

---

# Dynamic Analysis on Failure Modes of Tub Mounted Cranes

M. Koole

---

14-08-2015

MASTER OF SCIENCE THESIS





# Dynamic Analysis on Failure Modes of Tub Mounted Cranes

by

**M. Koole**

In partial fulfilment of the requirements for the degree of

**Master of Science**

in Offshore and Dredging Engineering at Delft University of Technology.

To be defended publicly on Friday August 14<sup>th</sup>, 2015 at 9:00 AM.

## Graduation committee

Chairman:	Prof. Dr. A.V. Metrikine	Delft University of Technology
Supervisor:	Ir. C. Keijndener	Delft University of Technology
	Ir. J.S. Hoving	Delft University of Technology
	Dr. Ir. M.A.N. Hendriks	Delft University of Technology
Company:	Ir. M. Bloem	Huisman Equipment B.V.

CONFIDENTIAL





---

# Abstract

---

The trend in Offshore Engineering is towards exploring in deeper waters and more harsh environments. As a consequence, topsides become larger and heavier. In order to keep up with the demand for more lifting capacity, Heerema announced a New Semi-submersible Crane Vessel (NSCV). This vessel will contain two 10 000mt Tub Mounted Cranes (TMC), which will be constructed by Huisman. In order to ensure safety, some level of redundancy has been implemented in the crane's hoisting systems. However, it was found that there was insufficient knowledge about the consequences of a wire failure in one of the hoisting systems.

In this thesis three possible failure cases were investigated: boom hoist cable failure, main hoist cable failure and a drop of the load. In addition, this thesis also looks at possible ways to reduce the dynamic effects of a wire failure.

Lagrange's equations were used to derive the equations of motion of the crane and the main hoist lower block. Using these equations of motion a dynamic model was created in MATLAB, using an Ordinary Differential Equation (ODE)-solver to solve the equations of motion. For all three cases animations were created in order to provide a visual validation of the models. Additional validation was performed by a comparison with results obtained using simpler models with only one or two degree(s) of freedom.

Parameter studies were performed on all three cases and different scenarios that could occur. For the boom hoist failure case the conclusion is drawn that none of the investigated parameters have a significant influence on the dynamic overshoot that occurs when one of the two wires fails. The overshoot is governed by the inertia of the load and boom.

This is not the case for main hoist failure, where the geometry of the main hoist block had a large influence on the resulting force in the wire. Other parameters that influenced the results of the analysis were the initial length of the main hoist system and the stiffness of the rigging between the hook and the load. With the current design the risk exists that when wire failure happens, the other wires will not be able to cope with the dynamic overshoot and the system will fail. However, it is unlikely that wire failure will happen due to overload in the normal operating case, as a safety factor of three is applied.

The third case, a drop of the load, proved to be the least severe case for the wires. Stress waves were witnessed in the results; however the effect of these were not significant. Even with the effects of stress waves taken into account the force in the wires remained below the initial value with the load still suspended from the crane. Further research on this case should focus on the bending of the boom.

Lastly, the influence of implementing a shock absorber in either the boom or the main hoist system was analyzed. For the boom hoist system the improvements were minimal, and the constant interaction of a damping system is undesired, which leads to the conclusion that it has no further potential. Implementing a shock absorber in the main hoist system resembles much of a Passive Heave Compensator (PHC) and could potentially improve the system. However, current PHC's do not have the right parameters to have a significant influence. The main reason for this is that the influence of the compensator is divided over many falls, which suppresses the influence.

Further research on this subject should focus on the behavior of the sheaves and falls in the system for two reasons: first, for determining the time it takes for a failing wire to un-reeve and lose its carrying capacity; second, in order to determine the effects of the reeving in a system with a shock absorber.

---

# Acknowledgements

---

This report contains the results of eight months of research carried out at Huisman Equipment BV as the final stage of my Master Offshore Engineering at Delft University of Technology. I would like to take this opportunity to thank the people that supported me throughout this research.

First, I would like to express my gratitude to ir. M. Bloem from Huisman Equipment for his guidance, support and advice in the past eight months. Your sincere interest in the topic was very contagious and motivated me a lot. I would also like to thank all my colleagues at Huisman for their interest and for the nice walks during lunch.

Furthermore, I would like to thank Professor Metrikine and Chris Keijdener from Delft University of Technology for their help and feedback during my research. I would also like to thank ir. J.S. Hoving and dr.ir. M.A.N. Hendriks for their participation in the graduation committee. I am also grateful to drs. D. Duppen for his useful comments on the report.

Last but certainly not least, I would like to thank my parents, brother, sister, girlfriend, friends and family for their endless support. Thank you for your encouragements and faith in me, not only during my graduation, but also throughout my years in Delft and my life in general.

*Marco Koole*  
*August 2015*



---

# Table of contents

---

<b>Abstract.....</b>	<b>V</b>
<b>Acknowledgements.....</b>	<b>VII</b>
<b>Table of contents .....</b>	<b>IX</b>
<b>List of Figures.....</b>	<b>XIII</b>
<b>List of Tables.....</b>	<b>XVII</b>
<b>Nomenclature.....</b>	<b>XIX</b>
<b>1 Introduction.....</b>	<b>1</b>
1.1 Problem definition .....	2
1.2 Base case and assumptions .....	3
1.3 Literature .....	4
1.4 Outline and content.....	5
<b>2 Preliminary analysis .....</b>	<b>7</b>
2.1 Lloyd’s Register and DNV .....	7
2.2 Analysis by Huisman.....	8
2.2.1 Calculation according to Lloyd’s Register .....	9
2.2.2 Calculation with impulse.....	11
2.2.3 Conclusion.....	12
<b>3 Crane details.....</b>	<b>13</b>
3.1 Load curve and load cases .....	14
3.2 Crane dimensions.....	15
3.3 Reeving boom hoist and wire stiffness.....	16
<b>4 Dynamic analysis .....</b>	<b>19</b>
4.1 Lagrange equations.....	19
4.2 Coordinate system and position vectors .....	20
4.3 Equations of Motion.....	22
4.4 Damping .....	25
4.5 Boom hoist failure .....	27
4.6 Main hoist failure .....	30
4.7 Drop of the load.....	34
4.8 Conclusions .....	36
<b>5 Modeling.....</b>	<b>37</b>

5.1	Coordinate system.....	37
5.2	Boom hoist length and luffing frame stiffness .....	38
5.3	Main hoist system .....	39
5.4	Boom stiffness .....	42
5.5	Stress wave effects .....	42
5.6	Specifics for each failure case .....	45
<b>6</b>	<b>Boom hoist failure analysis.....</b>	<b>47</b>
6.1	Effect of luffing frame stiffness .....	47
6.2	Effect of pivot friction .....	49
6.3	Effect of Main hoist length.....	50
6.4	Stress wave effect.....	51
6.5	Conclusions .....	53
<b>7</b>	<b>Main hoist failure analysis .....</b>	<b>55</b>
7.1	Detailed analysis of the free fall of the load .....	55
7.1.1	Outer wire failure .....	55
7.1.2	Inner wire failure.....	59
7.2	Effect of main hoist length on the maximum force .....	60
7.2.1	Outer wire failure .....	60
7.2.2	Inner wire failure.....	62
7.3	Stress wave effect.....	63
7.4	Influence of rigging .....	65
7.4.1	Outer wire failure .....	66
7.4.2	Inner wire failure.....	67
7.5	Dual lift with 20 000mt .....	70
7.6	Summary and Conclusions.....	73
7.6.1	Summary.....	73
7.6.2	Conclusions .....	74
<b>8</b>	<b>Drop of the load .....</b>	<b>77</b>
8.1	Results.....	77
8.1.1	82degrees, 10 000mt.....	77
8.1.2	68.3degrees, 10 000 mt.....	79
8.1.3	58.4degrees, 7,000mt.....	80
8.1.4	0degrees, 1588mt.....	81
8.2	Conclusions .....	81
<b>9</b>	<b>Concept design for mechanical equalizer .....</b>	<b>83</b>
9.1	Research.....	83
9.2	Concept .....	84
9.3	Assumptions.....	85
9.4	Equations of Motion for equalizer .....	86

9.5	Results without end buffer .....	87
9.6	Main hoist shock absorber .....	89
9.7	Effect of shock absorber on main hoist failure .....	92
9.8	Conclusions .....	93
<b>10</b>	<b>Conclusions and recommendations .....</b>	<b>95</b>
10.1	Conclusions .....	95
10.2	Recommendations.....	97
	<b>Bibliography .....</b>	<b>99</b>
	<b>Appendix A: Boom Angles .....</b>	<b>101</b>
	<b>Appendix B: Crane Details cont'd.....</b>	<b>103</b>
	<b>Appendix C: MATLAB Code.....</b>	<b>111</b>
	<b>Appendix D: End positions MH after failure.....</b>	<b>115</b>
	<b>Appendix E: Stress wave effect MH wire .....</b>	<b>117</b>
	<b>Appendix F: Heave Compensation System.....</b>	<b>119</b>
	<b>Appendix G: FMECA.....</b>	<b>121</b>
	<b>Appendix H: Main hoist concepts.....</b>	<b>123</b>



---

# List of Figures

---

Figure 1.1: SSCV Thialf performing decommissioning activities (www.heerema.com).....	1
Figure 1.2: 10 000mt TMC .....	2
Figure 1.3: Analysis sequence .....	5
Figure 2.1: Load with acting forces .....	9
Figure 2.2: $F_{\text{wire}}$ in time.....	10
Figure 2.3: Force balance .....	11
Figure 2.4: Energy accumulated in the wire .....	11
Figure 3.1: Nomenclature of the crane .....	13
Figure 3.2: Reeving configuration main hoist.....	14
Figure 3.3: Crane dimensions.....	15
Figure 3.4: Typical steel wire rope cross-section.....	16
Figure 4.1: Description of point P in two coordinate systems.....	21
Figure 4.2: Elementary rotations around X, Y and Z axis .....	21
Figure 4.3: Coordinate system.....	23
Figure 4.4: Elongation of boom hoist wires .....	24
Figure 4.5: Hysteretic damping, source: Rao; Mechanical Vibrations, Fifth Edition in SI Units.....	25
Figure 4.6: Time response and Wire force, load 10 000mt, no damping .....	27
Figure 4.7: Time response and Wire force, load 10 000mt, 82degrees .....	27
Figure 4.8: Time response and Wire force, load 10000mt, 68.3degrees.....	28
Figure 4.9: Time response and Wire force, load 7000mt, 58.4degrees .....	28
Figure 4.10: Time response and Wire force, load 4000mt, 41.6degrees.....	28
Figure 4.11: Time response and Wire force, load 1588mt, 0degrees .....	29
Figure 4.12: Main hoist equalizer, schematic view.....	30
Figure 4.13: Main hoist inner wire failure.....	30
Figure 4.14: Main hoist outer wire failure.....	30
Figure 4.15: Single DoF Main hoist system.....	31
Figure 4.16: Main hoist inner wire failure, force in remaining wire.....	32
Figure 4.17: Main hoist outer wire failure, force in remaining wire .....	32
Figure 4.18: Maximum wire force plotted against initial length of the Main hoist wire .....	33
Figure 4.19: Maximum wire force against damping factor, $v = 2.51$ [m/s].....	33
Figure 4.20: Drop of load analysis, 82° boom angle.....	34
Figure 4.21: Drop of load analysis, 68.3° boom angle .....	34
Figure 4.22: Drop of load analysis, 58.4° boom angle .....	35

Figure 4.23: Drop of load analysis, 41.6° boom angle ..... 35

Figure 4.24: Drop of load analysis, 0° boom angle..... 35

Figure 5.1: Coordinate system (figure courtesy of Z. Dix [2]) ..... 37

Figure 5.2: Total system ..... 38

Figure 5.3: Luffing frame equivalent stiffness ..... 38

Figure 5.4: Lower block system ..... 40

Figure 5.5: Discretizing of the boom..... 42

Figure 5.6: Wire expressed as mass spring elements..... 43

Figure 5.7: Boom Hoist wire discretization ..... 44

Figure 6.1: New approach to model luffing frame stiffness..... 47

Figure 6.2: Wire force boom Hoist, with luffing frame stiffness from ANSYS..... 48

Figure 6.3: Boom Hoist wire force, with and without luffing frame stiffness ..... 48

Figure 6.4: Maximum wire force against luffing frame stiffness ..... 48

Figure 6.5: Dynamic factor against luffing frame stiffness ..... 48

Figure 6.6: Pivot Friction..... 49

Figure 6.7: Maximum force in the wire against friction coefficient..... 49

Figure 6.8: Dynamic factor against friction coefficient ..... 49

Figure 6.9: Dynamic factor [Dynamic/Static(after failure)] against varying MH length ..... 50

Figure 6.10: Wire force in element closest to Luffing Frame ..... 52

Figure 6.11: Wire force in element closest to the boom ..... 52

Figure 7.1: Outer wire failure, Force on the inner wire ..... 56

Figure 7.2: Outer wire failure, Force on the inner wire ..... 56

Figure 7.3: Outer wire failure, Force on the inner wire ..... 57

Figure 7.4: Wire force with 1% damping ..... 58

Figure 7.5: Wire force with large damping values (~10%) ..... 58

Figure 7.6 Maximum wire force against damping factor ..... 59

Figure 7.7: Wire force with inner wire failure, load = 10 000mT ..... 60

Figure 7.8: Maximum force in remaining wire for different MH lengths, at outer wire failure ..... 61

Figure 7.9: Maximum wire force, 7000mt..... 61

Figure 7.10: Maximum wire force, 4000mt..... 61

Figure 7.11: Maximum wire force, 10 000mt ..... 62

Figure 7.12: Maximum wire force, 7000mt..... 62

Figure 7.13: Maximum wire force, 4000mt..... 62

Figure 7.14: Response of discretized and non-discretized wire ..... 64

Figure 7.15: Maximum force..... 64

Figure 7.16: SSCV Thialf in dual lift mode(source: Siemens AG) ..... 65

Figure 7.17: MH system including rigging ..... 65

Figure 7.18: Main hoist length = 30m, Rigging length = 20m..... 66

---

Figure 7.19: Maximum wire force against rigging stiffness .....	66
Figure 7.20: Force in failing wire .....	67
Figure 7.21: Force in remaining wire .....	67
Figure 7.22: Main hoist length = 30m, Rigging length = 20m.....	68
Figure 7.23: Slow dropping load (0.5s).....	68
Figure 7.24: Deflection of various parameters .....	69
Figure 7.25: Simplified system.....	69
Figure 7.26: Dual lift configuration.....	71
Figure 7.27: Main hoist length = 30m, Rigging length = 20m.....	72
Figure 8.1: 82 degrees loadcase, boom angle and wire force .....	77
Figure 8.2: 82 degrees loadcase, boom angle and wire force with Boom stop .....	78
Figure 8.3: Force and displacement of boom stop.....	78
Figure 8.4: Boom angle and wire force .....	80
Figure 8.5: Boom angle and wire force .....	81
Figure 9.1: Equalizer concept .....	84
Figure 9.2: Equalizer coordinate system and forces.....	86
Figure 9.3: Varying damping coefficient and stiffness.....	87
Figure 9.4: Varying mass and free path of the block .....	87
Figure 9.5: Wire force for all load cases.....	88
Figure 9.6: Main hoist shock absorber system .....	89
Figure 9.7: Boom hoist force and equalizer position XE .....	90
Figure 9.8: Implementation of existing PHC .....	91
Figure 9.9: Maximum wire force against damper stiffness.....	92
Figure 9.10: Main hoist wire force, outer wire failure.....	92
Figure 9.11: Maximum force against damping coefficient.....	93



---

# List of Tables

---

Table 3.1: The five load cases that are investigated.....	14
Table 3.2: Locations of components.....	15
Table 3.3: Wire properties boom hoist and main hoist.....	17
Table 4.1: Dynamic Factors.....	29
Table 4.2: Resulting forces on the wires after wire failure.....	31
Table 5.1: Specifics per failure case .....	45
Table 6.1: Summary of parametric study .....	53
Table 7.1: Variables used in analysis.....	55
Table 7.2: Parameters used for the analysis.....	60
Table 7.3: Natural frequencies .....	70
Table 7.4: Outer wire failure parameter study .....	73
Table 7.5: Inner wire failure parameter study .....	73
Table 9.1: PHC parameters .....	91
Table 9.2: Dynamic factor boom hoist wire .....	94



---

# Nomenclature

---

## Symbols

Symbol	Meaning	SI Units
$x, y, z$	Displacement	m
$\dot{x}, \dot{y}, \dot{z}$	Speed	m/s
$\ddot{x}, \ddot{y}, \ddot{z}$	Acceleration	m/s <sup>2</sup>
$A$	Area	m <sup>2</sup>
$C$	Wave speed	m/s
$c$	Damping coefficient	N-s/m
$D$	Diameter	m
$E$	Young's Modulus	N/m <sup>2</sup>
$F$	Force	N
$g$	Acceleration due to gravity	m/s <sup>2</sup>
$I$	Area moment of inertia	m <sup>4</sup>
$i, j$	Integer	
$k$	Stiffness coefficient	N/m
$L$	Length	m
$L_l$	Live load	kg
$M$	Mass	kg
$m$	Mass	kg
$mt$	Metric ton	1e3 kg
$q_j$	Generalized coordinate	
$\dot{q}_j$	Generalized velocity	m/s
$Q$	Non-conservative generalized force	
$r$	Position vector	
$t$	Time	s
$T$	Kinetic energy	J
$u$	Elongation	m
$V$	Potential energy	J
$V$	Volume	m <sup>3</sup>
$v_r$	Relative velocity	m/s

Symbol	Meaning	SI Units
$v$	Velocity	m/s
$W$	Working load	kN
$\alpha$	Angle	rad
$\varepsilon$	Strain	
$\delta$	Logarithmic decrement	
$\Delta$	Determinant	
$\mu$	Friction coefficient	
$\pi$	Ratio of a circle's circumference to its diameter	
$\psi$	Dynamic factor	
$\rho$	Mass density	kg/m <sup>3</sup>
$\sigma$	Stress	N/m <sup>2</sup>
$\theta$	Angle	rad
$\dot{\theta}$	Angular velocity	rad/s
$\ddot{\theta}$	Angular acceleration	rad/s <sup>2</sup>
$\varphi$	Rotation	rad

## Abbreviations

Abbreviation	Meaning
<b>ADAMS</b>	Multibody software
<b>ANSYS</b>	Finite element software
<b>Aux</b>	Auxiliary
<b>DNV</b>	Det Norske Veritas (international certification body)
<b>DOF</b>	Degree(s) Of Freedom
<b>FEM</b>	Finite Element Method
<b>FMECA</b>	Failure Mode Effect & Critically Analysis
<b>MBL</b>	Minimum Breaking Load
<b>NSCV</b>	New Semisubmersible Crane Vessel
<b>ODE</b>	Ordinary Differential Equation
<b>PHC</b>	Passive Heave Compensation
<b>SSCV</b>	Semi-Submersible Crane Vessel
<b>SWL</b>	Safe Working Load
<b>TMC</b>	Tub Mounted Crane

---

# 1 Introduction

---

Offshore technology has been developing fast in order to deplete natural resources (oil, gas, minerals etc.) from the seabed. The trend in Offshore Engineering is towards deeper water and more harsh environments. This trend has been going for some years, and will carry on in the foreseeable future. With the increasing difficulty of depleting offshore fields, there is a growth in demand for larger and heavier topsides.

Another trend that has been coming up is the removal and decommissioning of fields that have reached their lifetime. The structural integrity for these structures might have changed over the years, which makes a reverse installation more complicated than it seems. Also due to time restrictions it is preferred to remove as large as possible pieces in one go.

These trends have caused that the largest crane vessels are operating at their limits, and there is a growing demand for more lifting capacity. Whilst some companies came up with revolutionary designs, for example the Pioneering Spirit from Allseas, others stick to proven designs with an increased capacity.

Heerema Marine Contractors, another key-player in the offshore construction field, has recently announced the intent to construct a New Semisubmersible Crane Vessel (NSCV). The NSCV will carry two 10 000mt Tub Mounted Cranes (TMC). This is a significant increase compared to the Thialf (2x 7200mt), which is the largest Semi-Submersible Crane Vessel (SSCV) at present time. Figure (1.1) shows SSCV Thialf lifting a steel jacket structure [15].



**Figure 1.1: SSCV Thialf performing decommissioning activities (www.heerema.com)**

Huisman, worldwide specialist in lifting, drilling and subsea solutions, has received a Letter of Intent for the delivery of world's largest cranes onboard Heerema's planned NSCV. Huisman is known for their typical crane designs; mast cranes, pedestal cranes and knuckle boom cranes. These cranes

however, will be tub mounted, with an in-house designed and manufactured bearing for the slew system. The two cranes will be able to lift 10 000mt at a radius of 48m in offshore conditions.

With the design of such state of the art equipment, which pushes the human capabilities to the limit, new issues arise which haven't been investigated before. Safety is one of the key-elements in the offshore industry, lots of attention is paid to make offshore operations as safe as possible. Therefore the design specifications state that the boom hoist will contain two independent reeving systems, allowing the boom to be suspended (static) in either one of the ropes with full load suspended from the main hoist. However, little is known about the dynamic effects that are introduced when one of the two cables fails to carry the load.

### 1.1 Problem definition

As stated in the previous section little is known about the dynamic effects that are introduced when one of the cables in the boom hoist or main hoist fails to carry its load. Preliminary analysis (Section 2.2: Analysis by Huisman) has only delivered a dynamic factor, and lots of aspects that could influence the outcome have been neglected.

The goal of this study is to describe the dynamic effects of a single boom hoist cable failure, a single main hoist cable failure, or a drop of the load. Figure (1.2) shows the general configuration of the crane with the boom hoist and the main hoist.

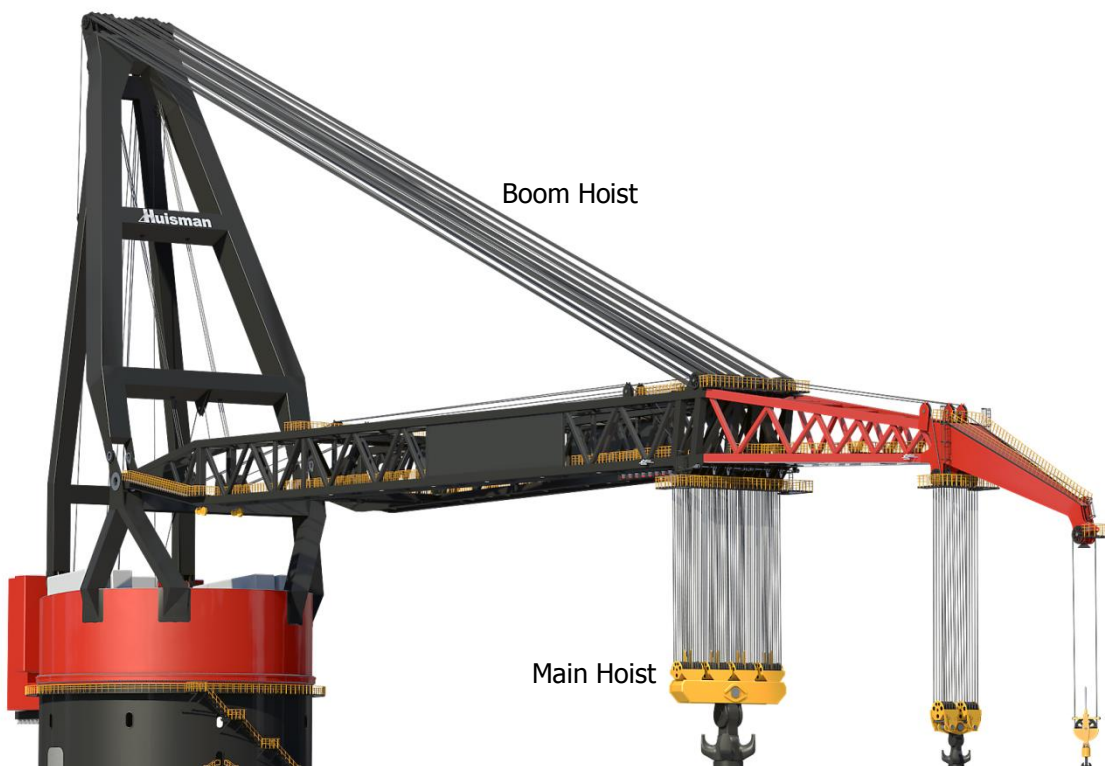


Figure 1.2: 10 000mt TMC

The boom hoist is single redundant; in case one cable breaks the other one has to take over the load. The main hoist has four independent hoisting cables, thus in case one of the cables fails to carry the load, the other three cables have to take over. This extra load on the remaining cable(s) will result in elongation and thus in a lowering of the boom/main hoist block and load. When the new equilibrium is reached the remaining hoist wires will carry the load that was originally carried by the two/four hoist wires. Besides this load, a momentum will be generated which requires an even larger force from the hoist wires to decelerate.

In the case of a dropping load (for example when the rigging fails) a momentum will also be generated. A load case will be considered with a dropping load, due to other reasons than cable snapping as mentioned in the other load cases. Due to the force in the wires of the boom hoist a drop of the load will result in a motion of the boom.

This makes the three defined load cases as follows:

- single boom hoist cable failure;
- single main hoist cable failure;
- drop of the load (due to other reasons than cable failure; rigging failure, hook failure etc.).

The main objectives of this thesis are:

- analysis of all components in the system;
- investigate the effect of stiffness and inertia of components, the effect of friction and other items that influence the dynamic behavior;
- determine the maximum dynamic loads on all components in the crane;
- find a concept design to reduce the dynamic effects.

## 1.2 Base case and assumptions

The 10 000 *mt* TMC's for Heerema are used as base case for this report. At the moment of this thesis these cranes are still in the design phase. The basic design has already been determined at this stage, so major changes are unlikely. Therefore this design will provide a good base case for this report. The crane configuration with its load curves can be found in Appendix B. The load cases will only be based on the main hoist load curve. No loads will be hoisted in the Aux hoist and the Whip hoist (see Figure (3.1) for reference of the Whip and Aux hoist).

A list of assumptions and boundary conditions is shown below:

- Movement of the vessel or crane due to wave action will not be taken into account;
- Wind forces will not be taken into account;

- The motions will be regarded as 2D motions, no swing effects will be taken into account;
- Flexibility and damping in the supports are taken into consideration;
- Flexibility and damping of the hoist rope are taken into consideration;
- Linear deformations in wire;
- The cause of wire failure will not be regarded in this thesis.

### 1.3 Literature

There are many papers and studies on the subject of offshore crane dynamics. However, most of these papers and studies address the problem of swing due to waves and displacements of the loads (hoisting, slewing and luffing). Analysis of such problems requires a system with 3D motions. For this research, the problem can be simplified into a 2D problem, which makes the use of 3D multi body software unnecessary. Still, in order to determine the equations of motions of a crane, some of these papers are deemed useful for this thesis, hence they are explained here.

Brzobohaty [1] has analyzed a crane losing its load, where a distinction was made between a sudden loss (0.1s) and a slow loss (1s) of the load. First a one dimensional mathematical model was created using the Newton's equations of motion. This model was then compared to a FEM (Finite Element Method) analysis with ANSYS. Results were found on the deflection and rotation of the boom, and in terms of stress in the boom. The fact that this report was only written in Czech, makes it hard to draw more conclusions from it.

Dix [2], Demmer [3] and Nugteren [4] all investigated the swing loads in offshore cranes. Their focus was mainly on the input from wave spectra and creating 3D models. Dix and Demmer used Lagrange's equations to establish the equations of motions in order to create a crane model. Nugteren only used a one dimensional pendulum as an analytic model, and is therefore less useful for this research.

Outside Huisman there are several papers available on the subject. The most relevant are elaborated in the next section.

Maczynski and Szczotka [9] have made a comparison of models for dynamic analysis of a mobile telescopic crane. An analytical model was created and then compared and verified with a numerical model in ADAMS. The comparison with two different methods is necessary in order to verify the model. The best way for comparison would be an actual experiment; however, this is not always possible.

Krukowski et al. [10] investigated the influence of a shock absorber on dynamics of an offshore pedestal crane. An analytical model was created with the Lagrange's equations of motion and the influence of a shock absorber in the hoisting cables was investigated. The result was that a shock absorber significantly decreases the dynamic overload experienced by the structural systems. Another aspect that was concluded is the fact that the flexibility of the boom only has a minor influence on the results.

No further literature was found on the subject. Although most of the literature presented is not exactly within the scope of this thesis, it provides a good basis to start with the analytical analysis. All other used literature can be found in the bibliography.

## 1.4 Outline and content

Figure (1.3) shows the analysis sequence for this thesis. First a simplistic model will be derived for all three failure cases in order to get some feeling on magnitude of loads and to determine how the detailed analysis should be performed.

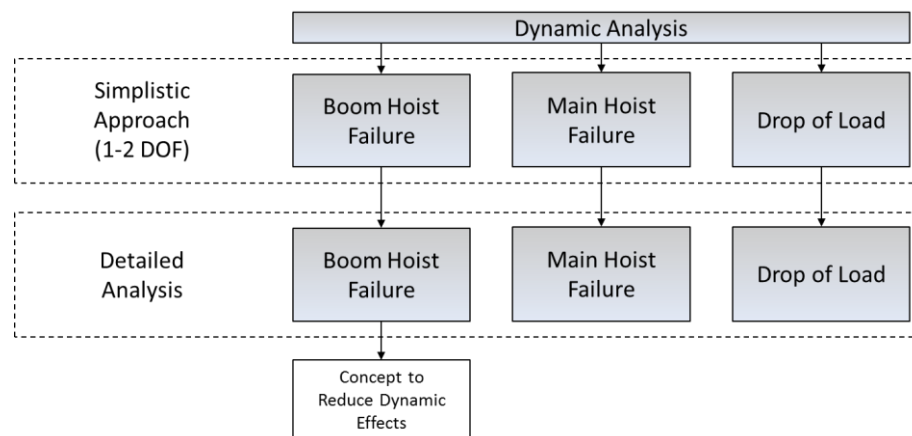


**Figure 1.3: Analysis sequence**

In Chapter 2 the preliminary analysis already conducted by Huisman is explained. This is a purely theoretical analysis based on energy and impulse balances, combined with formulae from the codes and regulations.

Chapter 3 shows the details of the crane, and the load cases based on the load curve of the crane. Also the wire properties and reeving diagrams can be found here. All details that are not presented in Chapter 3 but are still of interest for this thesis are listed in Appendix B.

The report continues with Chapter 4, in which the simplistic models are derived for all three failure cases. These models are based on a single or double degree of freedom system. The derivation of these systems has been done with the use of Lagrange's equations of motion, the principles of these equations are also found in Chapter 4. The first results on magnitudes of loads and impacts of the different load cases are reported in this section. From these results it is clear which effects need to be investigated in this thesis.

The implementation of different components in the system is discussed in Chapter 5. Also (a part of) the derivation of the equations of motion for the main hoist lower block is shown here. As a summary, a table is presented which shows which components will be implemented in each model for the three failure cases.

Then, in Chapter 6 the boom hoist failure is analyzed in detail. The effects of different components is analyzed and discussed.

Chapter 7 provides an in-depth analysis for the main hoist system. The distinction here will be made between inner – and outer wire failure. Also a dual lift analysis will be part of the analysis. Important parameters discussed in this section are: main hoist length, rigging stiffness and the stress wave effect.

In Chapter 8 a model with a discretized boom hoist wire is used to gain insight in the phenomena witnessed when drop of the load occurs.

An equalizer concept is proposed in Chapter 9. This concept is implemented in the model and its effects are analyzed. The goal of this is to determine whether it is viable to implement such an equalizer in the boom hoist reeving system.

Finally, the report will end with a conclusion and recommendations for future work.

Please note that, if not stated otherwise, all figures in this report are taken from internal Huisman documents or created by the author and are therefore not referenced.

---

## 2 Preliminary analysis

---

A preliminary analysis has been carried out by Huisman. The starting point for this analysis is based on the codes and regulations. Both the Det Norske Veritas (DNV) and Lloyd's Register state the same equations regarding dynamic forces. The calculation of this dynamic factor is explained in this section.

Two different approaches have been used to calculate the dynamic factor:

- calculation according to Lloyd's register;
- calculation with impulse.

Both approaches are explained in this chapter.

### 2.1 Lloyd's Register and DNV

The offshore industry is very strict in terms of codes and standards. Lloyd's register "Code for Lifting Appliances in a Marine Environment" [5] states the following about dynamic forces:

*"The dynamic force due to hoisting for offshore cranes is to include the effect of relative movement of the crane and load in addition to normal hoisting shock and dynamic effects. The hoisting factor is considered to be dependent of the design operational sea condition."*

The hoisting factor can be calculated from the following expression:

$$F_h = 1 + \frac{v_R}{g} \sqrt{\frac{k}{L_l}} \quad (2.1)$$

Where:

- $F_h$  = hoisting factor
- $k$  = the crane system stiffness, in N/m
- $L_l$  = live load, in kg
- $v_R$  = relative velocity, in m/s
- $g$  = 9.81 m/s<sup>2</sup>

To calculate the crane system stiffness the following combination of structural elements are to be considered:

- 1 hoist rope system;
- 2 luffing rope system;
- 3 pedestal;
- 4 crane house;

5 crane boom.

Other items may be considered additionally in the case where they are permanently installed on the crane. The stiffness of the wire rope is to be taken into account as per the rope manufacturer's recommendations using the Young's modulus and the associated area of the wire rope.

As an alternative to the method of determining the dynamic forces indicated above, Lloyd's register will consider submissions based on a dynamic analysis of the crane and associated structure (e.g., by means of a motion response analysis).

The DNV – code [6] states a similar equation for the dynamic factor:

$$\psi = 1 + V_R \sqrt{\frac{C}{W \cdot g}} \quad (2.2)$$

Where:

- $\psi$  = dynamic factor
- $C$  = geometric stiffness coefficient referred to hook position, in kN/m
- $g$  = 9.81 m/s<sup>2</sup>
- $W$  = working load, in kN
- $V_R$  = relative velocity (m/s) between load and hook at the time of pick-up

Comparing the two equations, one can easily obtain that these equations result in the same dynamic factor. The only difference lies in the unity, in which the load is expressed. Where Lloyd's uses  $kg$ , DNV uses  $kN$ . Redefining Equation (2.1), one obtains:

$$\frac{v}{g} \sqrt{\frac{k}{M}} = v \sqrt{\frac{k}{M \cdot g^2}} = v \sqrt{\frac{k}{W \cdot g}} \quad (2.3)$$

## 2.2 Analysis by Huisman

A preliminary analysis has been carried out by Huisman [3] in order to define the dynamic factor for a single boom hoist wire failure.

In order to obtain a result the following assumptions have been made:

1. the rotation of the boom is sufficiently small so that the whole system can be linearized around the working point;

2. while linearizing there exists an equivalent mass to describe the combined effect of both load and boom mass;
3. the stiffness of the boom hoist can be linearized to get an equivalent boom hoist stiffness;
4. initially the system is at rest (no velocity) and each boom hoist system is taking half the total load, then from this initial situation half of the supporting wires are removed from the equation;
5. no friction or damping is assumed so all potential energy from the lowering of the mass is transferred into kinetic energy;
6. the calculations have been performed according to Lloyd's register.

### 2.2.1 Calculation according to Lloyd's Register

The initial state of the loading is shown in Figure (2.1).

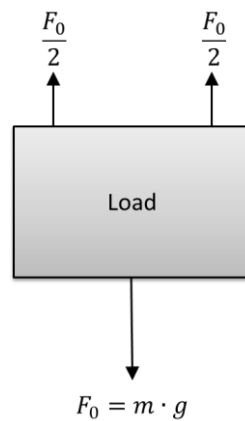


Figure 2.1: Load with acting forces

The force on the load can be described as:

$$F = F_0 - F_s \quad (2.4)$$

Where (after failure of one of the two wires):

$$F_s(x) = \frac{F_0}{2} + x \cdot k \quad (2.5)$$

With:

- x = elongation of wire
- k = stiffness of wire

Substituting Equation (2.5) into (2.4) one obtains:

$$F(x) = \frac{F_0}{2} - x \cdot k \quad (2.6)$$

Figure (2.2) shows the force in the wire over time. At  $t = 0$  there are two wires to support the load. Then one of the wires fails and the other wire needs to take the load from the failing wire. This results in an elongation of the wire. At the moment of maximum velocity there is no acceleration of the mass, so the net force on the mass is 0. Then, from Equation (2.6) the elongation can be determined as  $x = \frac{F_0}{2k}$ . The energy comes from moving the mass over the path from  $x = 0$  to  $x = \frac{F_0}{2k}$ , while the force on the mass is  $F(x) = \frac{F_0}{2} - x \cdot k$ .

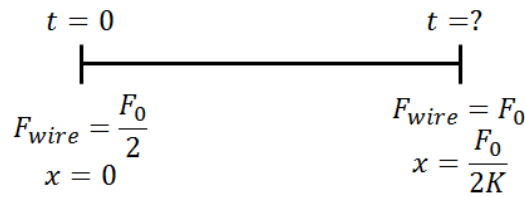


Figure 2.2:  $F_{wire}$  in time

The total energy of the fall can then be expressed as:

$$W = \int F dx = \int_0^{\frac{F_0}{2k}} \left( \frac{F_0}{2} - x \cdot k \right) dx = \left[ \frac{F_0}{2} x - k \frac{x^2}{2} \right]_{x=0}^{x=\frac{F_0}{2k}} \quad (2.7)$$

This results in:

$$W = \frac{F_0}{2} \frac{F_0}{2k} - \frac{k}{2} \frac{F_0^2}{k^2} = \frac{F_0^2}{8k} \quad (2.8)$$

The next step is to transfer the energy to a velocity of the mass:

$$W = \frac{1}{2} M v^2 = \frac{F_0^2}{8k} \rightarrow v^2 = \frac{F_0^2}{8k M} \quad (2.9)$$

Substituting  $F_0 = M \cdot g$  back into Equation (2.9) and taking the square root, one obtains:

$$v = \sqrt{\frac{M^2 g^2}{8k} \frac{2}{M}} \quad (2.10)$$

This velocity can be substituted in Equation (2.1) in order to obtain the dynamic factor:

$$F_h = 1 + \sqrt{\frac{M^2 g^2}{8k} \cdot \frac{2}{M} \cdot \frac{k}{M \cdot g \cdot g}} \quad (2.11)$$

$$F_h = 1 + \sqrt{\frac{2}{8}} = 1.5 \quad (2.12)$$

### 2.2.2 Calculation with impulse

Another approach to find the dynamic factor is to calculate the impulse generated by the energy stated in Equation (2.9). The maximum force is calculated by integrating the deceleration of the load. Figures (2.3) and (2.4) below show the force balance on the mass and the energy accumulated by the force in the wire and the elongation of the wire due to its stiffness.

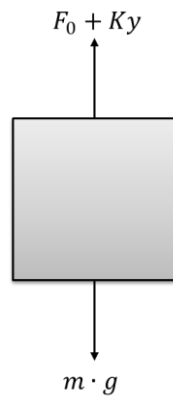


Figure 2.3: Force balance

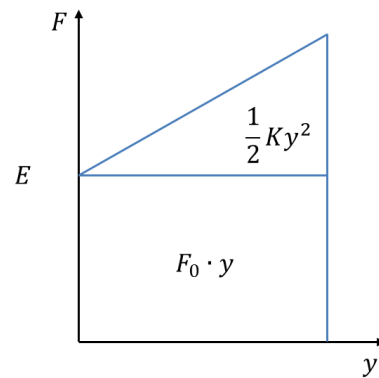


Figure 2.4: Energy accumulated in the wire

The energy balance that can be obtained from this is as follows:

$$W = \frac{1}{2}ky^2 + F_0y - Mgy = \frac{F_0^2}{8k} \quad (2.13)$$

In order to find the maximum deflection one needs to solve Equation (2.14):

$$\left(\frac{1}{2}k\right)y^2 + F_0y - F_0y - \frac{F_0^2}{8k} = 0 \quad (2.14)$$

This results in:

$$y_{max} = \frac{0 \pm \sqrt{4 \cdot \left(\frac{1}{2}k\right) \cdot \left(\frac{F_0^2}{8k}\right)}}{k} = \frac{\pm \sqrt{\frac{1}{4}F_0^2}}{k} = \frac{1}{2} \frac{F_0}{k} \quad (2.15)$$

The maximum force can then be determined as:

$$F_{max} = F_0 + ky_{max} = F_0 + \frac{1}{2}F_0 \quad (2.16)$$

And then the dynamic factor can be found to divide  $F_{max}$  by  $F_0$ :

$$\psi = \frac{F_0 \left(1 + \frac{1}{2}\right)}{F_0} = 1.5 \quad (2.17)$$

### 2.2.3 Conclusion

These two calculations show the dynamic factor determined by the ratio of energy in the system. Other parameters like boom hoist tackle stiffness or load do not seem to influence the final result. This leaves the dynamic factor to be  $\psi=1.5$ ; independent from any variables. However, many factors that might influence the outcome of this factor have not been taken into account. Therefore, a dynamic model is required for the crane as a whole in order to obtain more accurate results. Things that could be included in the model are: inertia, friction and other items that influence the dynamic behavior.

---

## 3 Crane details

---

As stated before, the 10 000 *mt* TMC's for Heerema's NSCV are used as a base case. This will be the largest offshore crane in the world, and is therefore an excellent example to use. This chapter will cover the most important details of the crane that were used for the analysis. This will be from a global perspective to detailed information about specific components.

Figure (3.1) shows the side view of the vessel with the crane. This so called 'nomenclature' shows all the names of the different components in the crane. The crane rotates as a whole around the tub. A bearing in the tub makes the rotation of the crane possible. The boom rotates around the pivot point. Two different boom angles are shown in Figure (3.1); one with a zero degree boom angle and one with a slight rotation of the boom.

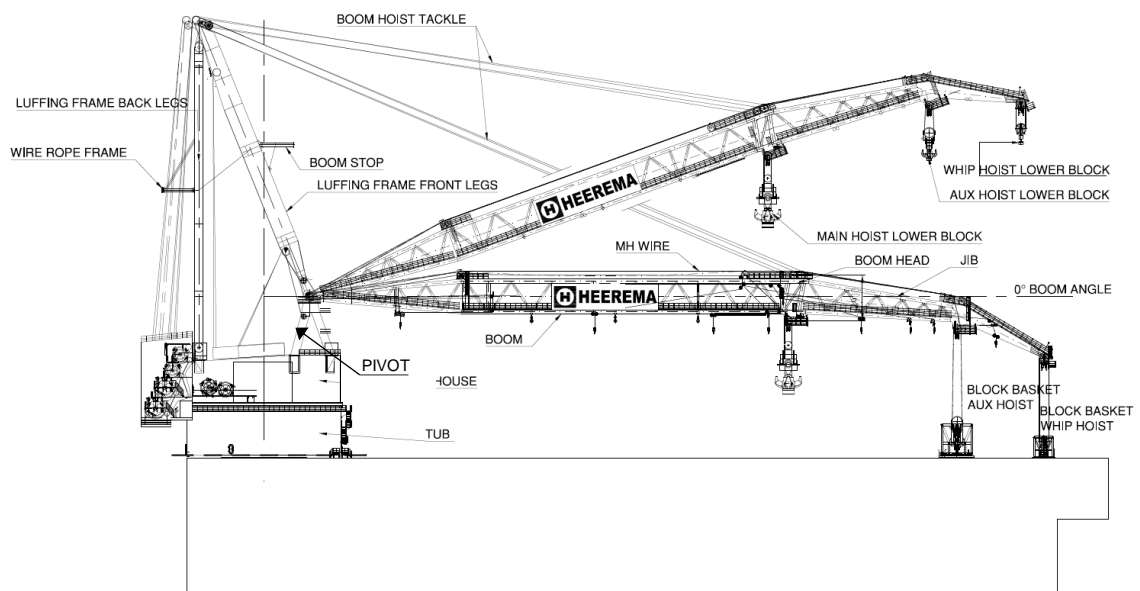


Figure 3.1: Nomenclature of the crane

### 3.1 Load curve and load cases

The load curve for the cranes can be found in Appendix B, Figure (B.1). The SWL (Safe Working Load) is displayed against the radius of the crane. Different reeving configurations for the main hoist are shown, however in this report only the maximum load cases are investigated, which means 80 falls. The reeving configuration is shown in Figure (3.2), there it can be seen that there are four independent main hoist wires in the system. In case of failure of one of the main hoist wires, there will be three remaining wires to carry the load.

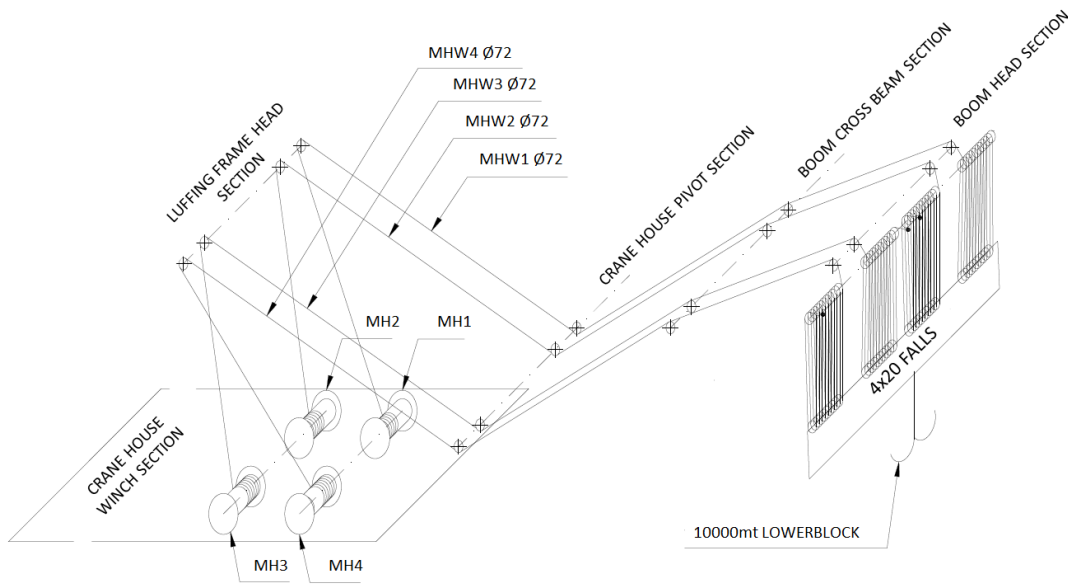


Figure 3.2: Reeving configuration main hoist

From the load curve, five load cases have been set. These load cases are shown in Table (3.1). The boom angle has an effect on stiffness of the boom hoist wires; therefore different load cases at multiple boom angles are investigated. Also at different sections of the load curve, different parameters are governing for the system. An elaboration of this can be found in Appendix (B), Figure (B.2). Appendix (A) shows a schematic view of the crane for all load cases listed in Table (3.1).

Table 3.1: The five load cases that are investigated

Main Hoist		
SWL [mt]	Radius [m]	Boom Angle [°]
10 000	26.7	82.0
10 000	48.0	68.3
7000	62.0	58.4
4000	82.0	41.6
1588	102.0	0.0

## 3.2 Crane dimensions

Figure (3.3) shows the crane dimensions. There are two axis systems in the crane, one which originates in the center of the tub and deck level, and one which originates in the pivot center. The various distances with respect to the pivot point or with respect to the center of the tub are shown in Table (3.2).

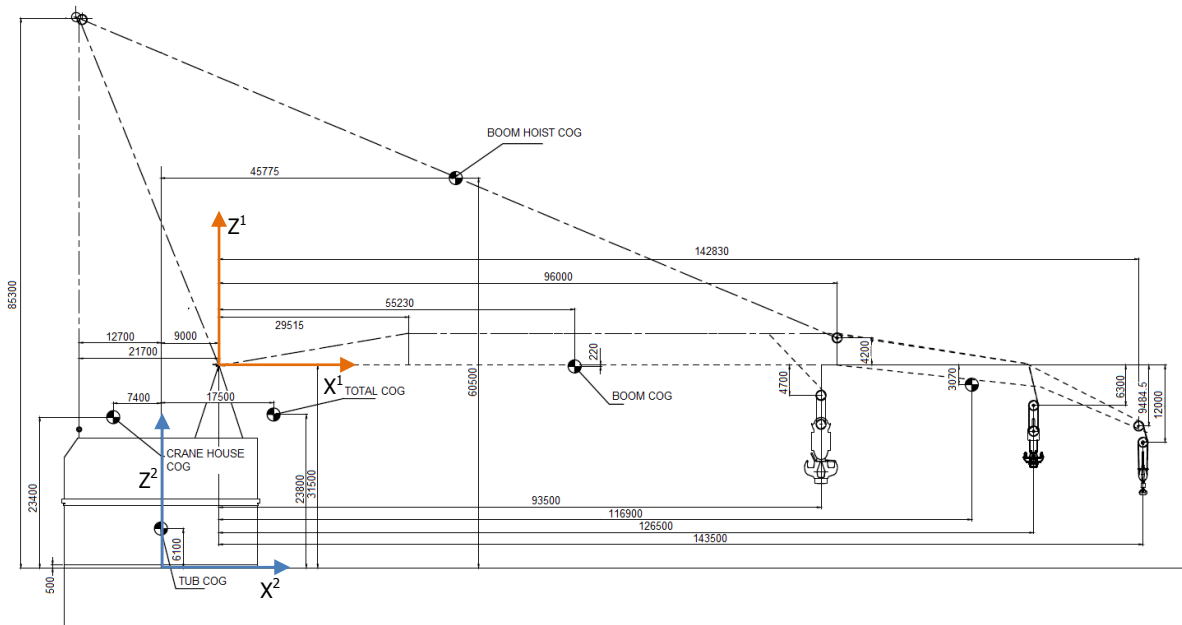


Figure 3.3: Crane dimensions

Table 3.2: Locations of components

Component	Summary		
	Weight [mt]	X_CoG [mm]	Z_CoG [mm]
Boom <sup>1</sup>	1463	55230	-220
Boom hoist wire <sup>2</sup>	258	45775	60500
Flyjib <sup>1</sup>	262	116900	-3070
Main hoist lower block <sup>1</sup>	480	93500	-4700
Aux hoist lower block <sup>1</sup>	130	126500	-6300
Whip hoist lower block <sup>1</sup>	10	143500	-12000
Crane house <sup>2</sup>	5583	-7400	23400
Pedestal <sup>2</sup>	909	0	6100
<b>Total</b>	<b>8492</b>		

<sup>1</sup>In boom coordinate system with respect to pivot

<sup>2</sup>In crane coordinate system with respect to deck level

### 3.3 Reeving boom hoist and wire stiffness

The reeving configuration for the boom hoist can be found in Appendix B (Figure B.2). There are two independent boom hoist wires in the system, operated by four winches. Both wires are reeved 20 times, which creates a total of 80 times the stiffness of a single wire.

The stiffness of the wires can be calculated with Hooke's law:

$$\sigma = E \cdot \varepsilon \quad (3.1)$$

$$\sigma = \frac{F}{A}, \quad A = \frac{(\pi \cdot d^2)}{4}, \quad F = k \cdot \Delta L, \quad \varepsilon = \frac{\Delta L}{L_0} \quad (3.2)$$

This results in the following equation:

$$k = \frac{E \cdot \pi \cdot d^2}{4 \cdot L_0} \quad (3.3)$$

The effective area of a steel rope is the area as defined in Equation (3.2) multiplied with a fill factor. Figure (3.4) shows a typical steel wire rope section [16]. It can be seen that not the whole cross-section is filled with steel, therefore the fill factor is introduced to indicate the percentage of steel. The fill factor for the cables in this research is 0.67.



Figure 3.4: Typical steel wire rope cross-section

The stiffness as calculated in Equation (3.3) is for a single wire only, the total stiffness for the system is determined as follows:

$$k_{system} = \sum_{i=1}^n k_{wire} = n \cdot k_{wire} \quad (3.4)$$

With  $n$  the total amount of wires in the system.

Table (3.3) shows the wire properties that are used in this research.

**Table 3.3: Wire properties boom hoist and main hoist**

<b>Property</b>	<b>Unit</b>	<b>Value</b>
Wire diameter	[mm]	72
Fill factor	[-]	0.67
Breaking strength	[kN]	4650
(MBL)	[mt]	474
Wire mass	[kg/m]	25.1
E	[MPa]	1.05e5



---

## 4 Dynamic analysis

---

In this chapter the method for the dynamic analysis is described. Generally speaking, in order to get numerical effectiveness, models should be as simple as possible; this reduces the risk of errors. However, one should bear in mind that oversimplification reduces the reflection of the actual system and should be avoided (Maczynski and Szczotka [9]). It is often the case that a problem is too complicated to solve with Newton's equations. Therefore a different approach was investigated to solve this problem. This approach is based on the Lagrange's equations. This method is more convenient for multi degree of freedom systems or systems in complex coordinate systems. At first it may seem that the Newton's equations could also suffice in this case, but with an eye on further analysis the choice was made to go with Lagrange's equations. An implementation of a device to reduce the dynamic effects would be more convenient in the Lagrange's system.

### 4.1 Lagrange equations

The Lagrange's equations are based on the conservation of energy. They are the beginning of a mathematical approach to mechanics. The Lagrange's equations use generalized coordinates to derive the equations of motions of a vibrating system. Lagrange's equations can be stated as:

$$\frac{d}{dt} \left( \frac{\delta T}{\delta \dot{q}_j} \right) - \frac{\delta T}{\delta q_j} + \frac{\delta V}{\delta q_j} = Q_j^n \quad j = 1, 2, \dots, n \quad (4.1)$$

Where:

- $\dot{q}_j = \frac{\delta q_j}{\delta t}$  = the generalized velocity;
- $Q_j^n$  = the non-conservative generalized force;
- $T$  = the kinetic energy of the system;
- $V$  = the potential energy of the system.

Another way to write the Lagrange's equations is:

$$\frac{d}{dt} \frac{\delta L}{\delta \dot{q}} - \frac{\delta L}{\delta q} = Q \quad (4.2)$$

In this equation  $L$  is the Lagrangian of the system and can be defined as:

$$L = T - V \quad (4.3)$$

Where  $T$  is the total kinetic energy and  $V$  is the total potential energy of the system.

In general, the kinetic energy of the system has to be determined for translational and rotational velocities. The translational velocity can be determined by differentiating the position vector. This vector describes the position of the center of gravity of a body with respect to the origin of a global coordinate system.

$$T = T_{trans} + T_{rot} \quad (4.4)$$
$$T = \frac{1}{2}M|\dot{r}|^2 + \frac{1}{2}I\dot{\theta}^2$$

Where

- $\theta$  = angle [rad]
- $r$  = position vector

The potential energy for the system can be expressed with the following expression:

$$V = Mgr_z + \frac{1}{2}kq_j^2 \quad (4.5)$$

Where:

- $r_z$  = vertical component position vector;
- $k$  = spring stiffness;
- $q_j$  = generalized elongation.

## 4.2 Coordinate system and position vectors

Equations (4.4) and (4.5) make use of position vectors to describe the positions of the components in the system. The positions of components are described with respect to a global coordinate system. In order to do this, rotation matrices are used. This section describes the use of rotation matrices to describe the coordinates.

As the problem will be regarded in a three-dimensional system later on in the research, the derivation is done for a three-dimensional space. A point's position with respect to an origin  $\{0\}$  can be described as:

$$r_P^0 = \begin{bmatrix} x_P \\ y_P \\ z_P \end{bmatrix} \quad (4.6)$$

In order to determine a rigid body's position in a three-dimensional space requires the definition of two coordinate systems:

- A global coordinate system;
- A coordinate system fixed to the body.

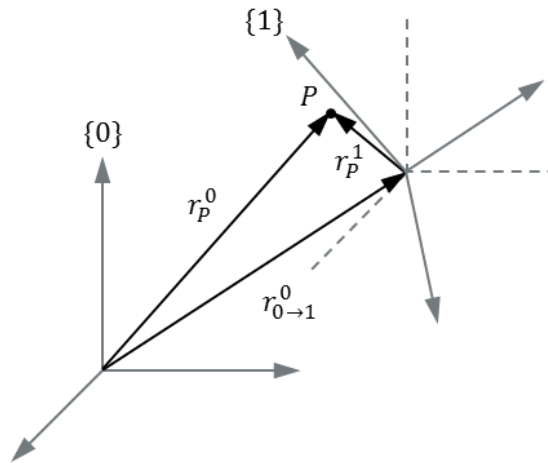


Figure 4.1: Description of point P in two coordinate systems

Figure (4.1) shows the description of a point in two coordinate systems;  $\{0\}$  is the global coordinate system and  $\{1\}$  is the local coordinate system attached to the body. The position of point P can now be described as:

$$r_P^0 = r_{0 \rightarrow 1}^0 + R_1^0 r_P^1 \quad (4.7)$$

Where  $R$  is the rotation matrix to transform the position of the load from a local coordinate system to the global coordinate system. In order to get better understanding of the principle of the rotation matrices, the rotation matrices for the elementary rotations are explained below.

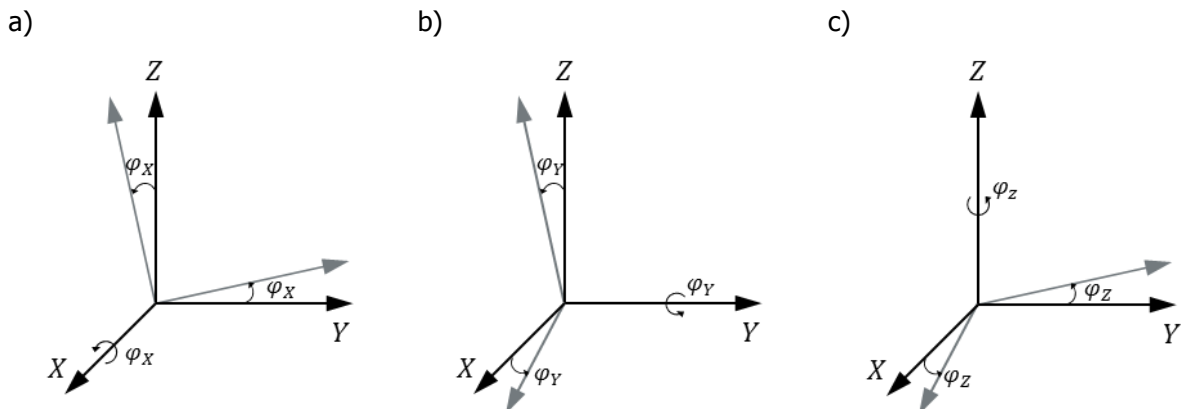


Figure 4.2: Elementary rotations around X, Y and Z axis

In Figure (4.2a) the rotation is around the X-axis by the angle  $\varphi_X$ , this rotation can be described by the following rotation matrix:

$$R_X(\varphi_X) = \begin{bmatrix} 1 & 0 & 0 \\ 0 & \cos(\varphi_X) & -\sin(\varphi_X) \\ 0 & \sin(\varphi_X) & \cos(\varphi_X) \end{bmatrix} \quad (4.8)$$

Subsequently, the rotations for  $\varphi_Y$  and  $\varphi_Z$  can be described with:

$$R_Y(\varphi_Y) = \begin{bmatrix} \cos(\varphi_Y) & 0 & \sin(\varphi_Y) \\ 0 & 1 & 0 \\ -\sin(\varphi_Y) & 0 & \cos(\varphi_Y) \end{bmatrix} \quad (4.9)$$

$$R_Z(\varphi_Z) = \begin{bmatrix} \cos(\varphi_Z) & -\sin(\varphi_Z) & 0 \\ \sin(\varphi_Z) & \cos(\varphi_Z) & 0 \\ 0 & 0 & 1 \end{bmatrix} \quad (4.10)$$

With these elementary rotation matrices every arbitrary rotation of a coordinate system relative to another can be described. The principle of the rotation matrices will be used to derive the equations of motions for the lower block system of the main hoist.

### 4.3 Equations of Motion

With the Lagrange's equations it is now possible to determine the equations of motion for this system. Figure (4.3) shows the coordinates in the system.

As there is no translation in this case, the kinetic energy of the system only consists of the rotational energy of the boom and the other components. This leads to the following equation for kinetic energy:

$$T = \frac{1}{2}I_b\dot{\theta}^2 + \sum_{n=1}^4 \frac{1}{2}I_n\dot{\theta}^2 + \frac{1}{2}M_l v_l^2 \quad (4.11)$$

with  $I_n = M_n L_n^2$

In Equation (4.11),  $n$  yields the following:

1. Jib;
2. Main hoist;
3. Aux hoist;
4. Whip hoist.

Equation (4.12) describes the potential energy of the system:

$$V = \sum_{n=1}^5 M_n g z_n + \frac{1}{2}k(\Delta u)^2 \quad (4.12)$$

Where  $n$  yields the following:

1. Jib;
2. Main hoist;

3. Aux hoist;
4. Whip hoist;
5. Boom.

And where:

$$z_n = L_n \cdot \sin(\theta + \alpha_n)$$

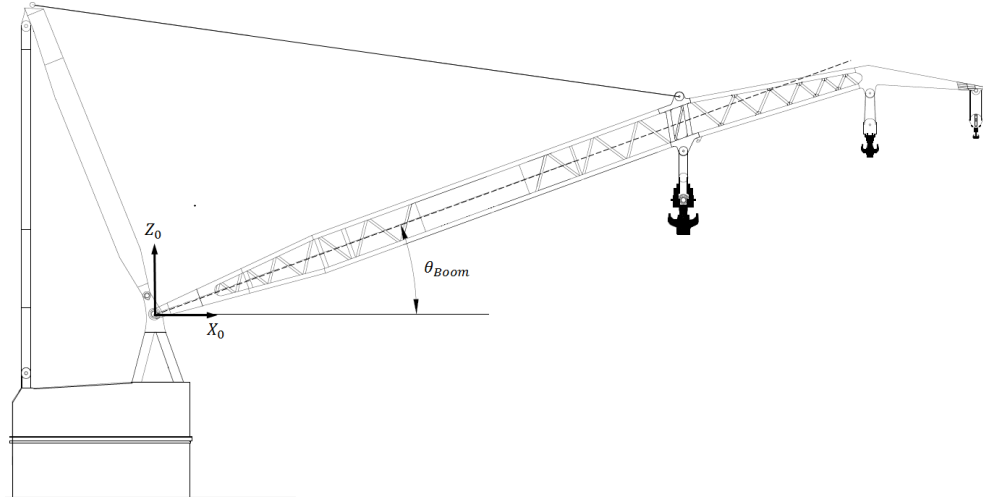


Figure 4.3: Coordinate system

The angle  $\alpha_n$  is due to the offsets of the locations of the components compared to the centerline of the boom. From Figure (4.4) it is possible to determine the elongation of the boom hoist wires. The initial position of the boom is shown as  $\theta_{initial}$ . The length of the boom hoist wires can then be calculated using the law of cosines. Doing the same for the present boom angle  $\theta$  and subtracting results in:

$$\Delta L_{BHwires} = \sqrt{L_1^2 + L_2^2 - 2 \cdot L_1 \cdot L_2 \cos(180 - \alpha_1 - \theta - \alpha_3)} - \sqrt{L_1^2 + L_2^2 - 2 \cdot L_1 \cdot L_2 \cos(180 - \alpha_1 - \theta_{initial} - \alpha_3)} \quad (4.13)$$

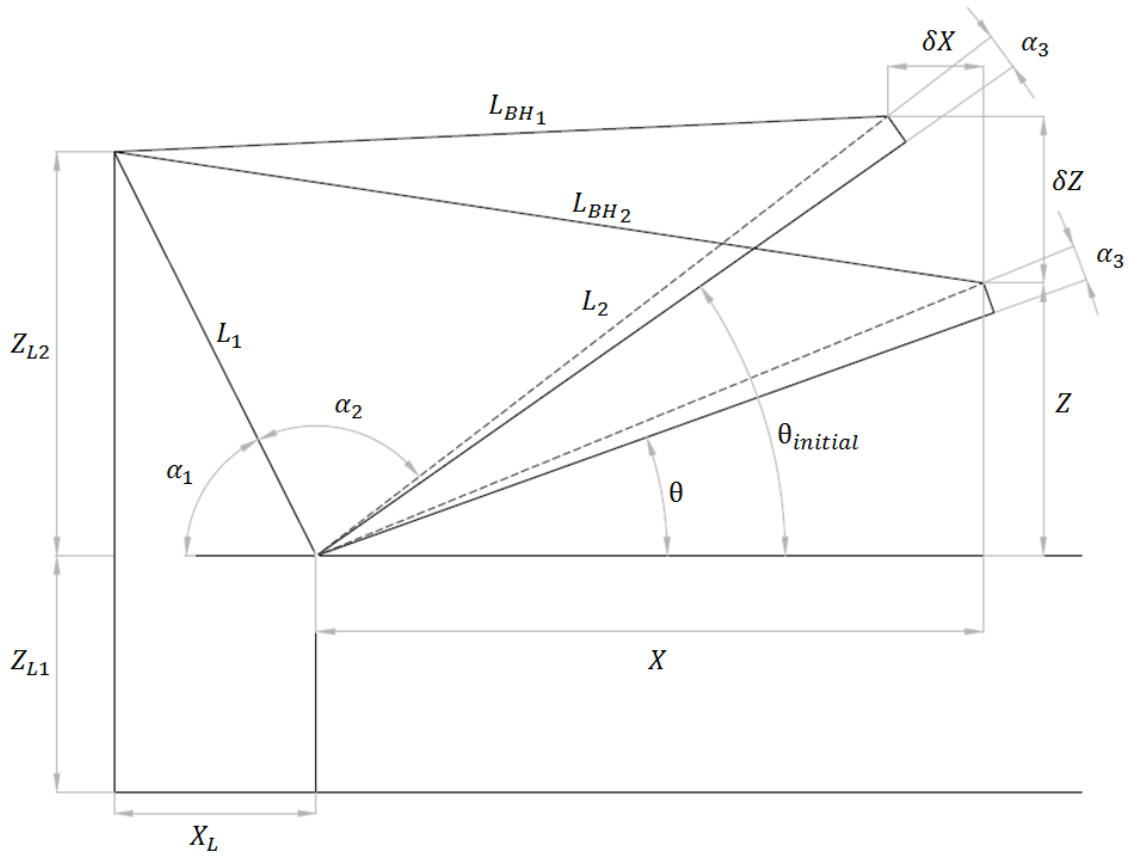


Figure 4.4: Elongation of boom hoist wires

Substituting Equation (4.11) back into Equation (4.1) results in:

$$\frac{d}{dt} \left( \frac{\delta T}{\delta \dot{\theta}} \right) = I_b \ddot{\theta} + \sum_{n=1}^4 I_n \ddot{\theta} + (m_l L_{MH}^2) \ddot{\theta} \quad (4.14)$$

Where the load is implemented as a point mass at the location of the main hoist. Then by substituting Equation (4.12) also back into Equation (4.1), one can obtain the following:

$$\begin{aligned} \frac{\delta V}{\delta \theta} = & \sum_{n=1}^5 M_n g \cdot L_n \cdot \cos(\theta - \alpha_n) \\ & + k \left( \sqrt{L_1^2 + L_2^2 - 2 \cdot L_1 \cdot L_2 \cos(180 - \alpha_1 - \theta - \alpha_3)} \right. \\ & \left. - \sqrt{L_1^2 + L_2^2 - 2 \cdot L_1 \cdot L_2 \cos(180 - \alpha_1 - \theta_{initial} - \alpha_3)} \right) \cdot \\ & \left( \frac{L_1 L_2 \sin(180 - \alpha_1 - \theta - \alpha_3)}{\sqrt{(L_1^2 - 2 L_1 L_2 \cos(180 - \alpha_1 - \theta - \alpha_3) + L_2^2)}} \right) \end{aligned} \quad (4.15)$$

The equation of motion for the generalized coordinate  $\theta$  is shown in Equation (4.16):

$$\ddot{\theta} = \left( \sum_{n=1}^5 M_n g \cdot L_n \cdot \cos(\theta - \alpha_n) + k \left( \sqrt{L_1^2 + L_2^2 - 2 \cdot L_1 \cdot L_2 \cos(180 - \alpha_1 - \theta - \alpha_3)} - \sqrt{L_1^2 + L_2^2 - 2 \cdot L_1 \cdot L_2 \cos(180 - \alpha_1 - \theta_{initial} - \alpha_3)} \right) \cdot \left( \frac{L_1 L_2 \sin(180 - \alpha_1 - \theta - \alpha_3)}{\sqrt{(L_1^2 - 2 L_1 L_2 \cos(180 - \alpha_1 - \theta - \alpha_3) + L_2^2)}} \right) \right) / (- (I_b + I_{jib} + I_{MH} + I_{AH} + I_{WH} + I_{load})) \quad (4.16)$$

## 4.4 Damping

The energy in a system will dissipate and the oscillation will fade out in time. The rate of damping will also influence the peak of the wire force overshoot; therefore it is important to make a realistic estimation of the damping factor. The main cause of damping is material damping in the boom hoist wires. In each loading and unloading cycle some energy will be dissipated, this phenomenon is known as hysteretic damping. Figure (4.5) shows a hysteric damping cycle and the rate of energy dissipation [8].

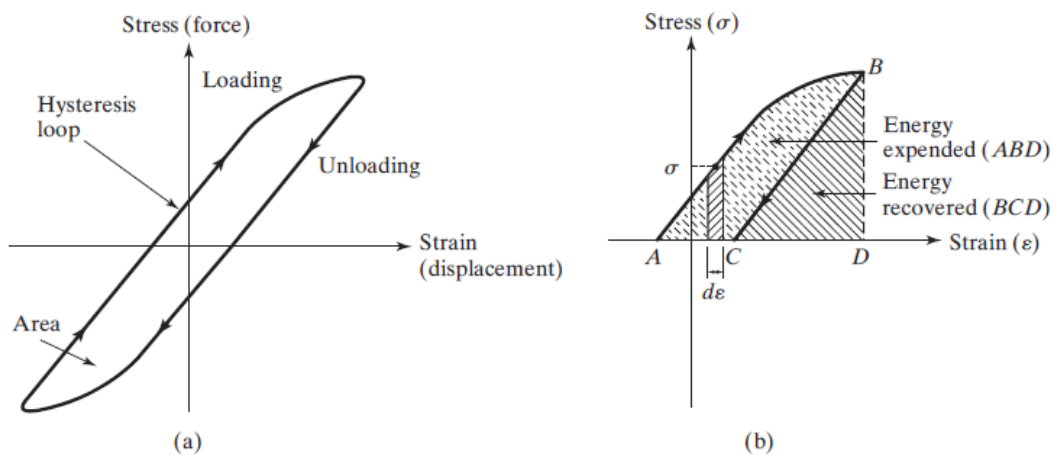


Figure 4.5: Hysteretic damping, source: Rao; Mechanical Vibrations, Fifth Edition in SI Units

It is not possible to apply the hysteretic damping model in time domain simulations; often an equivalent viscous damping is introduced to overcome this problem. Within the Lagrange equations the damping is implemented with the Rayleigh's Dissipation Function, which is based on viscous damping. The Rayleigh's Dissipation Function is defined by:

$$D = \frac{1}{2} \sum_{n=1}^n c_i \dot{q}_i^2 \quad (4.17)$$

In which:

$$c_i = \text{damping coefficient}$$

This could be substituted into Equation (4.1) as:

$$Q^{fr} = \frac{\delta D}{\delta \dot{q}_i} \quad (4.18)$$

Substituting Equation (4.17) into Equation (4.18), one obtains:

$$Q^{fr} = c \cdot \dot{q}_i \quad (4.19)$$

In this case the generalized coordinate is the elongation speed of the wire, which can be determined by differentiating Equation (4.13).

$$\frac{\Delta L}{dt} = \frac{2 \cdot L_1 L_2 \sin(180 - \alpha_1 - \alpha_3 - \theta) \cdot \dot{\theta}}{2 \cdot \sqrt{L_1^2 + L_2^2} - 2 \cdot L_1 L_2 \cos(180 - \alpha_1 - \alpha_3 - \theta)} \quad (4.20)$$

The damping constant  $c$  is set as a percentage of the critical damping of the system. This critical damping can be found as:

$$c_{crit} = 2 \cdot \sqrt{(I \cdot k)} \quad (4.21)$$

## 4.5 Boom hoist failure

In this section the results are shown of the response that is obtained with the Matlab ode45 solver. This solver is based on an explicit Runge-Kutta formula, the Dormand-Price pair. In general, the ode45 solver is the best function to apply as a first try to solve non-stiff problems. A stiff Ordinary Differential Equation (ODE) is an ODE for which numerical errors compound dramatically over time. This would require considerably smaller time steps to solve the ODE, which leads to long solving times. In case of a stiff problem a solver should be used, which can solve stiff ODE's more efficiently. The ode45 solver is a one-step solver; in order to compute  $y_{(tn)}$ , it needs only the solution at the immediately preceding time point,  $y_{(tn-1)}$ . The first plots, which can be seen in Figure (4.6), show the result without damping.

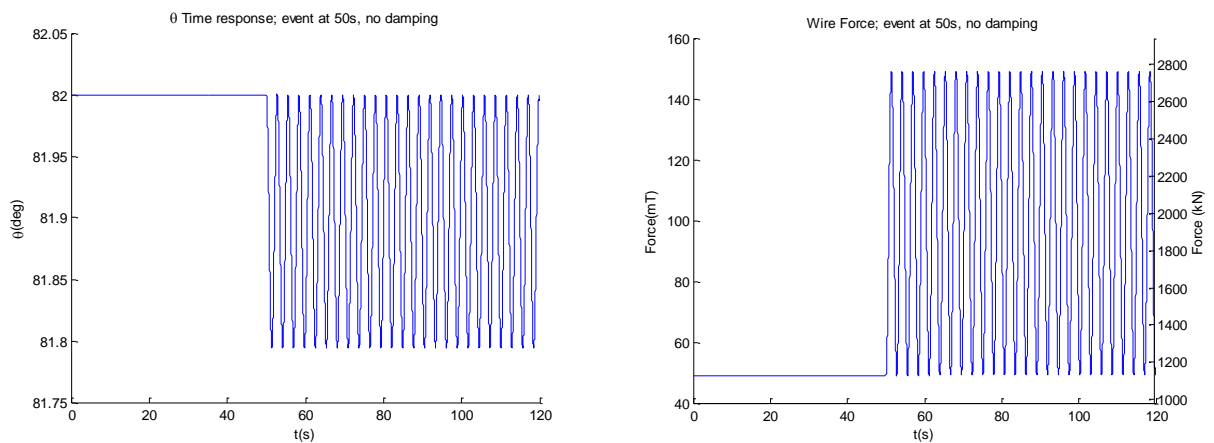


Figure 4.6: Time response and Wire force, load 10 000mt, no damping

With 3% damping added to the system as described in Section (4.4) the results are as follows:

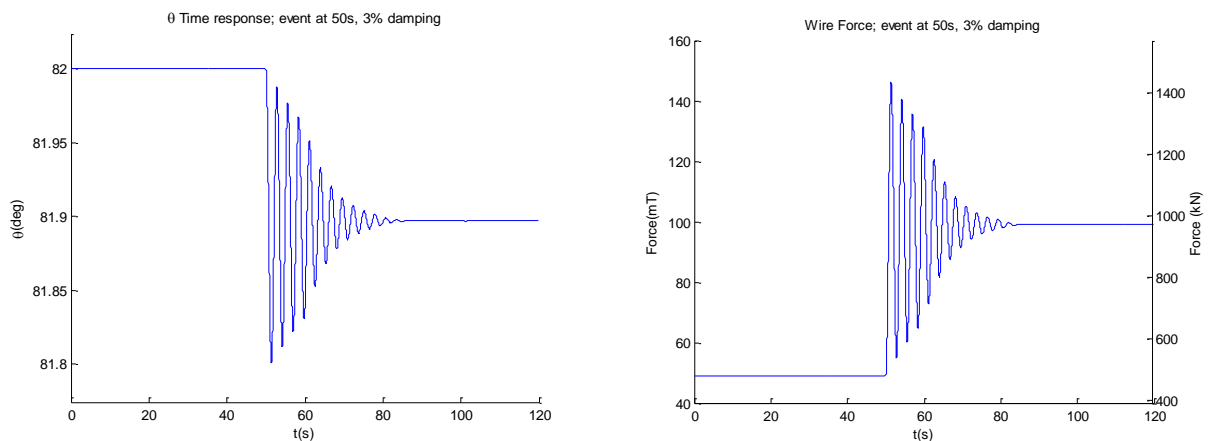


Figure 4.7: Time response and Wire force, load 10 000mt, 82degrees

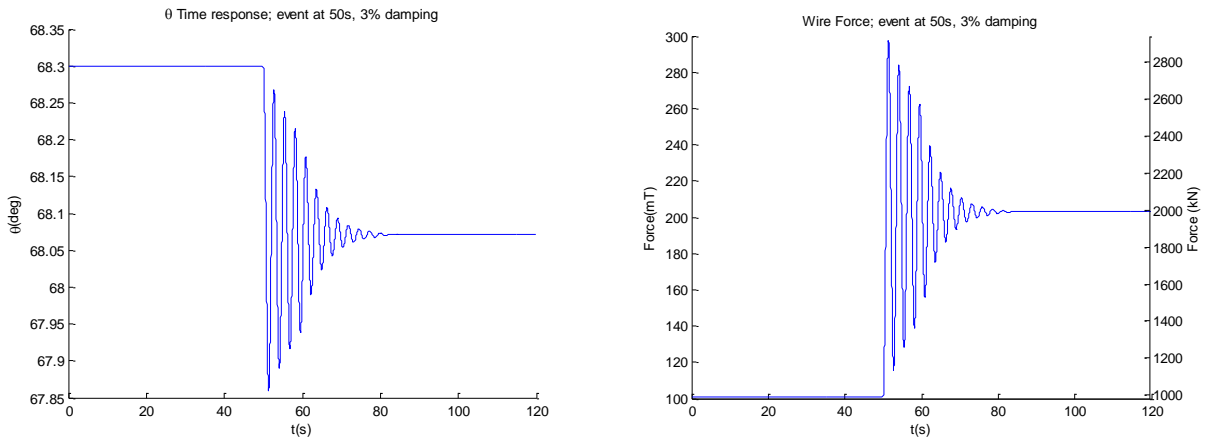


Figure 4.8: Time response and Wire force, load 10000mt, 68.3degrees

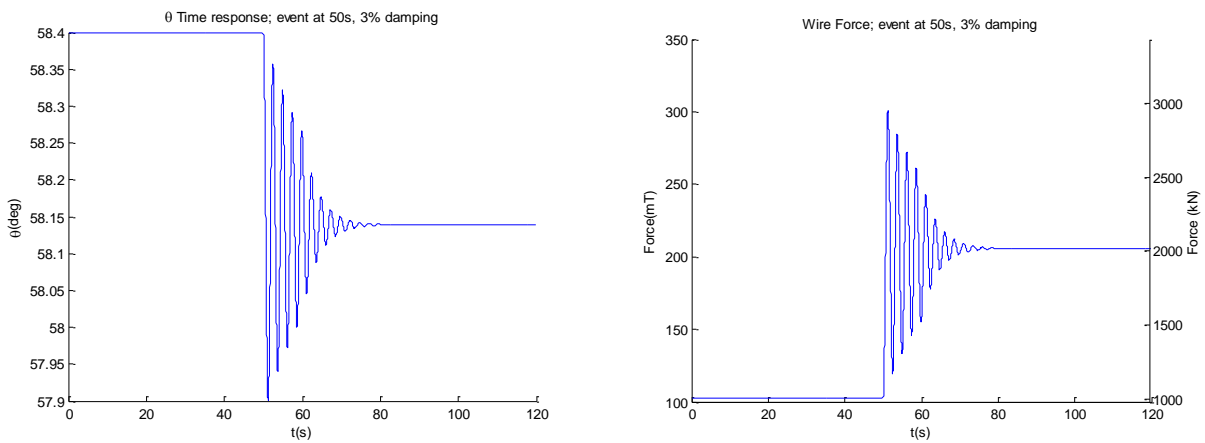


Figure 4.9: Time response and Wire force, load 7000mt, 58.4degrees

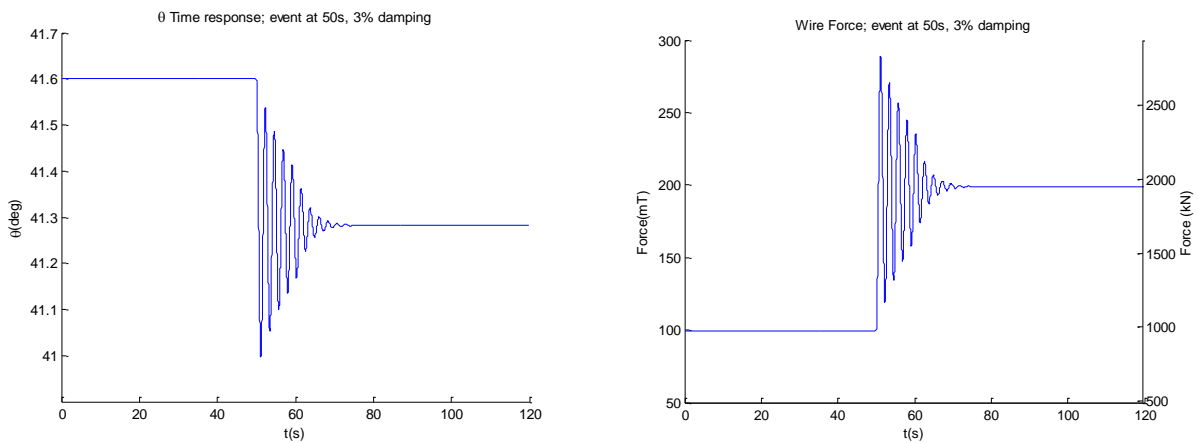


Figure 4.10: Time response and Wire force, load 4000mt, 41.6degrees

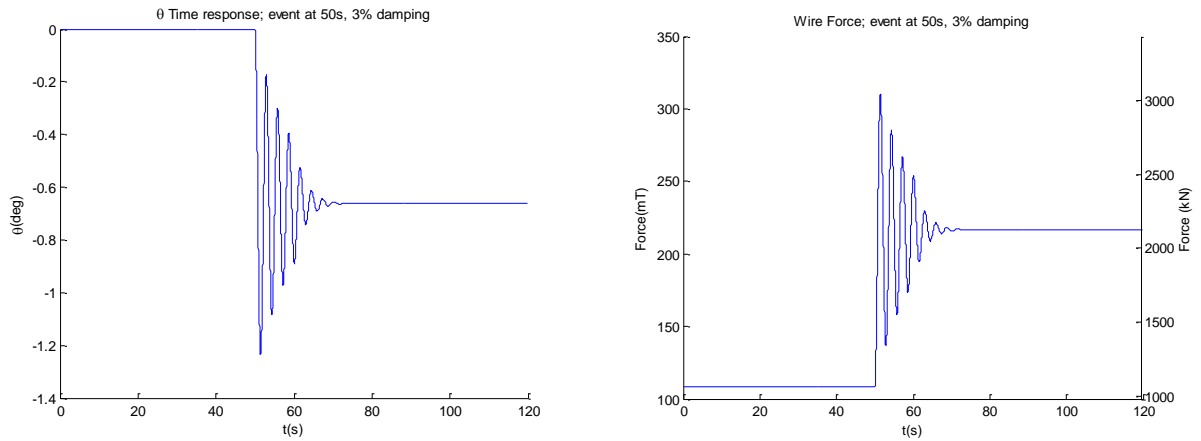


Figure 4.11: Time response and Wire force, load 1588mt, 0degrees

The dynamic factor of the load cases can be calculated with the following equation:

$$factor = \frac{F_{max}}{F_{mean}} \tag{4.22}$$

Table (4.1) shows the dynamic factors per load case.

Table 4.1: Dynamic Factors

Boom angle [°]	Load [mt]	F <sub>max</sub> [mt]	F <sub>static</sub> [mt]	Dynamic Factor
82.0	10 000	146.0	99.1	1.47
68.3	10 000	297.6	203.0	1.47
58.4	7000	300.4	205.8	1.46
41.6	4000	288.3	198.9	1.45
0	1588	309.9	216.7	1.43

This completes the preliminary analysis of the boom hoist failure. Now different effects can be built into the model in order to determine their effects on the system. Chapter 6 will elaborate more on the subject of boom hoist failure analysis.

## 4.6 Main hoist failure

In case of a wire failure, where one of the four wires snaps, there is some free fall before the system reaches equilibrium. The reason for this is the main hoist equalizing system, which connects the four wires to the lifting hook. From Figure (4.12) it can be seen that in case when one of the wires snaps, the block connecting two wires will rotate around its axis, which has the effect that the load will have a free fall. Two different cases can be distinguished; one where one of the inner wires fails, and one where one of the outer wires fails. In case of failure of one of the outer wires, the triangular block will rotate until the two joints are lined up vertically. When one of the inner wires fails, this will lead to less rotation of the block and that results in less free fall.

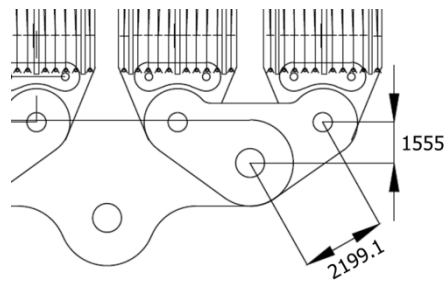


Figure 4.12: Main hoist equalizer, schematic view

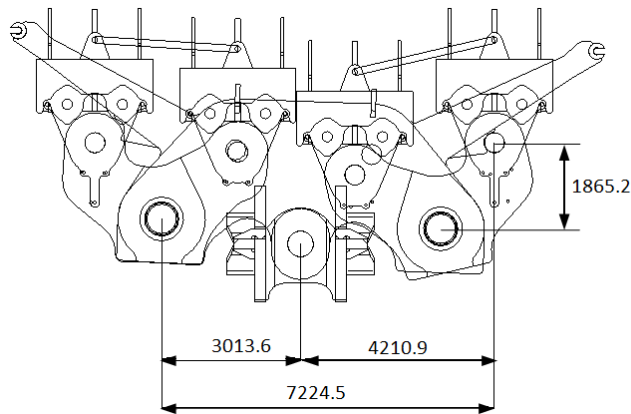


Figure 4.13: Main hoist inner wire failure

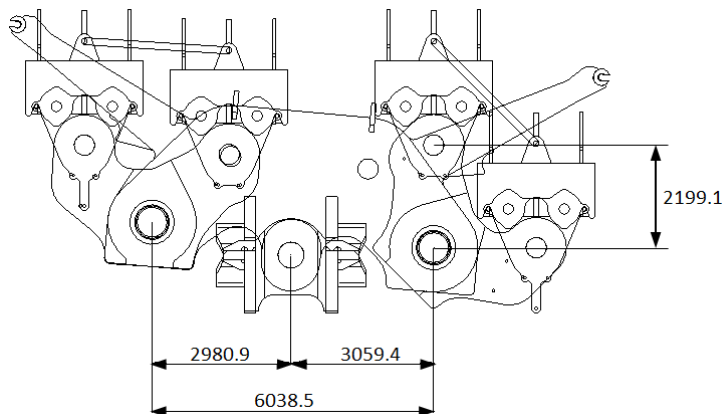


Figure 4.14: Main hoist outer wire failure

The free fall of the load in case of an inner wire failure can be approximated by the following equation:

$$Y_{free} = \frac{1865.2 - 1555}{2} = 155.1 [mm] \quad (4.23)$$

Equation (4.24) shows the free fall of the load for the case when one of the outer wires fails.

$$Y_{free} = \frac{2199.1 - 1555}{2} = 322.05 [mm] \quad (4.24)$$

Using conservation of energy the end speed of the mass can be calculated:

$$\frac{1}{2}mv^2 = mg\Delta h$$

$$v = \sqrt{2g\Delta h} \quad (4.25)$$

$$v_{inner} = \sqrt{2 \cdot 0.155 \cdot 9.81} = 1.74 [m/s]$$

$$v_{outer} = \sqrt{2 \cdot 0.322 \cdot 9.81} = 2.51 [m/s]$$

The first analysis that was carried out is with an initial speed as a result of free fall of the mass, so  $\dot{y}(0) = 1.74/2.51 [m/s]$ . The system has been regarded as a one degree of freedom system, which is depicted in Figure (4.15). The initial length  $L_0$  of the main hoist wires is set at  $10m$ .

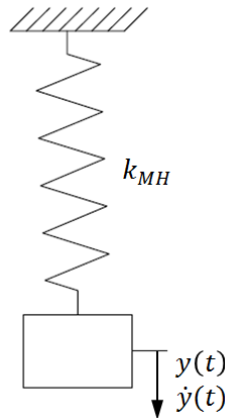


Figure 4.15: Single DoF Main hoist system

As there is a force balance in the main hoist equalizer the force on either side will be half of the total. After wire failure the momentum balance will set according to Figures (4.13) and (4.14). The resulting forces in the remaining wire after wire failure can be found in Table (4.2).

Table 4.2: Resulting forces on the wires after wire failure

	Load Before Wire Failure [mt]	Load After Wire Failure [mt]
Inner Wire Failure	2500	4171.36
Outer Wire Failure	2500	~5000

The force in the remaining wire at the side of wire failure is simulated in this situation. The results can be found in Figure (4.16) and Figure (4.17).

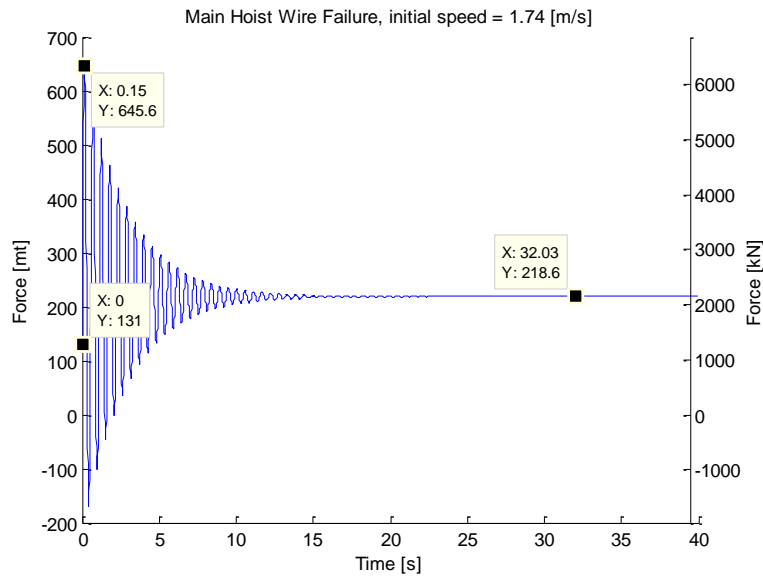


Figure 4.16: Main hoist inner wire failure, force in remaining wire

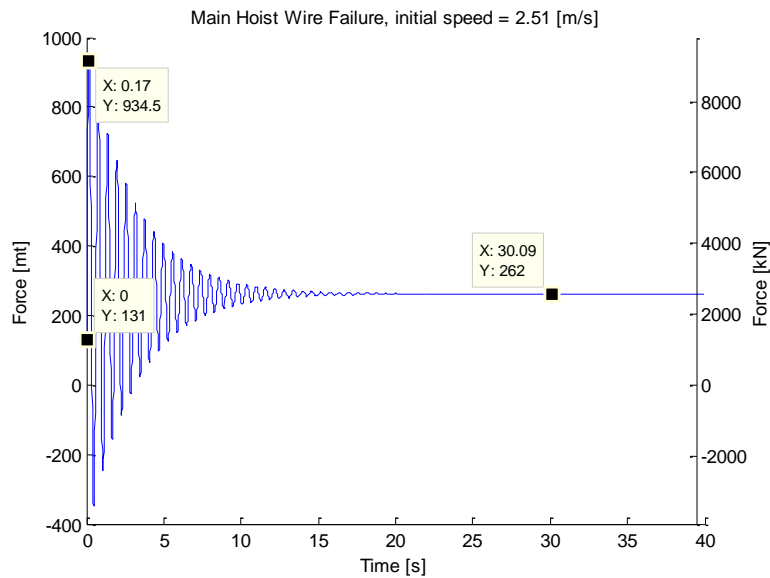


Figure 4.17: Main hoist outer wire failure, force in remaining wire

The breaking strength of the wires is given as 4650 kN. The maximum force that occurs in the wires is:

$$F_{wire} = 934.5 \cdot 9.81 = 9167.45 [kN] > 4650 [kN] \tag{4.26}$$

As can be seen in Equation (4.26) the force in the wire exceeds the breaking force. Therefore the preliminary conclusion can be drawn that a main hoist failure can be a potential catastrophe, with all the wires in the main hoist breaking.

In order to determine the effects of the initial length of the main hoist wire, a series of initial lengths have been inserted into the equation of motions. The results can be found in Figure (4.18).

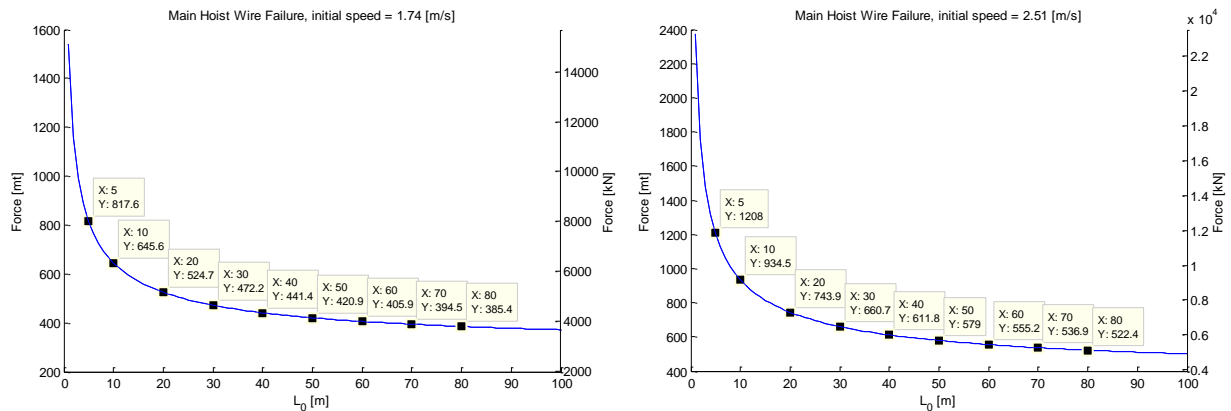


Figure 4.18: Maximum wire force plotted against initial length of the Main hoist wire

Figure (4.18) shows that the influence of initial main hoist wire length is large on the maximum force in the wires. It is unlikely that the short initial lengths ( $<30m$ ) will happen in reality, because the rigging of a 10 000mt structure will need some length in order to create a stable lift.

Another effect that influences the system is damping in the wire. Initially damping for the main hoist wire was set at the same value as for the boom hoist wire (3%), but it turned out that changes in damping have an influence on the outcome of the maximum force in the wire. Figure (4.19) shows the Maximum wire force with a varying damping factor.

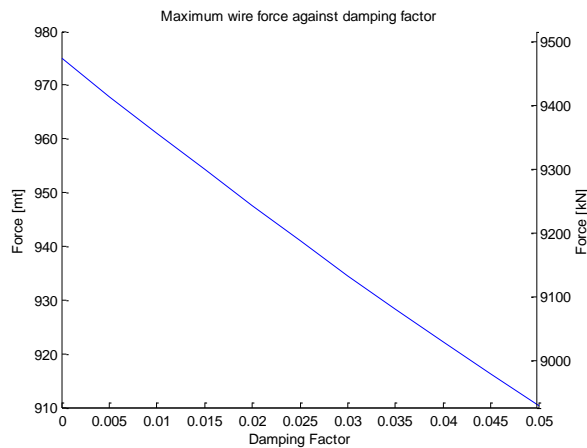


Figure 4.19: Maximum wire force against damping factor,  $v = 2.51$  [m/s]

From the figure the conclusion can be drawn that the influence of the damping factor is low ( $\sim 5\%$ ), therefore the assumption of a damping factor of 3% can be regarded as a valid assumption.

### 4.7 Drop of the load

In this section a drop of the load is simulated. The pretension in the boom hoist wires will cause a movement of the boom. Little research on this subject was performed in the past by Huisman [1]. The goal of this analysis is to gain more insight in the effects of a load loss. Initially the problem was modeled as a single degree of freedom problem according to Figure (4.4). Figures (4.20) – (4.24) show the results of the analysis.

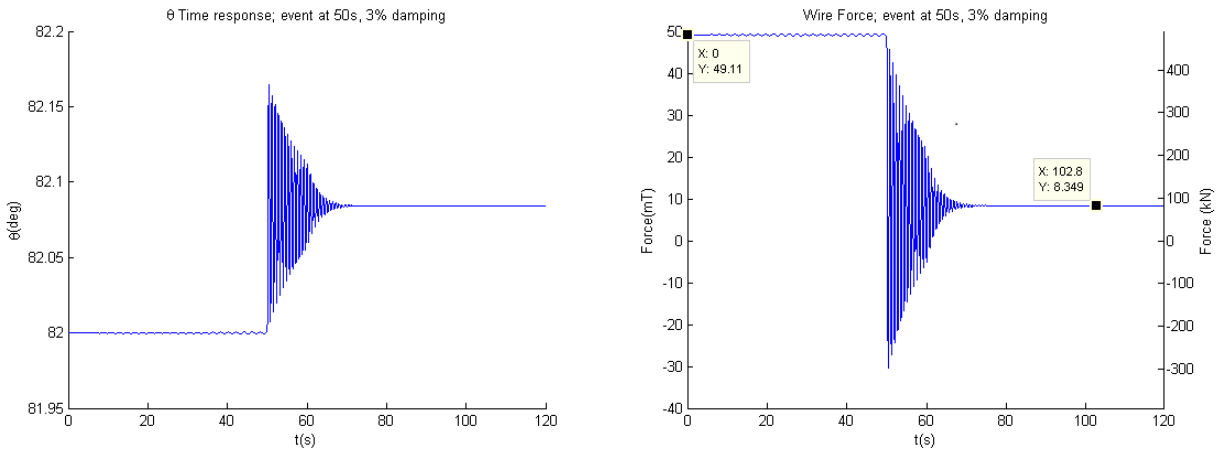


Figure 4.20: Drop of load analysis, 82° boom angle

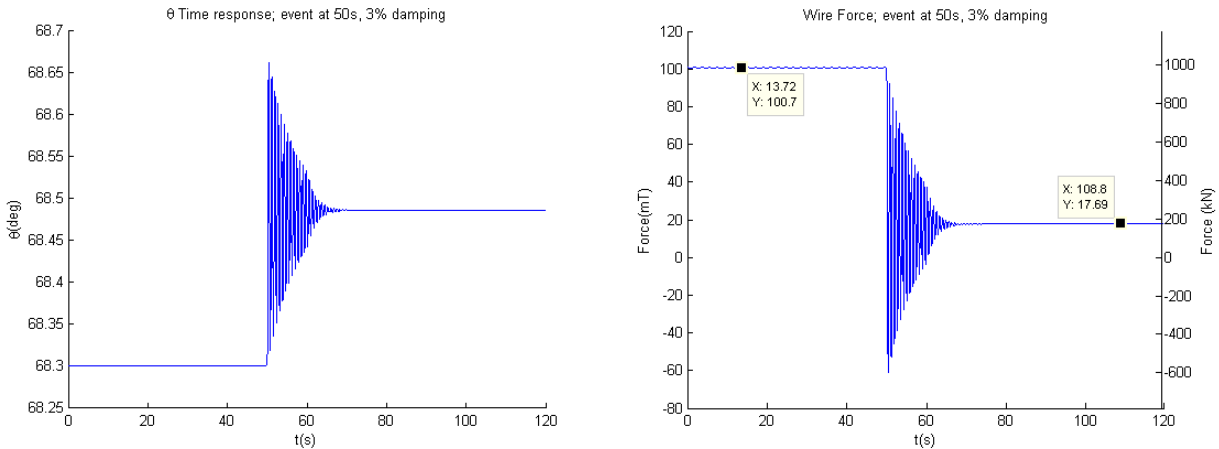


Figure 4.21: Drop of load analysis, 68.3° boom angle

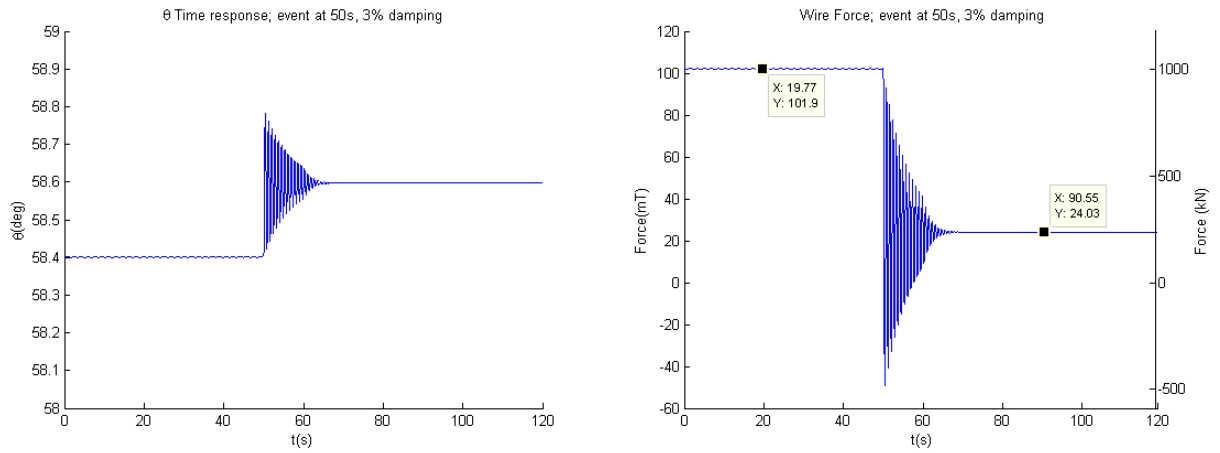


Figure 4.22: Drop of load analysis, 58.4° boom angle

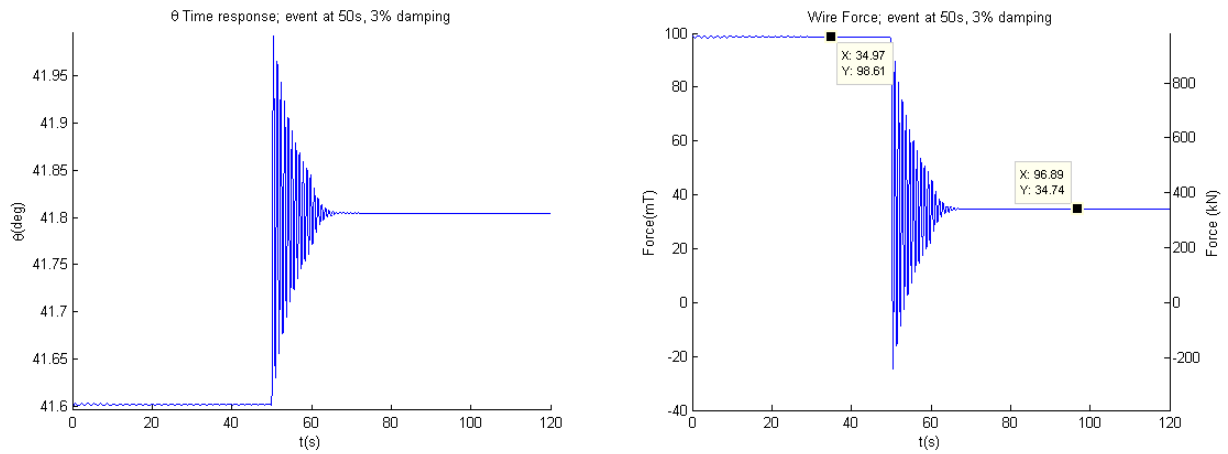


Figure 4.23: Drop of load analysis, 41.6° boom angle

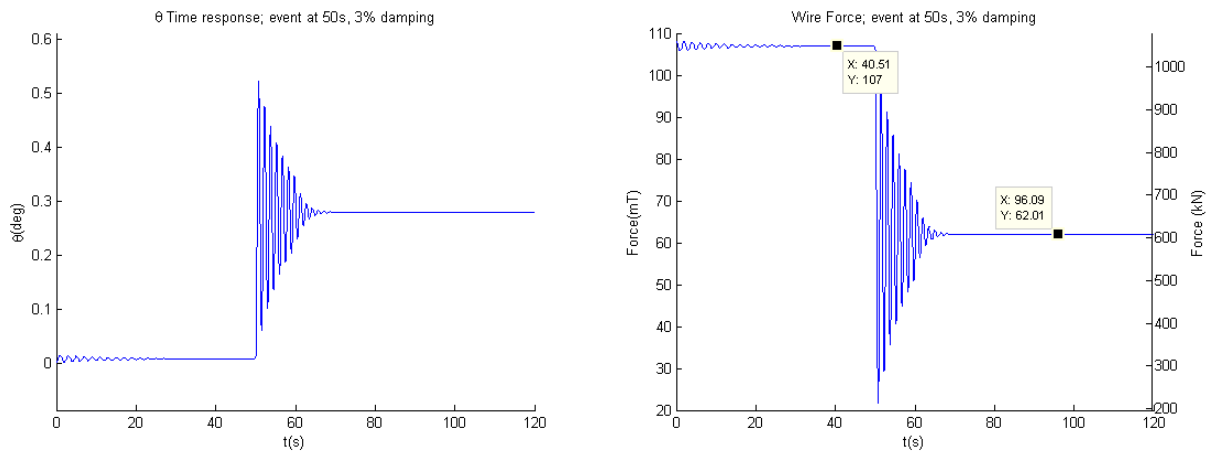


Figure 4.24: Drop of load analysis, 0° boom angle

Some of the figures show a negative wire force after the load loss. In reality this represents a 'slack' wire. Discretizing the cables would provide more insight on the moment that the wires are coming under tension again. Another interesting aspect would be to add the stiffness of the boom. The analysis would show the free vibration of the boom. This could then be compared to an analysis with FEM-software.

### 4.8 Conclusions

An elaboration was given on the Lagrange's equations and how one uses rotation matrices in order to derive the Lagrange's equations. First use of these equations was made in order to do a simplistic analysis of the system. The dynamic factors in case of the boom hoist failure were very close to the factors found in Chapter 2.

In case of wire failure in the main hoist system the stress in the wire will exceed the maximum allowable stress, which leads to failure in the entire system. It was also found that a more detailed analysis of the main hoist equalizer system is required in order to verify the impact speed of the load on the wires.

The case where the load drops out of the crane proved to have the least impact on the boom hoist wire force. For this case it would be more interesting to see how the boom will vibrate after the load has dropped out of the crane. Also the model should be able to represent 'slack' wire.

In the next chapter the Lagrange's equation are used to make a more detailed model of each failure case. Parameter studies will then show which components have considerable influences on the system.

---

## 5 Modeling

---

In this section the total equations of motion are explained for all aspects of the model. However, not all aspects are of interest in all three failure cases. Therefore some additional equations are added to the model, or simplifications are made when possible. These additions and simplifications will also be listed at the end of the chapter. The equations of motion are derived with Lagrange's equations as explained in Section (4.1), in terms of a global coordinate system.

### 5.1 Coordinate system

In order to derive the equations of motion the coordinate systems have to be specified. The pivoting point of the boom is taken as origin for the global coordinate system. Figure (5.1) shows the coordinate system. The position of the load can now be determined as follows:

$$\vec{r}_{load} = \vec{r}_{tip} + [R_{load}]\vec{r}_{MH} \quad (5.1)$$

Where  $[R_{load}]$  is the rotation matrix which transfers the position of the load from a local coordinate system to the global coordinate system. The working principle of rotation matrices is explained in Section (4.2).

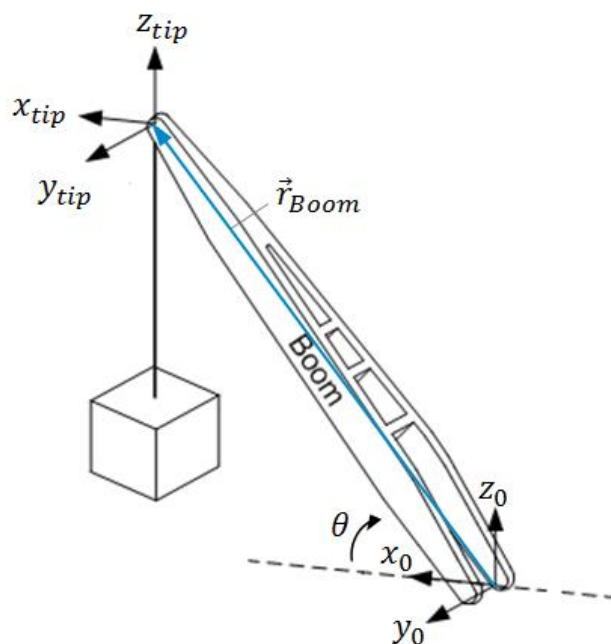


Figure 5.1: Coordinate system (figure courtesy of Z. Dix [2])

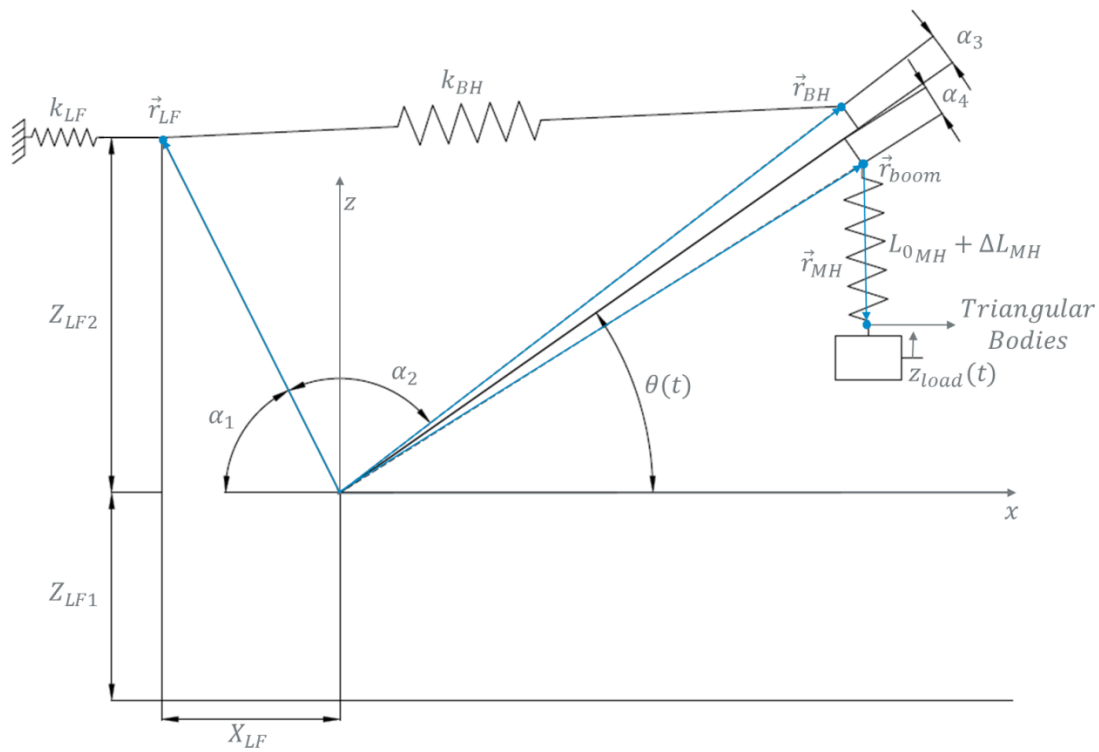


Figure 5.2: Total system

## 5.2 Boom hoist length and luffing frame stiffness

The luffing frame stiffness is implemented as a spring attached to the top of the frame. Its stiffness is determined with ANSYS and can be found in Appendix (B). Figure (5.2) shows the model with the luffing frame stiffness.

Figure (5.3) shows the point  $\vec{r}_{LF}$  of Figure (5.2), the luffing frame stiffness in the direction of the boom hoist wires is determined with Equation (5.2).

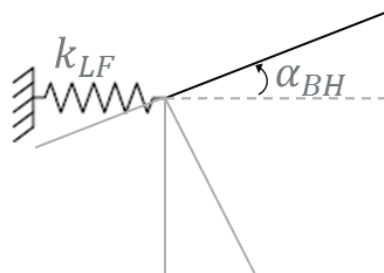


Figure 5.3: Luffing frame equivalent stiffness

$$k_{LF(BH\ direction)} = \frac{k_{LF}}{\cos(\alpha_{BH})} \quad (5.2)$$

The equivalent stiffness of the luffing frame and the boom hoist can be determined as follows:

$$\frac{1}{k_{eq}} = \frac{1}{k_{LF}} + \frac{1}{k_{BH}} \quad (5.3)$$

This makes the determination of the boom hoist stiffness at the given input angle slightly more complicated. Before, an iteration step was required in order to calculate the pretension in the boom hoist wire, to get a system that is in equilibrium at the start of the analysis. As it is necessary to exactly know the force in the boom hoist wires, the rate between the elongation of the equivalent luffing frame spring and the boom hoist wires has to be determined.

As the forces in the springs are equal, the following relation yields:

$$k_{LF}\delta_{LF} = k_{BH}\delta_{BH} = k_{eq}\delta_{eq} \quad (5.4)$$

Rewriting in terms of the elongations:

$$\delta_{LF} = \frac{k_{eq}\delta_{eq}}{k_{LF}} \text{ and } \delta_{BH} = \frac{k_{eq}\delta_{eq}}{k_{BH}} \quad (5.5)$$

With these relations, the iterations of finding the initial length of the boom hoist wire and its stiffness can be performed.

### 5.3 Main hoist system

The triangular bodies can be found in Figure (5.4). These bodies can rotate and translate in  $y$ ,  $z$ -direction. The position of the load can then be expressed in terms of rotation and translation of the triangular bodies together with the rotation of the boom tip.

The equations of motion for the lower block system are determined with Lagrange's equations. The number of degrees of freedom of the system is 6. There are two constraints;  $C_1$  and  $C_2$ . This makes the number of generalized coordinates ( $q_i$ ) as follows:

$$i = n - m \quad (5.6)$$

$$i = 9 - 4 = 5$$

Where:

$n$  = total number of degrees of freedom for all bodies;

$m$  = number of constraints.

This means that there are five generalized coordinates required in order to properly describe the system. One is free to choose the generalized coordinates in a way one sees fit for the problem. For this problem, the following generalized coordinates are used:  $(\varphi_1, \varphi_2, \varphi_3, z_3, y_3)$ . All other coordinates can be expressed in terms of these coordinates.

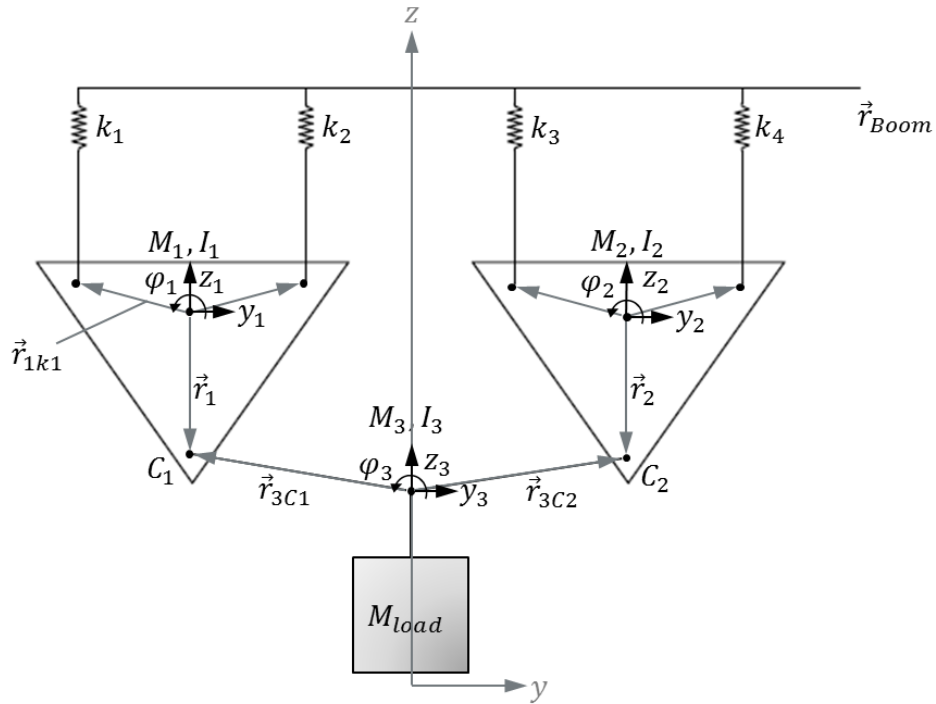


Figure 5.4: Lower block system

The two constraints  $C_1$  and  $C_2$  form the connection between the three bodies of the main hoist lower block. The third body is not shown in Figure (5.4), only the center of gravity and its connection with  $C_1, C_2$  and the load.

The first step is to express the position of  $C_1$  and  $C_2$  through body 1 and 2:

$$C_1 = \begin{bmatrix} y_1 \\ z_1 \end{bmatrix} + R(\varphi_1)\vec{r}_1 \tag{5.7}$$

$$C_2 = \begin{bmatrix} y_2 \\ z_2 \end{bmatrix} + R(\varphi_2)\vec{r}_2$$

Where:

$$R(\gamma) = \begin{bmatrix} \cos(\gamma) & -\sin(\gamma) \\ \sin(\gamma) & \cos(\gamma) \end{bmatrix} \tag{5.8}$$

For a clockwise rotation of the axis system.

The next step is expressing position C1 and C2 through body 3:

$$\begin{aligned} C_1 &= \begin{bmatrix} y_3 \\ z_3 \end{bmatrix} + R(\varphi_3)\vec{r}_{3C1} \\ C_2 &= \begin{bmatrix} y_3 \\ z_3 \end{bmatrix} + R(\varphi_3)\vec{r}_{3C2} \end{aligned} \quad (5.9)$$

Combining Equation (5.7) and (5.9) results in the expression of  $(y_1, z_1, y_2, z_2)$  in terms of generalized coordinates:

$$\begin{aligned} \begin{bmatrix} y_1 \\ z_1 \end{bmatrix} &= \begin{bmatrix} y_3 \\ z_3 \end{bmatrix} + R(\varphi_3)\vec{r}_{3C1} - R(\varphi_1)\vec{r}_1 \\ \begin{bmatrix} y_2 \\ z_2 \end{bmatrix} &= \begin{bmatrix} y_3 \\ z_3 \end{bmatrix} + R(\varphi_3)\vec{r}_{3C2} - R(\varphi_2)\vec{r}_2 \end{aligned} \quad (5.10)$$

The total kinetic energy of the system can then be expressed as:

$$\begin{aligned} T &= \frac{1}{2}M_1 \left| \begin{bmatrix} \dot{y}_1 \\ \dot{z}_1 \end{bmatrix} \right|^2 + \frac{1}{2}I_1\dot{\varphi}_1^2 + \frac{1}{2}M_2 \left| \begin{bmatrix} \dot{y}_2 \\ \dot{z}_2 \end{bmatrix} \right|^2 + \frac{1}{2}I_2\dot{\varphi}_2^2 + \frac{1}{2}M_3 \left| \begin{bmatrix} \dot{y}_3 \\ \dot{z}_3 \end{bmatrix} \right|^2 + \frac{1}{2}I_3\dot{\varphi}_3^2 + \\ &\quad \frac{1}{2}M_{load} \left| \begin{bmatrix} \dot{y}_3 \\ \dot{z}_3 \end{bmatrix} \right|^2 \end{aligned} \quad (5.11)$$

In Equation (5.11),  $y_1, z_1, y_2, z_2$  will be substituted for the equations from Equation (5.10).

The potential energy of the system consists of the gravity components of the bodies and the load, and consists of the energy in the main hoist wires. The main hoist wire is modeled as a spring, thus the energy in the wires can be determined with:

$$V_{MH} = \frac{1}{2} \cdot k_i \cdot \left( \left| \vec{r}_{Boom_{ki}} - \left( \begin{bmatrix} y_i \\ z_i \end{bmatrix} + R(\varphi_i)\vec{r}_{i_{ki}} \right) \right| - L_0 \right)^2 \quad (5.12)$$

Where:

$$\vec{r}_{Boom_{ki}} = \begin{bmatrix} y_{b,i} \\ L_{Boom}\sin(\theta - \alpha_4) \end{bmatrix}$$

Together with the potential energy due to gravity this results in the total potential energy of the system:

$$V = M_1gz_1 + M_2gz_2 + M_3gz_3 + M_{load} \cdot gz_3 + E_{wires} \quad (5.13)$$

Further derivation is carried out with a Symbolic Math Toolbox in Matlab, called MuPAD. Because the equations become lengthier in the process, they will not be shown in the report anymore.

## 5.4 Boom stiffness

The boom stiffness can be modeled by means of Rigid Finite Element Method (Wittbrott *et al.* [12]). The boom is then split up in a number of rigid elements connected by massless spring elements, see Figure (5.5). Then, with Lagrange's equations it is possible to derive the equations of motions for the rigid finite elements (rfe).

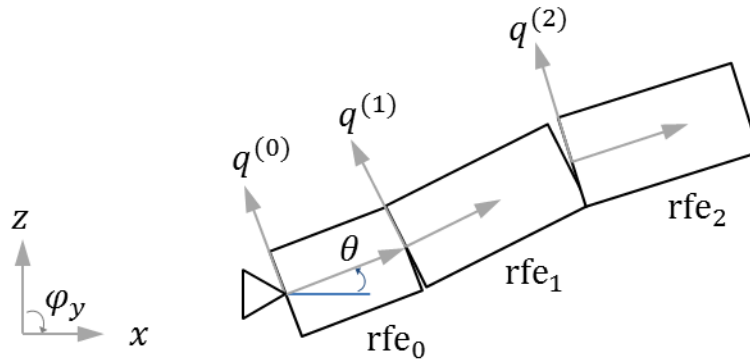


Figure 5.5: Discretizing of the boom

The first element is added to the crane house and does not have its own generalized coordinates. It has a rotational connection with the boom angle ( $\theta$ ) as input. The succeeding elements can then be expressed as vectors with respect to its predecessors. With these vectors representing the locations of the elements, the equations of motion can be determined with Lagrange's equations. This, however, does require some elaborate matrix-transformations. Therefore these transformations will not be shown in this report.

Also it was found in literature that discretizing the boom has only minor influence, research by Krukowski [10] shows that the influence of modeling the boom as a flexible element has only minor influence on the results. It states that *'for preliminary calculations or for test purposes, the flexibility of the boom can be omitted'*.<sup>1</sup> As for this thesis the focus lays on the reeving system and reducing the force in the wires, the boom stiffness is neglected. If, however, one is interested in implementing this method in the model, (Wittbrott *et al.* [12]) offers an excellent guide for this method.

## 5.5 Stress wave effects

When the event of a wire failure occurs, the wire becomes slack for a short period of time. After this period, the wire comes back under tension. This sudden tension will generate a stress wave which will

<sup>1</sup> Krukowski *et al.*, "The Influence of a Shock Absorber on Dynamics of an Offshore Pedestal Crane", Journal of Theoretical and Applied Mechanics, Volume 50 No. 4, 2012, p. 965.

propagate through the wire. The wave propagation phenomenon can be explained on the analogy of Figure (5.6):

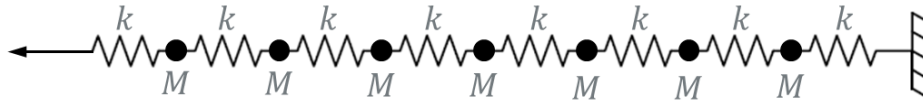


**Figure 5.6: Wire expressed as mass spring elements**

In Figure (5.6) a wire model is composed of discrete masses and springs. The disturbance, which is depicted by the arrow on the left, causes the first mass to move. This movement will be transmitted to the next mass by the springs. At this point the most right mass has not yet 'felt' the movement of the left masses. The displacements of the masses and its transmissions will generate a wave, traveling from left to right.

The stress generated by the propagating wave can be calculated using Equation (5.14) [13].

$$\sigma = \rho CV(x, t) \quad (5.14)$$

Where

$\rho$  = mass density;

$V$  = speed of a particle along the rod;

$C$  = wave speed, given by:

$$C = \sqrt{\frac{E}{\rho}} \quad (5.15)$$

At the boundary the wave is reflected. The reflection of a wave is dependent on the boundary conditions. For this case the wave is reflected at the fixed end with no change in sign. Effectively, the stress in the cable becomes double the stress of the propagated wave; this is shown in Equation (5.16).

$$\sigma_{max} = 2\rho CV(x, t) \quad (5.16)$$

In order to determine whether there are stress load effects present in case of boom hoist failure, the boom hoist wire has to be discretized, see Figure (5.7). The boom hoist wire is divided into sections, each represented by a mass and a spring element. The mass elements have two degrees of freedom; one in x-direction and one in z-direction. The most left spring is connected to the luffing frame and the most right spring to the boom hoist sheaves. The force in each spring section is then calculated with the locations of the masses. For a discretization with  $N$  wires, the stiffness and mass are calculated as follows:

$$d = \frac{L_{wire}}{N + 1}$$

$$m = \rho_{wire} A_{wire} d$$

$$k = \frac{EA}{d}$$
(5.17)

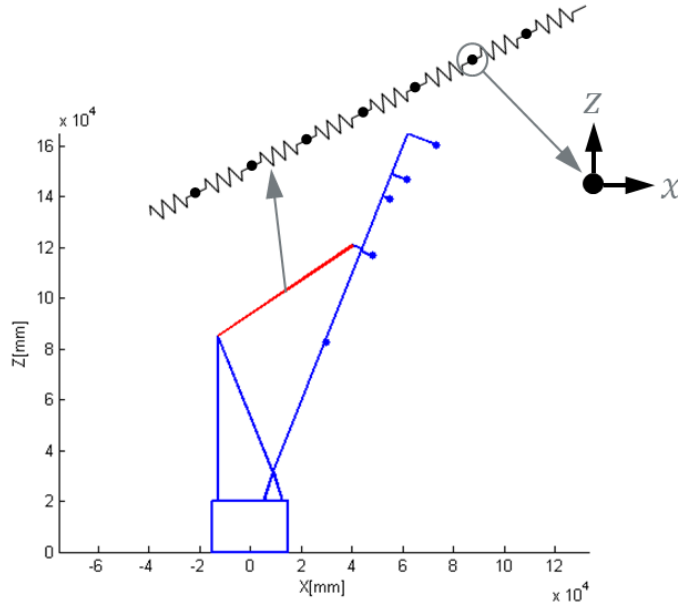


Figure 5.7: Boom Hoist wire discretization

The equations of motions are defined by the following equations:

$$m_1 \ddot{x}_1 = \sum F_x$$

$$m_1 \ddot{z}_1 = \sum F_z$$
(5.18)

Where the force in the springs is determined with the following equations:

$$\Delta L = \sqrt{(X_2 - X_1)^2 + (Z_2 - Z_1)^2} - d_{element}$$

$$F = \Delta L \cdot k$$

$$\vec{r} = \frac{1}{\Delta L} \begin{bmatrix} (X_2 - X_1) \\ (Z_2 - Z_1) \end{bmatrix}$$

$$\vec{F} = F \cdot \vec{r}$$
(5.19)

The same relation holds for the damping in the wire:

$$\frac{dL}{dt} = \sqrt{(\dot{X}_2 - \dot{X}_1)^2 + (\dot{Z}_2 - \dot{Z}_1)^2}$$
(5.20)

$$F = \frac{dL}{dt} \cdot c$$

$$\vec{r} = \frac{1}{\frac{dL}{dt}} \begin{bmatrix} (\dot{X}_2 - \dot{X}_1) \\ (\dot{Z}_2 - \dot{Z}_1) \end{bmatrix}$$

$$\vec{F} = F \cdot \vec{r}$$

## 5.6 Specifics for each failure case

Not all aspects of the model are required for all failure cases, e.g. for the boom hoist failure and drop of the load the main hoist system is not of any influence. It is then arguable if it would make any difference to leave the system in the equations or take it out of the equations. For this research the choice is made to create three separate models, one for each failure case with specific details for that failure case. To clarify which components are used in the models, a table is set up; this is shown in Table (5.1).

Table 5.1: Specifics per failure case

	<b>Luffing Frame</b>	<b>Main Hoist Wire</b>	<b>Main Hoist System</b>	<b>Boom Stiffness</b>	<b>Wire Discretization</b>
Boom Hoist Failure	X	X	-	-	X
Main Hoist Failure	X	X	X	-	-
Drop of Load	X	X	-	-	X

For the boom hoist failure and drop of the load the same model is used, hence the specific details are the same.



---

## 6 Boom hoist failure analysis

---

In Section (4.5) a simplified boom hoist failure analysis was performed. There are several components in the system that could influence the outcome of the dynamic analysis. In this section the various components are implemented in the analysis and their effects will be determined. The components that are regarded are:

- Effect of luffing frame stiffness;
- Effect of pivot friction;
- Effect of main hoist length;
- Effect of stress wave.

The base model that is used consists of a two degree of freedom system, with one being the boom angle, and one the vertical displacement of the load, as can be seen in Figure (5.2). All analyses are carried out with a boom angle of  $68.3\text{ degrees}$ , and a load of  $10\,000\text{ mt}$ .

### 6.1 Effect of luffing frame stiffness

In Section (5.2) the luffing frame stiffness was combined with the boom hoist wire, this introduces some complications when trying to extract the force in the boom hoist wire from the system. Therefore an additional degree of freedom is added to the system to allow for movement of the luffing frame in x-direction. The new system is shown in Figure (6.1).

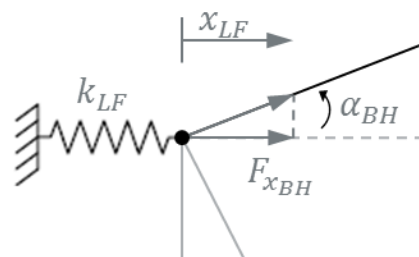


**Figure 6.1: New approach to model luffing frame stiffness**

The results of the analysis are shown in Figure (6.2) and (6.3). From Figure (6.3) it can be obtained that the peak of the force is delayed with luffing frame stiffness compared to the peak force without luffing frame stiffness. Also the peak force obtained with luffing frame is a little lower; however, this effect is not significant.

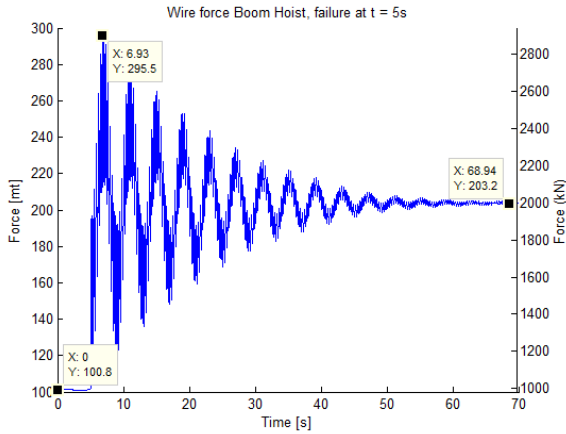


Figure 6.2: Wire force boom Hoist, with luffing frame stiffness from ANSYS

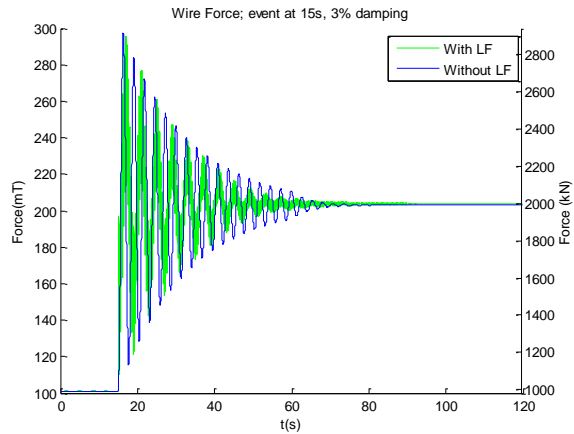


Figure 6.3: Boom Hoist wire force, with and without luffing frame stiffness

Although the stiffness for the luffing frame is obtained from an ANSYS analysis and is therefore likely to be accurate, there might be some derivations in the stiffness in reality. Also it is interesting to see the influence of changing luffing frame stiffness on the dynamic factor. Figure (6.4) and (6.5) show the maximum force and dynamic factor against the luffing frame stiffness. As would be expected, the maximum force in the boom hoist wire reduces with lower luffing frame stiffness.

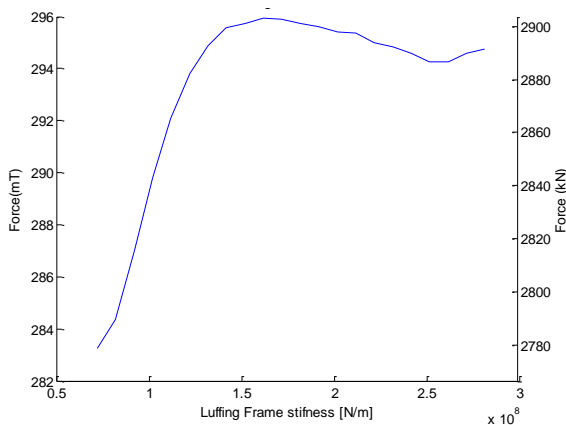


Figure 6.4: Maximum wire force against luffing frame stiffness

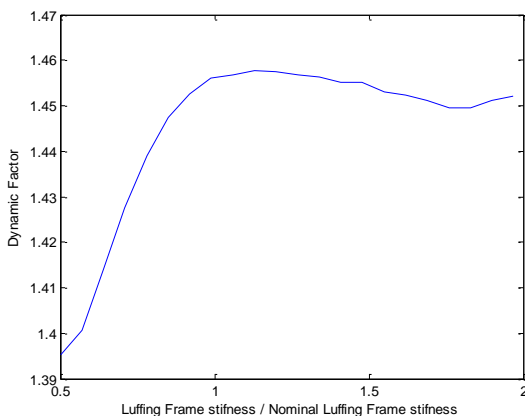


Figure 6.5: Dynamic factor against luffing frame stiffness

## 6.2 Effect of pivot friction

The connection of the boom to the crane house is created with a bearing; this bearing will generate some friction when the boom is rotating. The friction generated by the bearing is a function of the friction coefficient  $\mu$  and the axial force of the boom, see Figure (6.6). The moment created by the friction force will always be directed opposite to the rotational velocity of the boom.

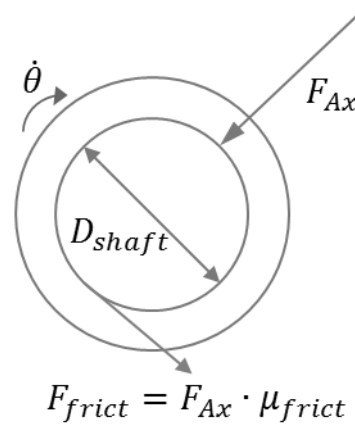


Figure 6.6: Pivot Friction

The friction coefficient is assumed to be 0.15 (Appendix (B): Bearing material selection) for this case, but in order to get insight in the effect of changes in friction coefficient; a plot is created with the coefficient ranging from 0-1. Figure (6.7) shows the maximum force in the boom hoist wire against the friction coefficient and Figure (6.8) expresses the maximum force as dynamic factor. It can be concluded that the influence of friction in the pivot on the system is low, for a friction coefficient of 0.15 the effect is negligible.

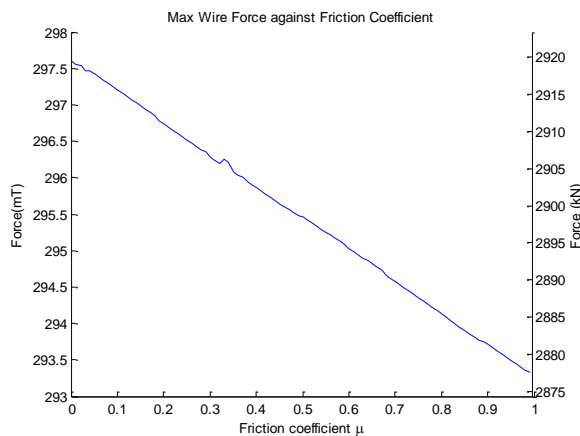


Figure 6.7: Maximum force in the wire against friction coefficient

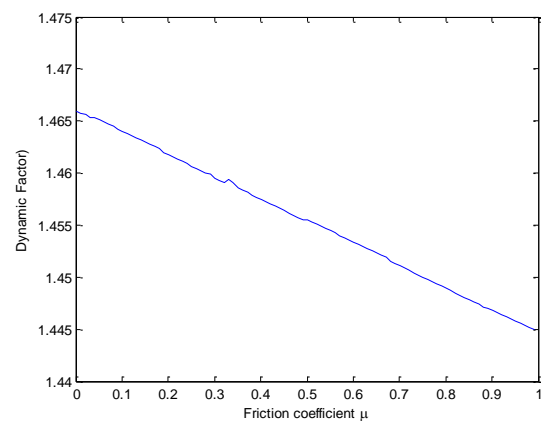
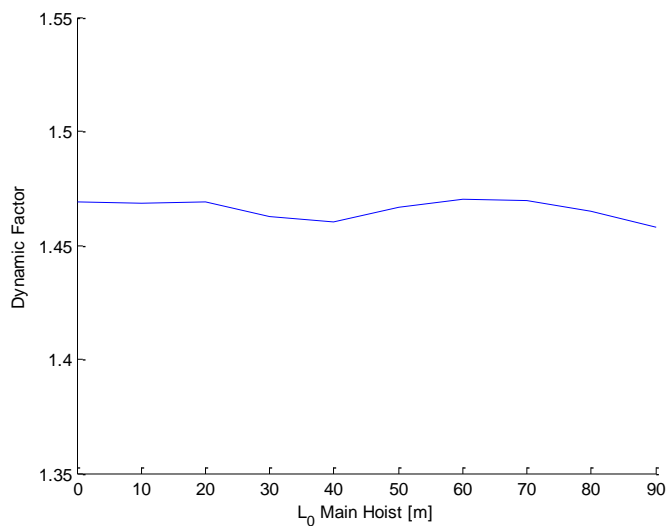


Figure 6.8: Dynamic factor against friction coefficient

### 6.3 Effect of Main hoist length

When the boom hoist wire fails, the load will drop. The movement of the load will lead to an elongation of the main hoist wire. This elongation combined with the damping in the main hoist wire might have a reducing effect on the maximum load in the boom hoist wire. As the stiffness changes over the length of the main hoist wires, a series of simulations were run with different initial main hoist lengths. The results of these simulations can be found in Figure (6.9).



**Figure 6.9: Dynamic factor [Dynamic/Static(after failure)] against varying MH length**

Figure (6.9) shows no clear relation in main hoist length versus dynamic factor. The difference remains small so there is no significant influence. One might expect a decreasing line with respect to the main hoist length, however this is not the case. The natural period of the system changes over length of the main hoist system, this might cause the fluctuations in dynamic factor.

## 6.4 Stress wave effect

When a shock load occurs on a system, often shock load effects are present. The stress wave 'travels' through the wire from the location where the shock is introduced to the fixed point of the wire. At this point the stress wave is reflected, which leads to a doubling of the stress wave stress. To be able to 'see' this stress wave, the wire is split up into multiple mass spring elements. Each of the elements is able to move in X – and Z – direction. A more detailed description of the stress wave effect can be found in Section (5.5).

For the case shown in the report, the wire is split up into 20 mass elements. Figure (6.10) shows the force in the spring element closest to the luffing frame. If there are stress wave effects present, one would expect an increase in wire force close to the luffing frame. This effect however, is not witnessed in Figure (6.10). The force in the wire close to the luffing frame is not different than the force in the element closest to the boom, see Figure (6.11). Also, the time instant at which the peak force is present,  $t = 6.94s$ , does not differ from the two elements. A reasonable explanation for the absence of a stress wave is that the wire is already under high pretension when the load is carried by the two boom hoist wires. At the moment of failure the load is directly connected to the boom, so the increase of velocity of the load is directly transferred to the wire. Therefore no stress wave effects are witnessed in this system.

Note that the absolute value of the force is lower than the forces previously found, this is not an effect of the discretization of the wire. The luffing frame stiffness is also included in this model, which causes a little reduction of the maximum force, and due to the modeling of the wire the damping of the wire is slightly larger, which also reduces the maximum force.

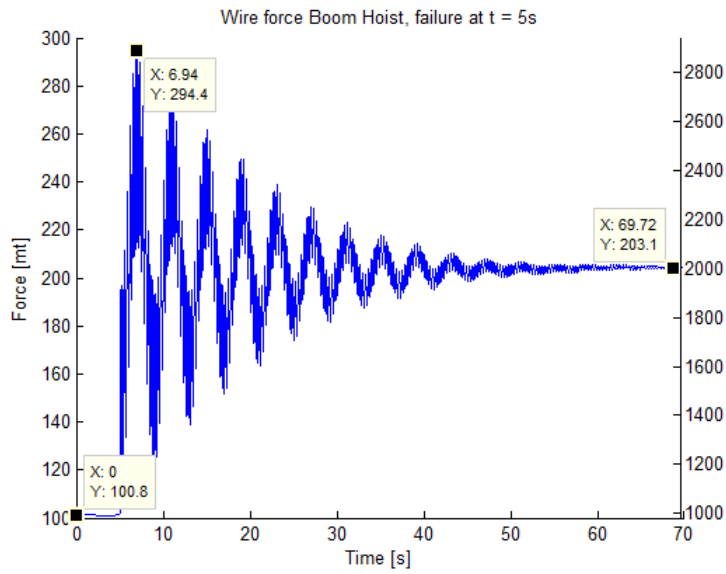


Figure 6.10: Wire force in element closest to Luffing Frame

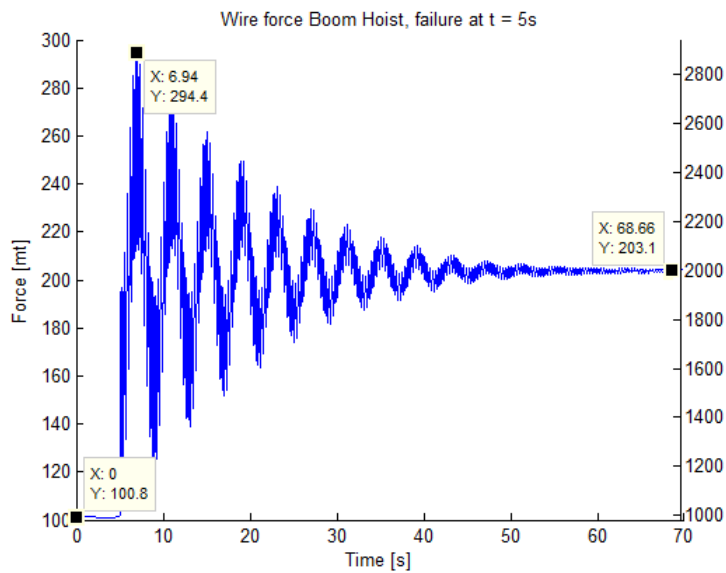


Figure 6.11: Wire force in element closest to the boom

## 6.5 Conclusions

For the case of boom hoist failure, different parameters have been analyzed. As a base case the maximum outreach with maximum load was used, this is 10 000mt at 68.3degrees. The results of the various analyses can be found in Table (6.1). From these results the conclusion can be drawn that none of the investigated parameters have significant influence on the outcome of the dynamic factor. Therefore it can be concluded that independent of any variables, the dynamic factor in case of boom hoist failure is 1.47. This also validates the results of the preliminary analysis from Chapter 2. This also implies that, when a reduction of the dynamic factor is required, a subsystem will need to be designed and implemented into the model. The implementation of such a system will be further investigated in Chapter 9.

**Table 6.1: Summary of parametric study**

<b>Parameter</b>	<b>Value Parameter</b>	<b>Unit Parameter</b>	<b>Uncertainty Parameter [%]</b>	<b>Influence [%]</b>	<b>Max Force [mt]</b>	<b>Range Dynamic Factor</b>
Nominal	-	-	-	-	297.6	1.47
Luffing frame stiffness	143e3	[kN/m]	10	<1	295.5	1.45-1.46
Pivot friction	0.15	-	10	<1	297	1.46-1.465
Main hoist length	30-80	[m]	-	<1	-	1.45-1.46
Stress wave effect	-	-	-	-	-	-



---

# 7 Main hoist failure analysis

---

Section (4.6) only covers a simplified analysis of the main hoist failure case. The equations of motions have been derived in Section (5.3). In this section a more in depth analysis is performed on the main hoist case. The lower block system is analyzed, which results in a different impact speed of the load. Other effects that will be investigated include:

- Detailed analysis of the free fall of the load
- Effect of main hoist length on the maximum force
- Stress wave through the main hoist wire

The section will be concluded with a summary of the parametric study carried out on the different factors that influence the outcome of the dynamic analysis.

## 7.1 Detailed analysis of the free fall of the load

As explained in Section (4.6), two cases of main hoist failure can be distinguished; inner and outer failure. Both cases are analyzed in this chapter. If not stated otherwise, the values that are used for the analysis are:

**Table 7.1: Variables used in analysis**

	<b>Units</b>	<b>Symbol</b>	<b>Value</b>
Boom angle	[°]	$\theta$	68.3
Main hoist initial length	[m]	$L_{0MH}$	10
Load	[mt]	-	10 000

As stated before, the equations of motions were derived in Section (5.3). A depiction of the model can be found in Appendix D, together with a concise validation of the model. This validation is carried out by analyzing the equilibrium positions of the system after wire failure.

### 7.1.1 Outer wire failure

The outer wire failure case is the most governing failure case for the system. The load will have a certain free fall path in which it will accumulate speed, which results in a high impact on the remaining main hoist wire. Figure (7.1) shows the force on the inner wire before and after wire failure, which occurs at  $t = 3$ .

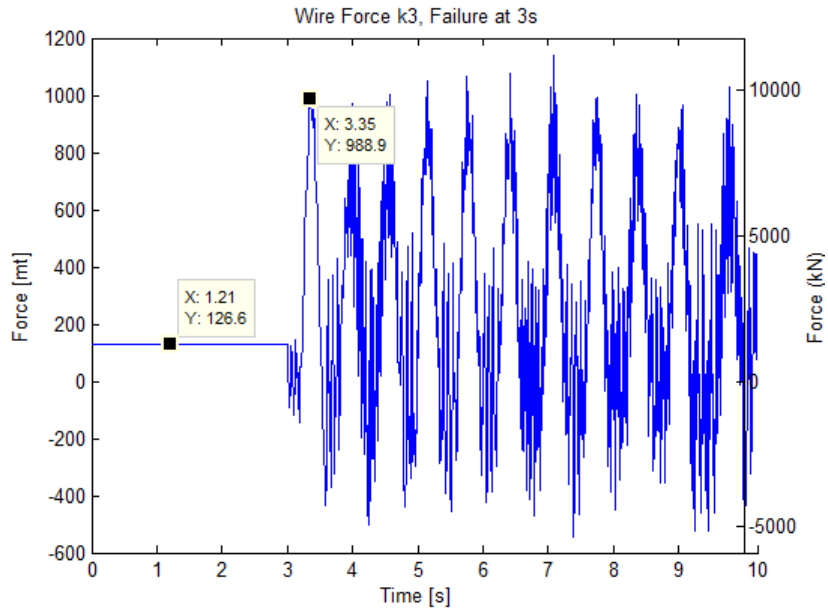


Figure 7.1: Outer wire failure, Force on the inner wire

One thing that can be obtained from Figure (7.1) is that the force gets negative before it reaches its peak at  $t = 3.35$ . This physical explanation for this is that the triangular body, to which the wires are connected, rotates faster than the load falls down. However, in reality a negative force (compression) in a wire is impossible. The term that is used for a wire that is not under tension is 'slack'. In Figure (7.2) the model is altered in such a way that the stiffness of the spring is factored with  $1/100$  when the elongation becomes negative. A value of 0 for the stiffness leads to numeric instability of the system, hence the factored value.

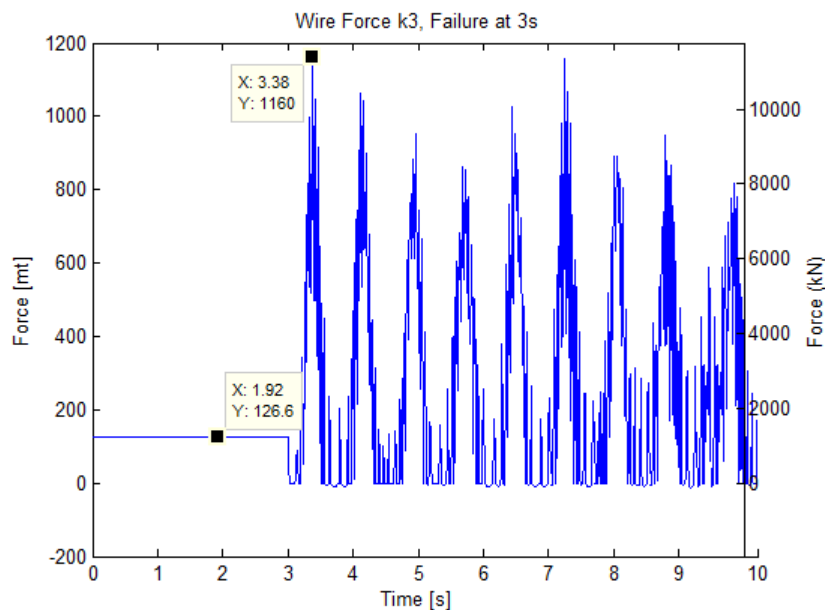


Figure 7.2: Outer wire failure, Force on the inner wire

As expected the peak force in Figure (7.2) exceeds the force in Figure (7.1) because the free fall path of the load increases. Both the force obtained in Figure (7.1) and in Figure (7.2) lie within the same order of magnitude as the force obtained in Section (4.6).

The next step in modeling the system is adding the boom hoist stiffness and the luffing frame stiffness to the system. Up till now, the boom tip position has been taken as a rigid point with respect to time. However, the impact of the dropping load will most likely cause a little lowering of the boom, which will result in a lower maximum force on the main hoist wires after failure.

Figure (7.3) shows the results of the main hoist failure analysis with the boom stiffness and luffing frame stiffness included in the model. As expected the peak force at  $t = 3.37$  is reduced due to the lowering of the boom.

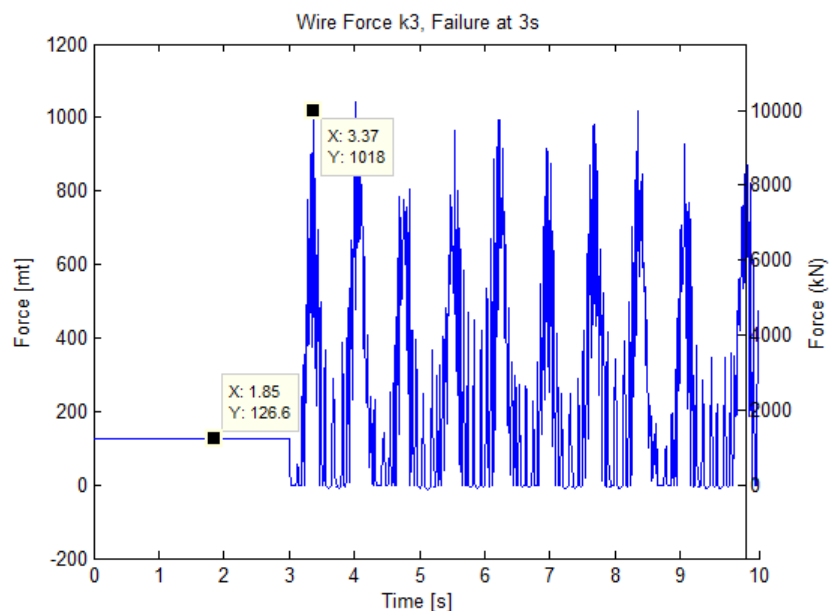


Figure 7.3: Outer wire failure, Force on the inner wire

The final step in completion of the model is adding damping to the system. All previous analysis where carried out without damping in the system. There are several mechanisms in which damping occur;

- Elongation of the wire (friction in the wire);
- Friction in the bearings of the triangles;
- Friction in the bearing between the transverse body and the hook;
- Friction in the bearing of the pivot point of the boom;
- Sheave friction and rope bending.

The damping is added to the system as a viscous damping, with the damping factor taken as a percentage of the critical damping of the system. For reference see Equation (4.17 – 4.21).

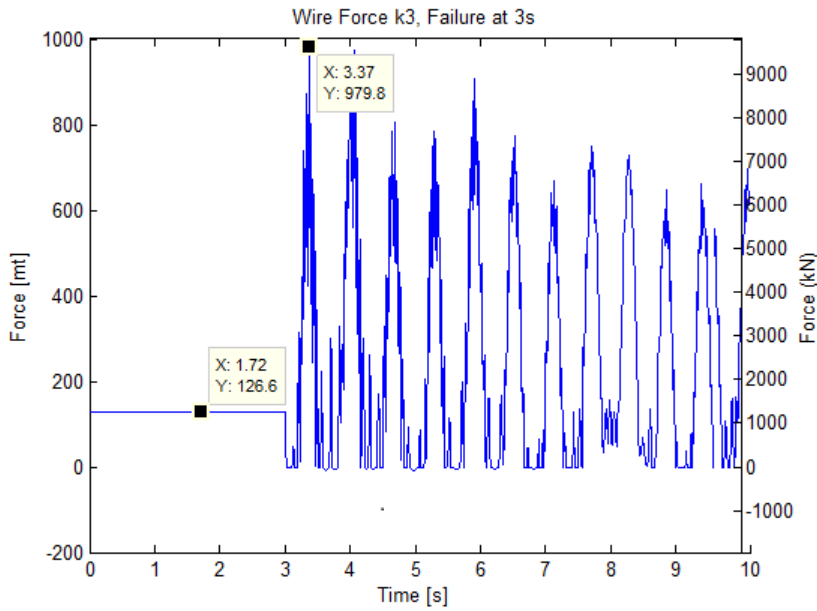


Figure 7.4: Wire force with 1% damping

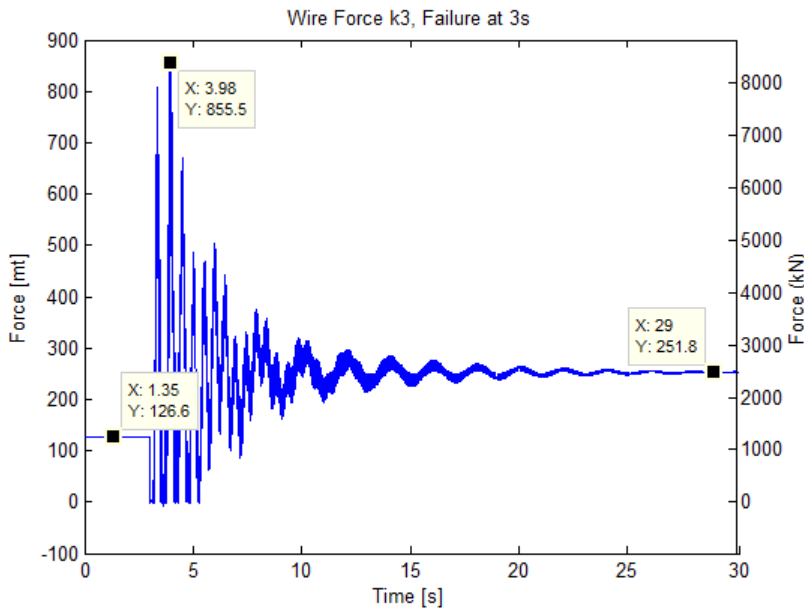
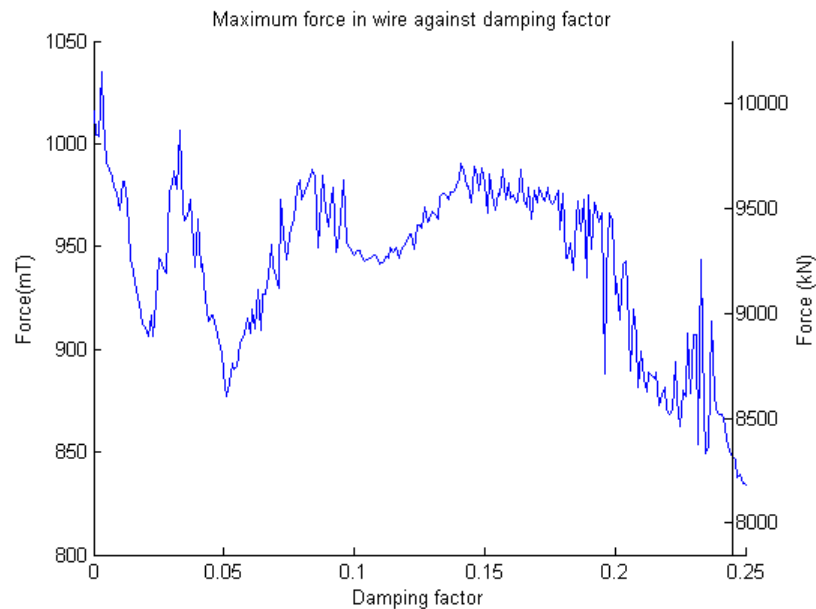


Figure 7.5: Wire force with large damping values (~10%)

Figure (7.5) shows the response of the system with large damping values. The purpose of this check is to determine whether the system reaches equilibrium with expected values for the force in the wire. As expected, the equilibrium after wire failure of one of the wire consists of double the initial wire force. The arms which generate the momentum around the pivot are approximately equal (see Figure (4.14) for reference), therefore the forces found are deemed valid.



**Figure 7.6 Maximum wire force against damping factor**

Figure (7.6) shows a plot of the maximum force in the wire compared with the damping factor of the triangular blocks. With a damping factor ranging from 0 till 0.1 the maximum force fluctuates a lot. The reason for this is that the triangular blocks will accelerate a lot which influences the outcome of the maximum force. From 0.1 till 0.18 the outcome of the force is more consistent, so the damping factor for the triangles is set at 0.1 (10% of critical damping.)

### 7.1.2 Inner wire failure

The inner wire failure cannot be modeled with the same model, because there is a mechanical restriction in the system. This restriction limits the rotation of the triangular block at  $15\text{ degrees}$ . Therefore the simulation is run till the block reaches  $15\text{ degrees}$ , then with an event function the ODE solver is stopped at this time. The speed of the rotation of the triangular body will then be inverted and factored with  $1/10$ , and then the ODE solver is started with the new initial conditions. This way the bouncing off the hard stop is simulated in a primitive manner.

Figure (7.7) shows the response of the wire force, with a load of  $10\ 000\text{ mt}$ . As expected, the peak of the force in the wire is much lower than in case of outer wire failure. The maximum force that can be found in Figure (7.7) is  $752.1\text{ mt}$ . This force is a bit higher than the force found previously in Figure (4.16), which is  $669.7\text{ mt}$ . It is worth noting that the first peak in Figure (7.7) is  $664.5\text{ mt}$ , which is almost equal to the  $669.7\text{ mt}$  found in the simplified analysis. The difference suggests that including the horizontal motion of the block has a significant effect on the maximum force found in the wire.

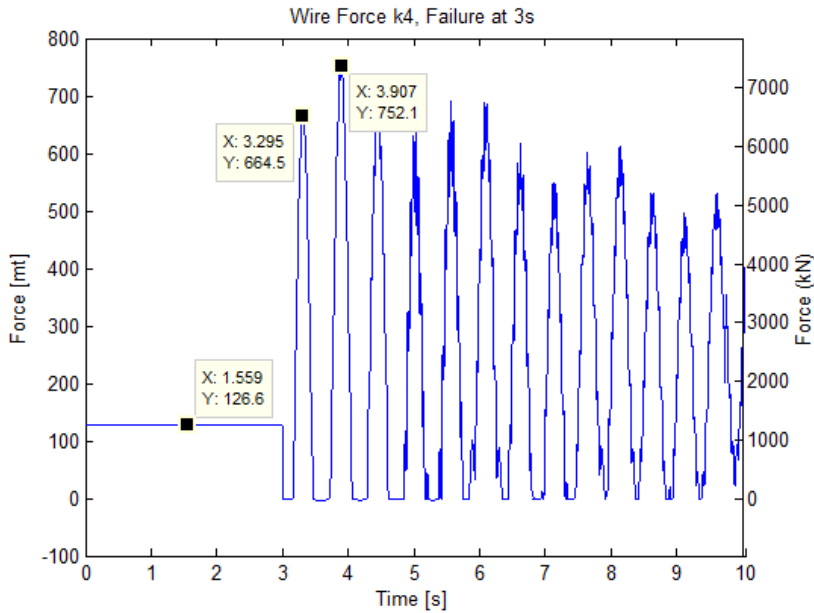


Figure 7.7: Wire force with inner wire failure, load = 10 000mT

## 7.2 Effect of main hoist length on the maximum force

An effect that has already been witnessed in Section (4.6) is that the initial length of the main hoist wires does influence the maximum force a lot. Therefore the effect of the main hoist length is investigated on the model, and the results are presented in this section. Again, the distinction is made between outer wire failure and inner wire failure.

### 7.2.1 Outer wire failure

In this section the effect of the initial length of the main hoist wire on the maximum force in the wire in the case of outer wire will be examined. A preliminary analysis on this has already been carried out and the results will be compared.

If not stated otherwise, the values that are used for the analysis are:

Table 7.2: Parameters used for the analysis

	Units	Symbol	Value
Boom angle	[°]	$\theta$	68.3
Main hoist initial length	[m]	$L_{0MH}$	5-100
Load	[mT]	-	10000
Damping triangles	[%]	-	10
Damping other components	[%]	-	1

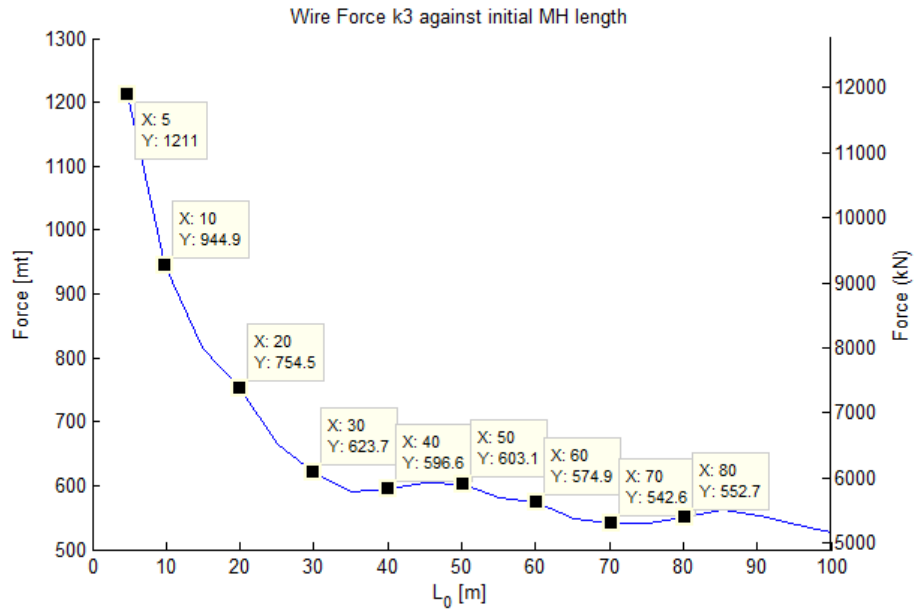


Figure 7.8: Maximum force in remaining wire for different MH lengths, at outer wire failure

Figure (7.8) shows the outer wire failure case, with the force in the remaining wire plotted against different main hoist lengths. From Figure (7.8) it can be obtained that the initial length of the main hoist wire has a large influence on the resulting force. The largest forces are seen in the region from 5 – 10m. From 30m onwards the maximum load is almost constant at approximately 6000kN. The figure shows large resemblance with Figure (4.18) which can be seen as a validation of the model.

Another conclusion that can be drawn from Figure (7.8) is that an outer wire failure will lead to forces that exceed the limits for the other wire. The MBL for the wire is 4650kN, which is exceeded for all lengths of  $L_0$ . A series of simulations is required in order to determine the boom angle and corresponding load on the load-curve at which the failure of the outer wire will not cause failure of the inner wire. Figure (7.9) and (7.10) show the maximum forces for the other load cases.

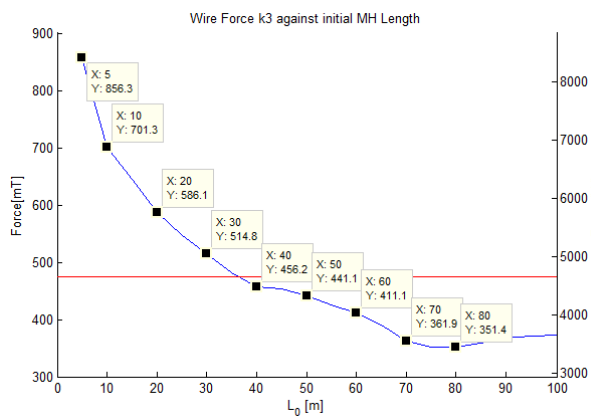


Figure 7.9: Maximum wire force, 7000mt

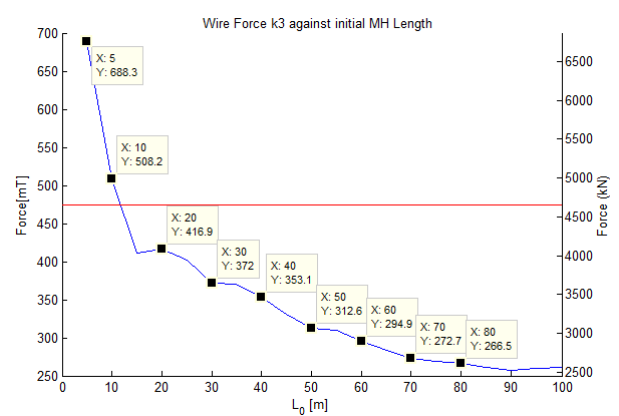


Figure 7.10: Maximum wire force, 4000mt

### 7.2.2 Inner wire failure

For inner wire failure the same analysis are carried out with respect to main hoist length. The results of the simulations for varying main hoist length with a load of 10 000mt can be found in Figure (7.11).

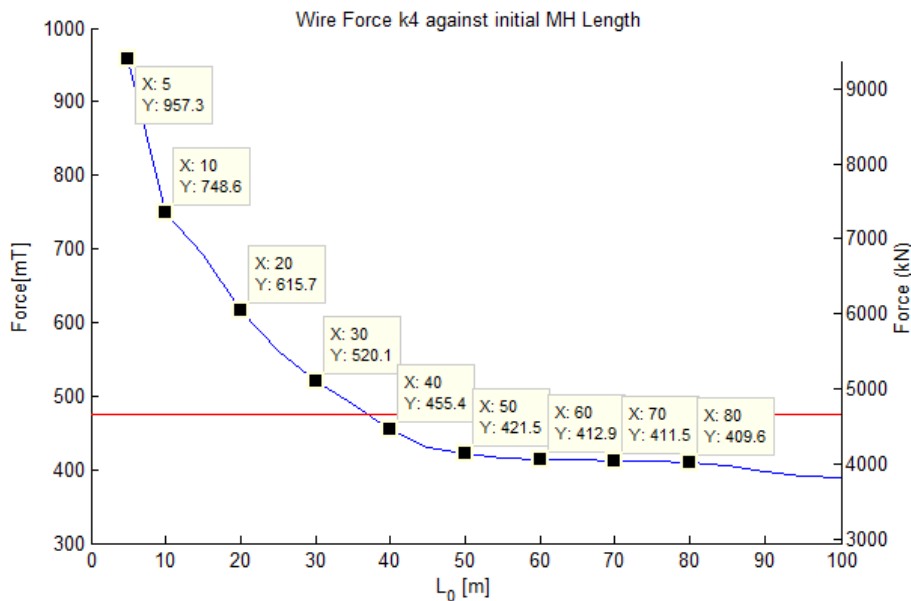


Figure 7.11: Maximum wire force, 10 000mt

The declining trend that was obtained in previous analysis can also be obtained here. Also in these figures the red lines resembles the MBL of the wire. For the 10 000mt case, the maximum line pull will remain below this value from a main hoist length of 40m.

The other load cases have also been investigated, the results of this can be found in Figure (7.12) and (7.13). For these cases the boom hoist stiffness also changes due to the other boom angles that correspond to these cases.

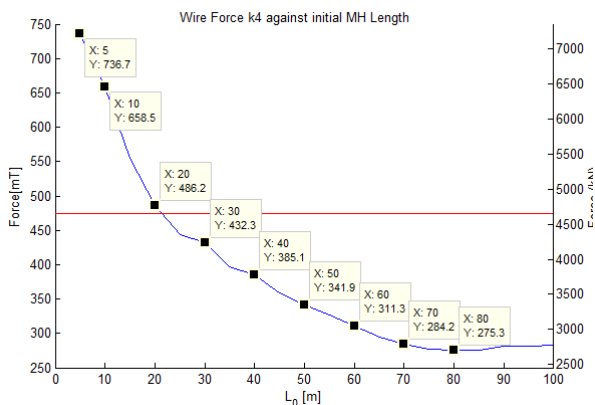


Figure 7.12: Maximum wire force, 7000mt

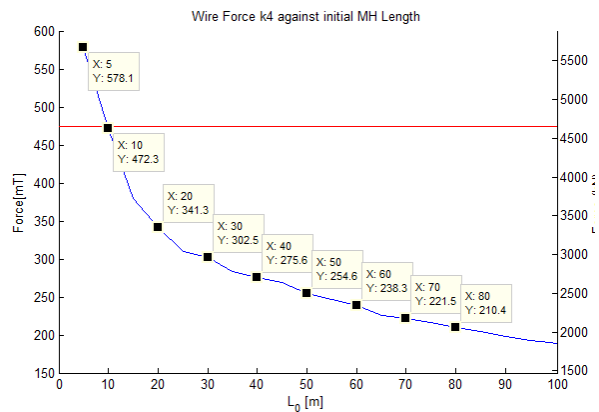


Figure 7.13: Maximum wire force, 4000mt

### 7.3 Stress wave effect

Section (5.5) shows the formulas that are used for the stress wave calculation. The particle speed  $V$  in Equation (5.14) and (5.16) is taken as the speed of the dropping when the wire comes under tension. In this case, this is the speed obtained in Section (4.6) for outer wire failure and with a free fall of the load of  $322.05\text{mm}$ .

For the values of the steel wires used in the crane the maximum stress calculation is as follows:

$$\rho_{\text{wire}} = 5260 \text{ kg/m}^3$$

$$E_{\text{wire}} = 1.05e5 \text{ MPa}$$

$$C_{\text{wire}} = \sqrt{\frac{1.05e11}{5260}} = 4467.88 \text{ m/s}$$

$$V_{\text{load}} = 2.51 \text{ m/s}$$

$$\sigma_{\text{max}} = 118.0 \text{ MPa}$$

$$F = \sigma_{\text{max}} A_{\text{wire}} = 118.0e6 \cdot 0.072^2 \pi \cdot 0.25 = 480 \text{ kN} = 49.0 \text{ mt}$$

This is only a small percentage of the loads that have been obtained in Figure (7.8), in the order of 5%. Therefore the decision is made to not implement the discretized wire into the system, as this would lead to long computation times. However, an analysis was carried out to validate the values that have been calculated. In order to do this, the one degree of freedom system from Section (4.6) is expanded with a discretized wire. This discretized wire consists of 20 mass and 21 spring elements. The results of the analyses are shown in Figure (7.14) and Figure (7.15). Comparing to the force that was obtained in Section (4.6), which was  $934 \text{ kN}$ , the force in obtained here is higher. This is due to the effect that here the pretension of the wire is set to 0 to match the findings in this chapter; due to the rotation of the triangular body the pretension releases. This increases the force in the wire slightly. Still no stress wave effects are found in this analysis. The difference with or without discretized wire is minimal, around  $4 \text{ mt}$  instead of the calculated  $49 \text{ mt}$ .

In order to gain more insight in the stress wave effect, some more extensive analysis has been done in Appendix E. There it becomes clear that the model is able to show the stress wave effects if these are present. Therefore the conclusion can be drawn that the static force of the load is much higher than the stress wave effects due the impact of the translating load, therefore the decision is made to not further implement the discretized wire in the detailed main hoist model.

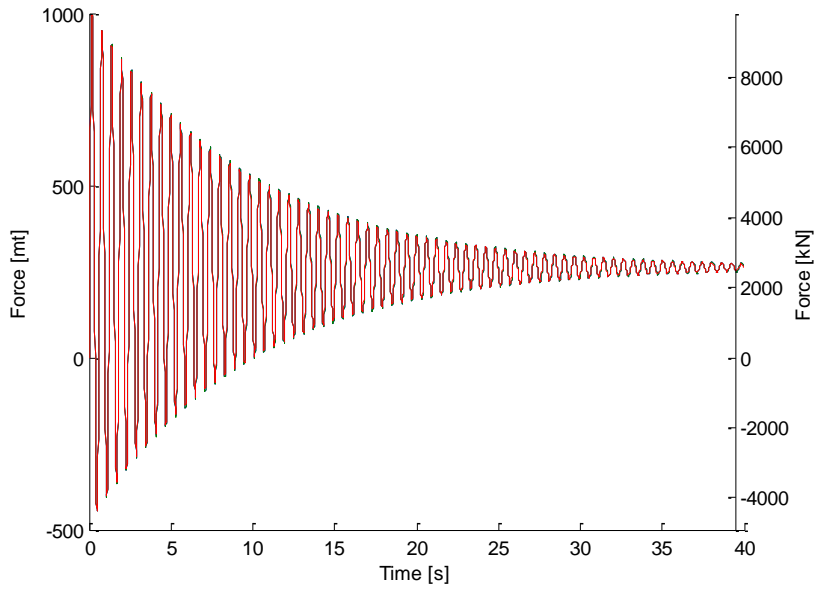


Figure 7.14: Response of discretized and non-discretized wire

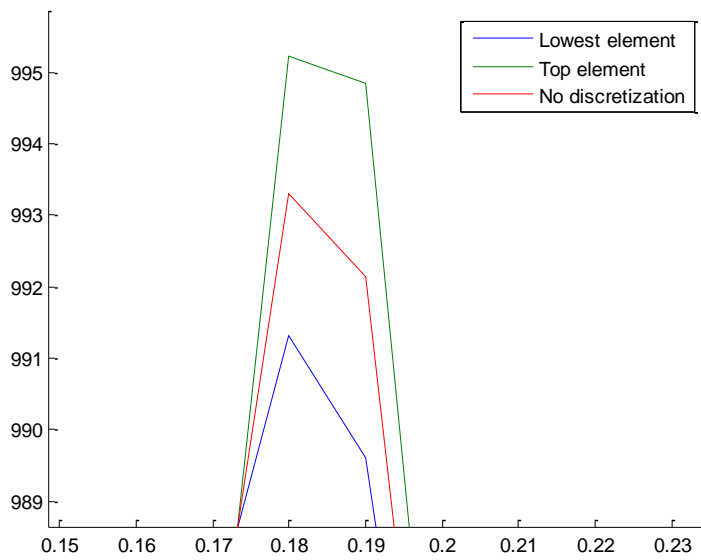


Figure 7.15: Maximum force

## 7.4 Influence of rigging

The connection between the hook and the load has been considered as rigid up till this point. In reality, some rigging wires and spreader bars are used to connect the load to the hook, see Figure (7.16) [19]. This rigging will have a stiffness, which will have an influence on the dynamic factor. In this section the influence of rigging is analyzed. The module in Figure (7.16) has a weight of 12 000 *mt*, the capacity of the NSCV will be 20 000 *mt* in dual lift mode.



Figure 7.16: SSCV Thialf in dual lift mode(source: Siemens AG)

The stiffness of the rigging is implemented in the system as one equivalent spring element with a stiffness  $k_{rigging}$ . This stiffness is based on experience by the company and has a value of 432 424 *kN/m*. The main hoist system including the rigging is shown in Figure (7.17).

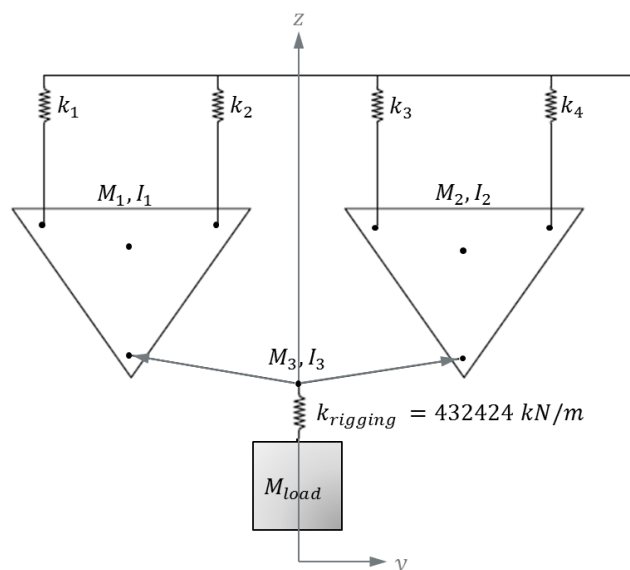


Figure 7.17: MH system including rigging

### 7.4.1 Outer wire failure

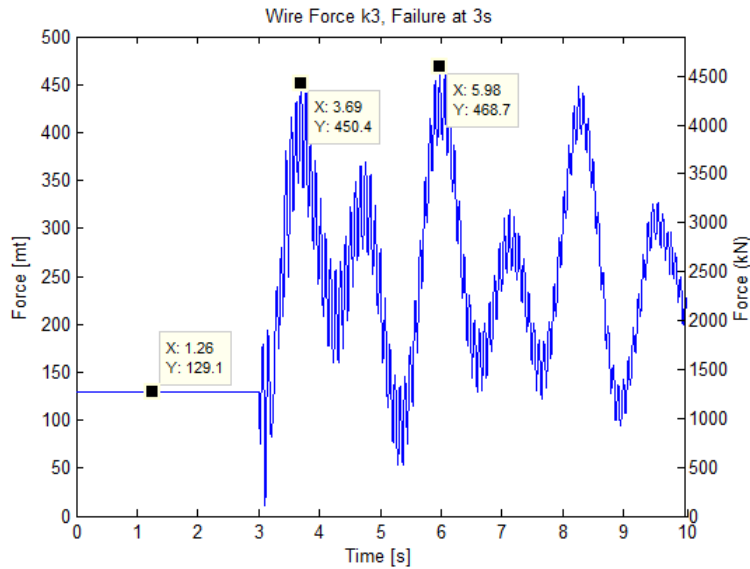


Figure 7.18: Main hoist length = 30m, Rigging length = 20m

Figure (7.18) shows the maximum wire force in the remaining wire. The influence of the rigging is large. The maximum force in the wire found in Figure (7.8) was  $623.7\text{ mt}$ , with the rigging included this force drops to  $468.7\text{ mt}$ , which is a reduction of 25%. The rigging value however, was based on a rough estimation, this introduces an uncertainty. To see the influence of the rigging stiffness, a series is run with a stiffness varying from 0.5 to 4 times the nominal rigging stiffness. The results can be found in Figure (7.19). From 0.5 -1.5 times the nominal rigging stiffness the maximum wire force remains approximately equal, at higher values a linear increase is witnessed. It is likely that the rigging will have a stiffness in the same order as the main hoist, which in this case is 0.5 times the nominal rigging. Therefore higher stiffness of the rigging can be excluded, and the maximum force is within 5% of  $450\text{ mt}$ .

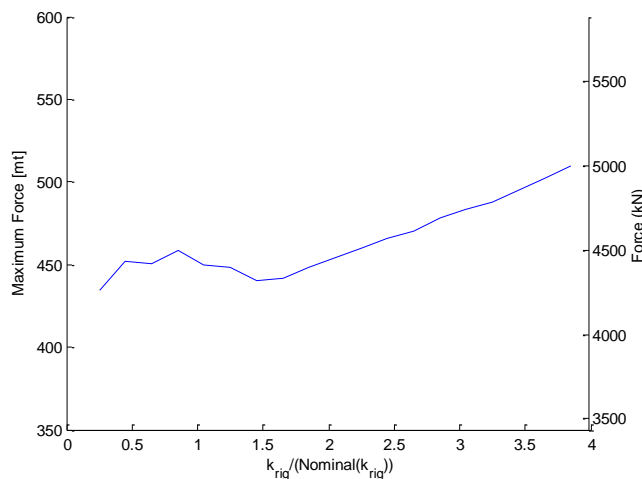


Figure 7.19: Maximum wire force against rigging stiffness

In case of wire failure, it will take some time for the wires to lose their carrying capacity, this is due to the un-reeving of the wires over the sheaves. As a conservative assumption, the time that it takes for the failing wire to fully lose its carrying capacity is 0.5s. The characteristic of the force in the wire is shown in Figure (7.20), Figure (7.21) shows the force in the remaining wire.

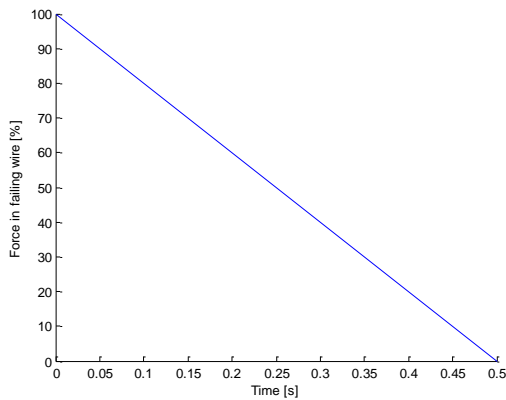


Figure 7.20: Force in failing wire

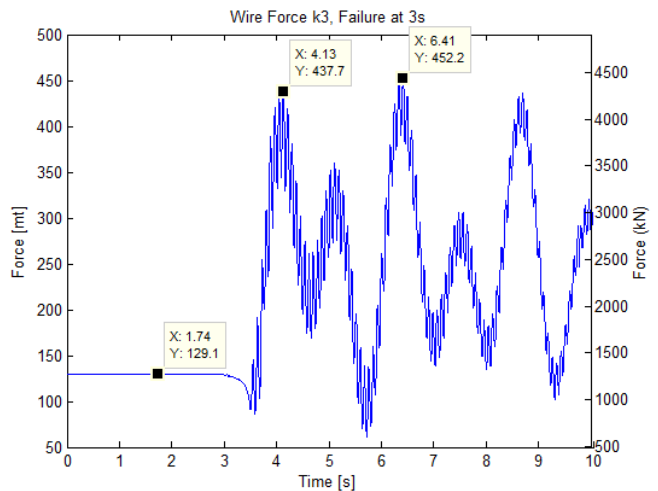


Figure 7.21: Force in remaining wire

When the time it takes for a wire to lose its capacity is taken into account, the peak load drops with approximately 3.5%. However, the process in case of wire failure is hard to measure, the reeving system is very complex and there are a lot of falls present. Therefore the 0.5s it takes for the wire to lose its carrying capacity is a very uncertain value. Tests should be carried out to determine whether this effect may or may not be taken into account. Realizing such tests is complex and costly; therefore this effect will not be taken into account in the end statement on main hoist failure.

#### 7.4.2 Inner wire failure

For inner wire failure the same effects have been analyzed; the influence of rigging and the influence of a slowly dropping carrying capacity of the wire. The results of these analyses can be found in Figure (7.22) and Figure (7.23).

One thing that is remarkable in Figure (7.23) is that the fluctuations of the force are larger than the fluctuations found in Figure (7.18). This is further explained with Figure (7.24) so no attention will be paid to it here. As expected from outer wire failure, the rigging reduces the peak loads in the system, but the differences are smaller. Compared to the force found in Section (7.2.2), which is 520.1 mt, the reduction is 15%, where in case of outer wire failure a reduction of 25% was found. Including the load curve of the failing wire (Figure 7.20) yields an additional reduction of 19% which is in fact much more than the 3.5% for outer wire failure.

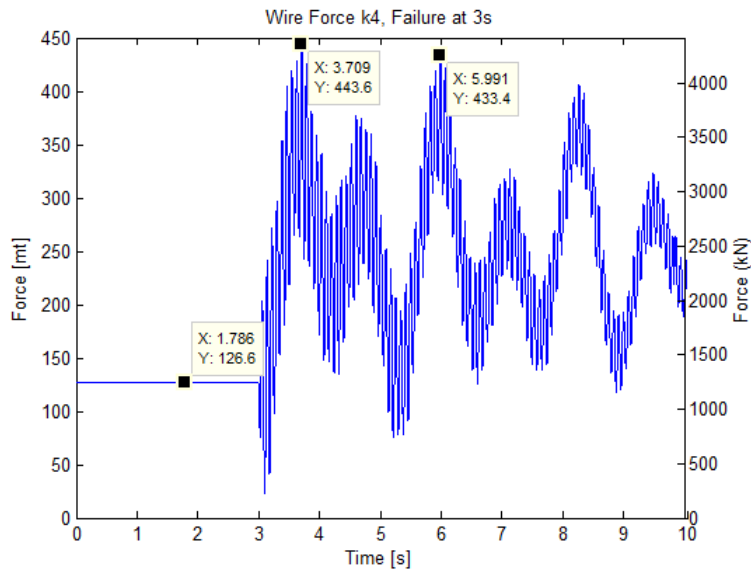


Figure 7.22: Main hoist length = 30m, Rigging length = 20m

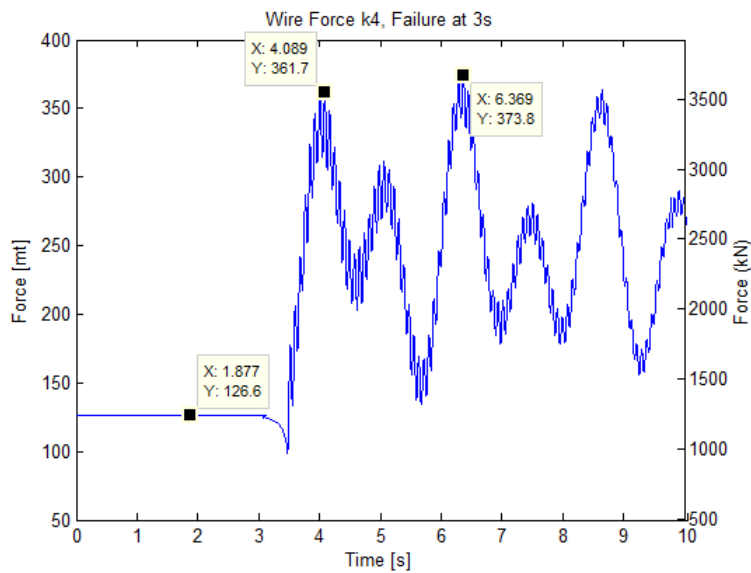


Figure 7.23: Slow dropping load (0.5s)

The explanation for the large vibrations found in Figure (7.22) is given here. First it has to be determined which variable introduces the large fluctuations. Therefore Figure (7.24) shows the relative position of the three governing variables. It is clear that the variable that fluctuates the most is  $z_3$ , which is the z-position of the main hoist block.

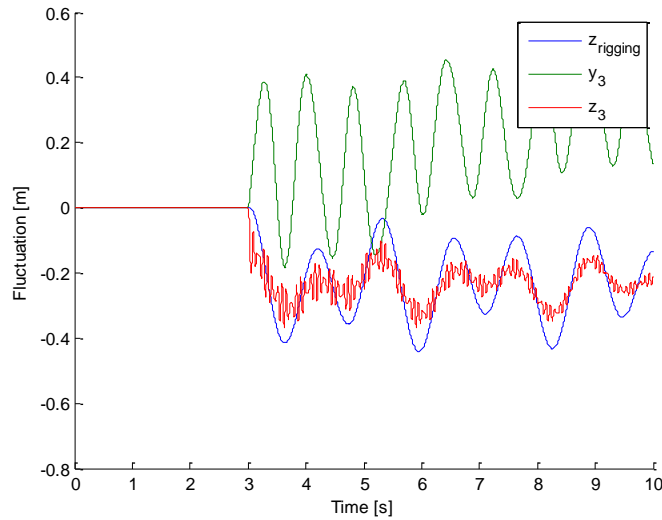


Figure 7.24: Deflection of various parameters

From Figure (7.24) the period of vibration is measured with Matlab. The period between two peaks is 0.073s. The frequency at which the main hoist block vibrates can then be found as:

$$\omega_{inner} = \frac{2\pi}{T} = \frac{2\pi}{0.073} = 86.07 \text{ [rad/s]} \quad (7.1)$$

For the case of outer wire failure, a period of 0.085s is measured from Figure (7.19), this corresponds with the following frequency:

$$\omega_{outer} = \frac{2\pi}{T} = \frac{2\pi}{0.085} = 73.92 \text{ [rad/s]} \quad (7.2)$$

A Free-Vibration analysis of the system is carried out in order to determine the natural frequencies of the system. For this analysis a simplified version of the system is introduced in Figure (7.25).

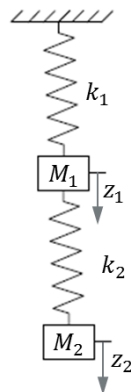


Figure 7.25: Simplified system

The equations of motions in matrix form are:

$$\begin{bmatrix} M_1 & 0 \\ 0 & M_2 \end{bmatrix} \ddot{\vec{z}}(t) + \begin{bmatrix} k_1 + k_2 & -k_2 \\ -k_2 & k_2 \end{bmatrix} \vec{z}(t) = f(t) \quad (7.3)$$

The natural frequencies can be found by solving:

$$\det \begin{vmatrix} -\omega^2 M_1 + (k_1 + k_2) & -k_2 \\ -k_2 & -\omega^2 M_2 + k_2 \end{vmatrix} = 0 \quad (7.4)$$

The system is solved with Matlab in order to reduce the chance of calculation errors. For  $k_1$  the value of the three main hoist wires after wire failure is used, for  $k_2$  the previously mentioned rigging stiffness. The results of the calculations can be found in Table (7.3).

**Table 7.3: Natural frequencies**

	Symbol	Value	Unit
1 <sup>st</sup> natural frequency	$\omega_1$	88.04	[rad/s]
2 <sup>nd</sup> natural frequency	$\omega_2$	4.95	[rad/s]

The first natural frequency of the system lies very close to the frequency in which the system vibrates after failure, found in Equation (7.4). Therefore the excitation is larger, which introduces larger fluctuations in force. This also explains why the reduction in peak force is more significant when gradually releasing the wire tension in the failing wire instead of snapping it. Because when the wire snaps, the pulse will cause the system to vibrate in its natural frequency. Note that this is only the case for these values in particular, for other rigging and main hoist length combinations the natural periods of the system change.

## 7.5 Dual lift with 20 000mt

In Figure (7.16) the SSCV Thialf is shown performing a dual lift. The NSCV will be able to perform a dual lift of 20 000mt. Based on the dimensions and weight of the load in in Figure (7.16) an estimation is made on the dimensions of a 20 000mt load. With a dual lift the rotational inertia of the load will have an influence, where previously this effect could not be witnessed.

Figure (7.26) shows the schematic view of a dual lift. The distance between the centerlines of the tubs of the cranes is 67.5m. The crane model on the left has the main hoist system included; the right crane is a simplification of the main hoist system with equivalent stiffness and mass. The length of the main hoist and rigging are kept equal to the values used in Section (7.4) in order to make a comparison possible. The rotational inertia of the load is calculated with Equation (7.8).

$$I_{Load} = \frac{1}{12} \cdot M \cdot (L^2 + H^2) = \frac{1}{12} \cdot 20000e3 \cdot (125^2 + 45^2) = 2.942e10 \text{ [kg} \cdot \text{m}^2] \quad (7.5)$$

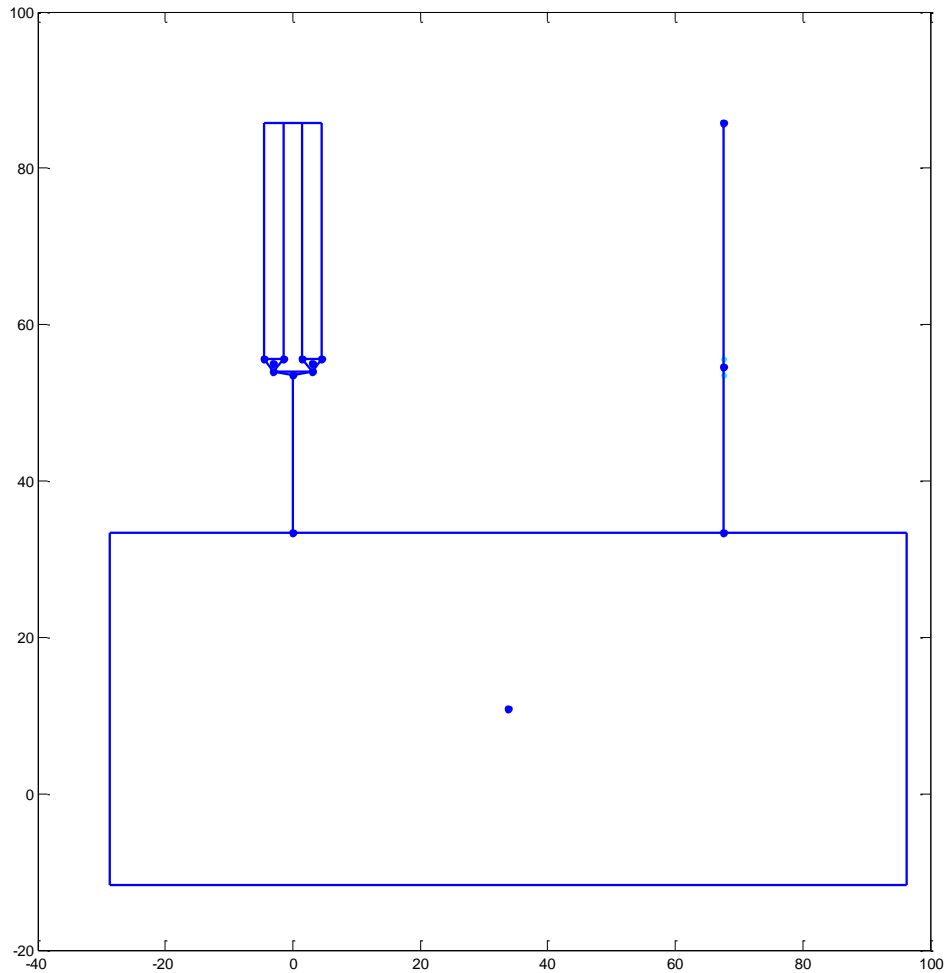


Figure 7.26: Dual lift configuration

The results of the analysis can be found in Figure (7.27). Because the load is more restricted in the y-plane, the force in the wire is more constant than found in the other main hoist failure analyses. Furthermore, the peak is approximately the same as in case of a single lift; 468.8mt for a single lift against 448.8mt for the dual lift.

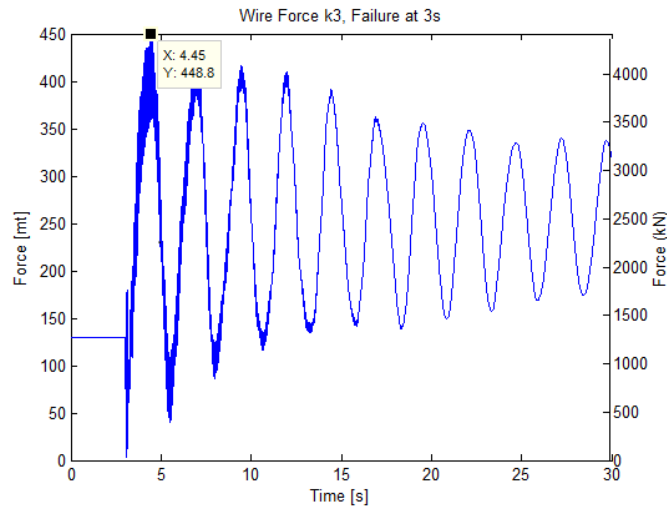


Figure 7.27: Main hoist length = 30m, Rigging length = 20m

## 7.6 Summary and Conclusions

A more detailed model was created of the main hoist system, and has been analyzed in this chapter. In this section the results from the analyses will be summarized in tables, after which a conclusion will be drawn on the subject.

### 7.6.1 Summary

The influence of various parameters was investigated, of which the results can be found in Table (7.4) for outer wire failure and Table (7.5) for inner wire failure. Note that the dynamic factor for outer wire failure is based on a nominal wire tension of 261.8mt and for inner wire failure on 218.5mt. The influence of parameters is always compared to the preceding parameter, e.g. the influence of rigging is compared to the '30m MH no rigging' case and not to the 'Multi-body system'.

**Table 7.4: Outer wire failure parameter study**

Parameter	Value Parameter	Unit Parameter	Uncertainty Parameter [%]	Influence [%]	Max Force [mt]	Range Dynamic Factor
1 DoF	-	-	-	-	946	3.6
Multi-body system	-	-	-	+4.5	988.9	3.77
Slack wire	-	-	-	+17.3	1160	4.43
LF & BH stiffness	-	N/m	5	-12.2	1018	3.70-4.08
Damping	0.01	% of critical	10	-3.8	979.8	3.55-3.92
Main hoist length	10-80	m	-	Variable	944.9-552.7	3.61-2.11
Stress wave effect	-	-	-	-	-	-
30m MH no rigging	-	-	-	-	623.7	2.38
Rigging	432424	kN/m	10	-24.9	468.7	1.59-1.98
Slow drop (0.5s)	0.5	s	(-) <sup>1</sup>	-3.5	452.2	1.72 <sup>2</sup>
Dual-lift	-	-	-	-4.2	448.8	1.71

<sup>1</sup> The uncertainty of the slowly dropping load cannot be expressed in a quantity here, because no test or reference is present.

<sup>2</sup> Note that the uncertainty of the rigging has not been taken into account for this value

**Table 7.5: Inner wire failure parameter study**

Parameter	Value Parameter	Unit Parameter	Uncertainty Parameter [%]	Influence [%]	Max Force [mt]	Range Dynamic Factor
1 DoF	-	-	-	-	652.7	2.98
Multi-body system with slack wire and LF & BH stiffness	-	-	-	+15	752.1	3.44
Main hoist length	10-80	m	-	Variable	409.6-748.6	1.87-3.42
Stress wave effect	-	-	-	-	-	-
30m MH no rigging	-	-	-	-	520.1	2.38
Rigging	432424	kN/m	10	-14.7	443.6	1.88-2.17
Slow drop (0.5s)	0.5	s	(-) <sup>1</sup>	-15.7	373.8	1.72

<sup>1</sup> The uncertainty of the slowly dropping load cannot be expressed in a quantity here, because no test or reference is present.

The tables show that the values that are obtained are very close to the values that have been obtained previously in the 1 DoF analyses. Table (7.4) is more detailed than Table (7.5) because in Table (7.4) the model has been expanded stepwise, and for Table (7.5) the same model was used with most of the components included.

The largest influence that is witnessed is the influence of rigging; adding an additional spring between the load and the main hoist block significantly lowers the force in the wire. As a 'rule of thumb' the rigging stiffness is always taken equal to the main hoist stiffness.

### 7.6.2 Conclusions

The most important conclusion that can be drawn from this section is not explicitly about the values itself, but more about how the values are used by the companies. A lot of employees base their 'gut feeling' on the absolute value of the dynamic factor, without checking its implementations. Therefore the presented values in this section can cause a lot of confusion, i.e. the dynamic factor for inner and outer wire failure can be the same, but the maximum force in the wire that occurs can still differ. This is a direct consequence of basing the dynamic factor on the force in the wire after failure.

It would be much more convenient to base the dynamic factor on the load before wire failure, as this is the same for both cases. Based on the assumption that the rigging stiffness is approximately the main hoist stiffness and the assumption that the minimum main hoist length is always longer than 30m, the following values are obtained:

---

$$\text{Dynamic factor outer wire failure} = \frac{468.7}{131} = 3.6$$

---

And:

---

$$\text{Dynamic factor inner wire failure} = \frac{443.6}{131} = 3.4$$

---

These values provide a solid base for further calculations, this way no inconsistencies exist about the absolute value of the wire force that will occur in the wire.

Secondly, there is a chance that when outer wire failure occurs, that the remaining wire will also fail. This will have major consequences on the system, with even a drop of load as a consequence. As there is little room for improvements on the system itself, the recommendation is to carry an extensive Failure Mode Effect and Critically Analysis (FMECA) (see Appendix F) out for the case of outer wire failure. At this stage the likelihood of wire failure is unknown to the author, but the consequences would be devastating. Therefore the urge exists to examine what the consequences would be if it happens, and if there are measurements to be made. These measurements can be directed against prevention of wire failure, or the mechanics of the main hoist lower block should be revised to see whether this can be improved to reduce the wire force.

Lastly, engineers should remain critical to the results gathered with advanced software. The implementation of multibody systems can be complex, and although multibody software packages provide useful tools, the outcome is highly subjective to the input. At the time of writing this thesis another company carried out a similar analysis on the same subject, with advanced multibody dynamics software. However, the simplifications of the system to be able to implement it in a multibody package were wrong. This led to the results that the dynamic factor for a 30m main hoist length was lower than for a 120m main hoist length. In an early stage of this thesis, it was already determined that a longer main hoist length leads to a lower force, which is shown in Figure (4.18). These findings still hold after implementing the more detailed system, so it can be concluded that there was a mistake in the analysis of the other company which led to improper results.



---

## 8 Drop of the load

---

The simplistic analysis for the drop of the load case has already been conducted in Section (4.7). There the conclusion could already be drawn that this load case is the least severe case for the boom/main hoist wires. However, still some inconsistencies existed, for example the slack wire wasn't modeled properly. In the analyses carried out compression forces in the spring element existed, which cannot exist in steel wire ropes. For the boom hoist failure case a model is created with a discretized boom hoist wire, see Section (5.5). This model is used in this section to validate and update the loads that have been found in Section (4.7).

### 8.1 Results

In this section the results are displayed for the various load cases. The focus will lay on the stress wave effect occurring when the wires come under tension after being slack for a certain period of time. Also for the *82degrees* loadcase the effect of the boom stop will be investigated.

#### 8.1.1 82degrees, 10 000mt

First, the *82degrees* loadcase is analyzed. The results obtained for this loadcase are found in Figure (8.1). The discretized wire causes that the force doesn't become negative anymore, which was the case in Section (4.7), therefore the results are more realistic. It is also concluded that the force does not exceed the initial value before drop of the load. This makes the drop of the load case the least severe case for the boom hoist wires.

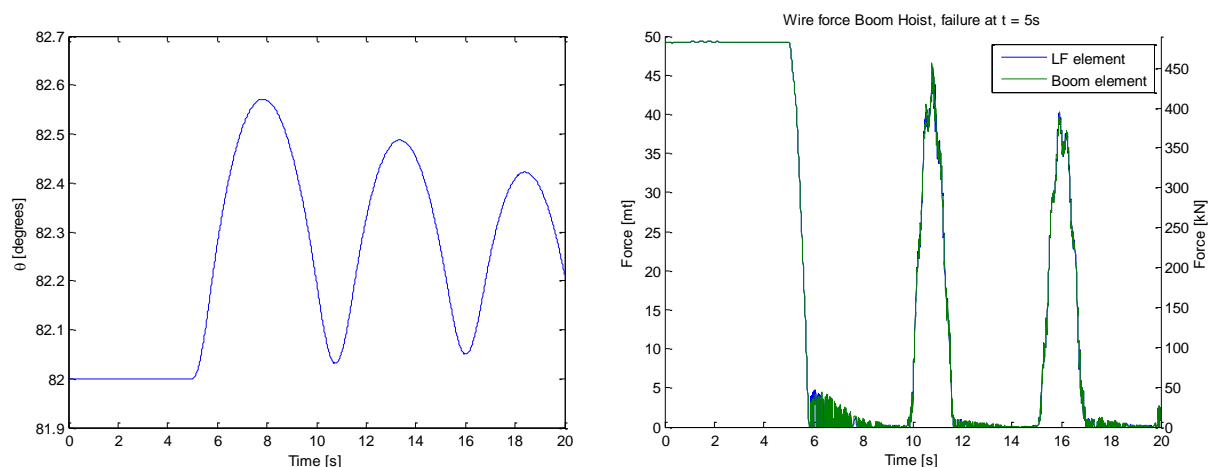


Figure 8.1: 82 degrees loadcase, boom angle and wire force

It must be noted that the motion shown in Figure (8.1) cannot happen in reality. This is due to the fact that the boom is held against the boom stop when operating in the 82degrees position. A depiction of the boom stop can be found in Appendix B. The force on the boom stop can be easily determined with a momentum balance, and from there the required strength of the boom stop can be determined. The boom stop is designed as a first failing mechanism, because then damage to the boom and/or luffing frame can be prevented. The system is coupled through the stiffness of the boom stop; this could reduce the occurring load in the boom stop. Therefore the stiffness of the boom stop is implemented into the model in order to determine the maximum occurring force in the boom stop. The calculation for the stiffness of the boom stop can also be found in Appendix B.

Figure (8.2) shows the results of the drop of load analysis with the boom stop implemented, as can be seen, due to the force that is excited on the boom by the boom stop, no slack wire occurs. Also the natural period increases significantly due to the high stiffness of the boom stop.

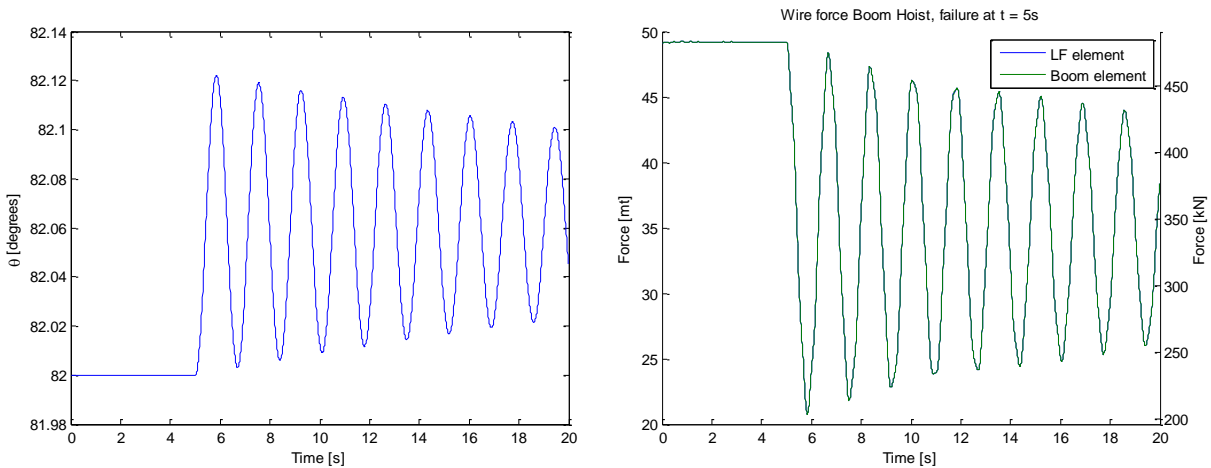


Figure 8.2: 82 degrees loadcase, boom angle and wire force with Boom stop

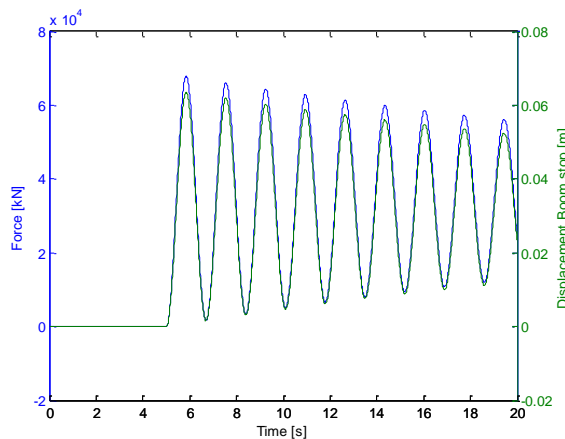


Figure 8.3: Force and displacement of boom stop

It is relevant to determine the force in the boom stop, which is why Figure (8.3) shows the deflection and force of the boom stop. The static force if the stiffness of the boom stop is not taken into account can be calculated as follows:

$$F_{Boomstop} = \frac{\sum M_{Boom}}{L_{Boomstop}} = F_{Xwires} \cdot \frac{L_{wires}}{L_{Boomstop}} = 2.2853e7 \cdot \frac{95.65}{30.06} = 7.27e7 \text{ N} \quad (8.1)$$

This force is, as expected, higher than the force that can be obtained from Figure (8.3). The magnitude of this force is  $6.79e7 \text{ N}$ . However, the difference is small, and both forces are much higher than the allowable force of the main chord.

With two main chords of the dimensions and material shown in Appendix (B), the maximum allowable force can be calculated as follows:

$$F = \sigma \cdot A \quad (8.2)$$

With  $\sigma$  the yield strength of steel St52, which is  $355 \text{ MPa}$ , the following maximum force can be obtained:

$$F = 355e6 \cdot 2 \cdot (0.559^2 - 0.535^2) \cdot \pi \cdot \frac{1}{4} = 2.02e7 \text{ N} \quad (8.3)$$

This leads to the conclusion that the boom stop will fail under the compression load, but this has been already accounted for. It will not lead to damage to the boom or the luffing frame as calculated by Huisman, which are the vital components of the system.

### 8.1.2 68.3degrees, 10 000mt

The case that is discussed in this section is the case of maximum outreach, which is  $48 \text{ m}$  with a boom angle of  $68.3 \text{ degrees}$ . The initial wire tension for this case is twice the tension of the  $82 \text{ degree}$  load case; this is due to the more disadvantageous moment of the load. The results of the analysis can be found in Figure (8.4). Something worth noticing from these results is the larger fluctuation that exists in the force. This fluctuation can be explained with the shockwave effect, which was mentioned previously in the report. When the wire comes under tension after being slack for a certain period of time, a stress wave travels through the wire which can increase the stress at boundaries. Remarkable is that this way the maximum force in the wire even exceeds the initial force with the  $10\,000 \text{ mt}$  load suspended from the hook. Still, the values remain way below the breaking limit of the wire, so no concerns are necessary.

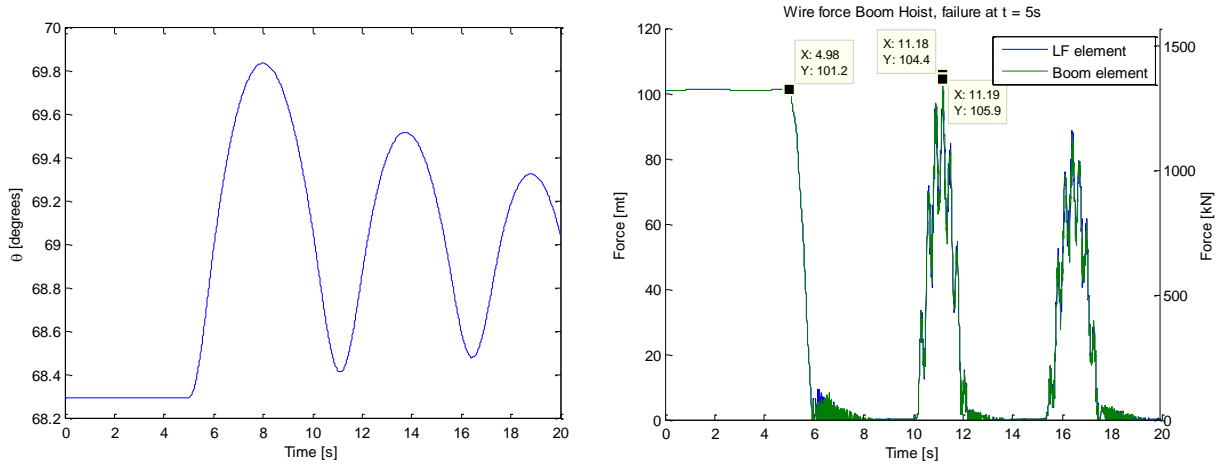


Figure 8.4: Boom angle and wire force

### 8.1.3 58.4degrees, 7,000mt

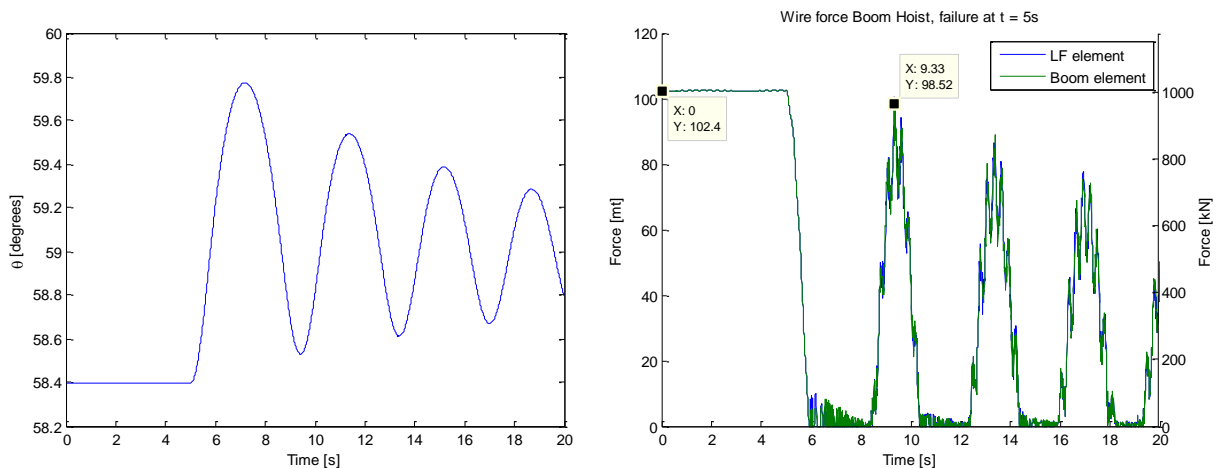


Figure 8.5: Boom angle and wire force

As the boom angle decreases, the initial wire length of the boom hoist increases. This decreases the stiffness, and as a consequence the initial elongation of the wire increases. The various load cases are analyzed in order to determine whether the wire will get slack and stress waves occur. As can be obtained from Figure (8.5) the slack wire effect still occurs. The force, however, does not exceed the initial value anymore. Also the stress wave effect is less visible than in the 68.3degrees loadcase. The last case that is investigated is with 0degrees boom angle. Although the load in this case is much lower, 1588mt over 10 000mt, the weight of the boom has a more disadvantageous moment in the 0degree case. Therefore, the wire force that occurs in this case might even be larger than in other cases.

### 8.1.4 0degrees, 1588mt

The results of this analysis can be found in Figure (8.5). As explained before, the initial elongation increases with decreasing boom angle. In this case the pretension in the wire will not be completely dissolved by the rotation of the boom. Therefore, the slack wire effect does not occur in this case, which significantly reduces the maximum force that occurs in the wires.

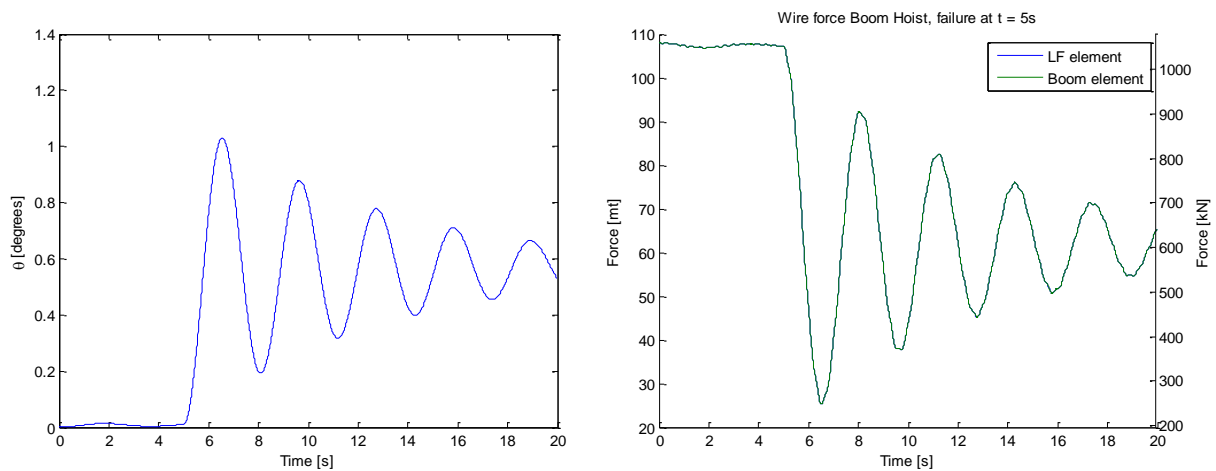


Figure 8.5: Boom angle and wire force

## 8.2 Conclusions

This section covered a more in-depth analysis of the drop of the load case. The boom hoist wires have been discretized in order to get more insight in the forces that occur in the wires. With the discretization of the wires, the issue of slack wire is solved. The wire is able to transfer forces in x – and z – direction, therefore in case of slack wire no compression can occur due to the out of plane forces. In case of the simplified main hoist model with discretized wire (Section 7.3) the wire is only able to transfer loads in z – direction, hence also compression forces occur.

With the discretized wires the model is also able to show stress wave effects when the wire comes under tension after being slack for a certain period of time. This can lead to higher forces in the wires than expected, for the 68.3degree loadcase the force even exceeds the initial value with load. For the 82degree loadcase the influence of the boom stop has also been investigated, as a result the slack wire does not occur anymore. The boom stop itself will fail under the compression load of the boom; this is to prevent damage to more vital parts of the crane.

Compared to the other load cases, this case is the least severe for the steel wire ropes in the system. The forces are approximately equal to the normal operating case, so no further investigation is required on this field. It would however be interesting to see how the boom acts under these loads in terms of bending. A study on this has already been performed for a much lighter crane by Brzobohaty [1].



---

# 9 Concept design for mechanical equalizer

---

In Chapter 6 the influence of several parameters on the dynamic factor for boom hoist wire was investigated. It was found that none of the parameters have a significant influence on the dynamic factor. The two independent boom hoist systems are to be controlled with a control system operating on the winches in order to keep the forces in the wires equal. However, for safety reasons, one might desire a mechanical system over a computer system in order to equalize the forces in the wires. A mechanical system is more robust and less sensitive to disturbances. Another advantage of the mechanical equalizer could be that a shock absorber could be implemented into the system, which could reduce the dynamic overloading in case of wire failure. The usage of heave compensators in cranes with shock absorbers is pretty common these days, however the loads that can be lifted with these cranes are much less than the 10 000  $mt$  that these cranes are able to lift. In this chapter the possibility and the technical feasibility of a mechanical equalizer, with the capacity to reduce the dynamic overload in case of wire failure, is investigated.

## 9.1 Research

As mentioned before, Krukowski [10] investigated the influence of a shock absorber on the dynamics of an offshore pedestal crane. A mathematical crane model was derived using Lagrange's equations and the shock absorber was attached to the boom hoist wire. The results showed were promising, reductions in the order of 30% on the peak load were achieved. It also showed that implementing the bending flexibility of the boom does not influence the results, and it is therefore allowed to omit the flexibility of the boom in preliminary calculations. The calculations however, were carried out with a load of 18  $mt$  (18 000  $kg$ ), which is much lower than the 10 000  $mt$  in this research. This means a study has to be performed in order to see whether it is practically possible to construct a shock absorber with such dimensions that it is fit for this purpose.

Van den Berg [14] investigated the optimization of the buffer in a passive heave compensator. The working principle of this can be found in Appendix F. A passive heave compensator shows great resemblance with the proposed equalizer for this system. The focus on the investigation was on the material used for the end buffer of the shock absorber. As it is likely that the shock absorber will hit the end buffer in the boom hoist equalizer, the experiences gained in that research can be very useful for this thesis. The maximum load that was tested for the system in the thesis of van den Berg was 1200  $mt$ , which is still a factor 10 lower than the load in this thesis.

## 9.2 Concept

The concept that is investigated in this chapter is based on an existing concept within Huisman. A preliminary implementation in the 10 000mt cranes has already been carried out. It was found that the additional free fall introduced by the equalizer cannot be absorbed by a spring-damper system. The analysis, however, focused on one single configuration of the system only. As a result, there is little insight present on which factors have the most influence on the dynamic factor. Therefore in this thesis the focus will lay on a parameter study on the equalizer, which will result in a recommendation towards Huisman about the equalizer.

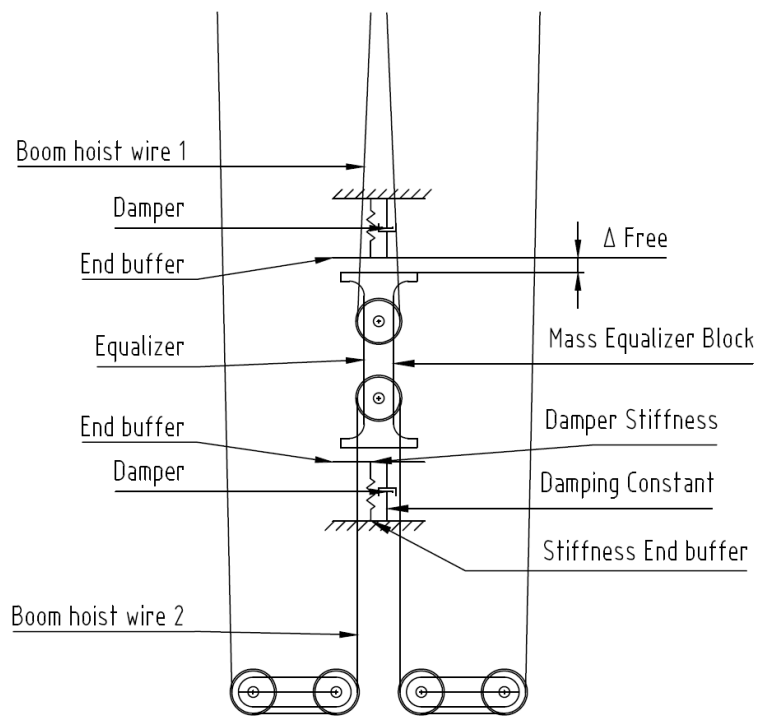


Figure 9.1: Equalizer concept

The boom hoist equalizer is depicted in Figure (9.1). The boom hoist equalizer is placed on the luffing frame, which means dimensions of the mass-block and damper are restricted. The boom hoist equalizer has two main purposes:

- To equalize the force in the wires when there is a difference in drum speed ~ operating case
- To reduce the dynamic loads in case of a wire failure ~ failure case

These purposes are however contradictory. For equalizing purposes the free motion of the block needs to be as large as possible in order to provide the system some time to catch up in case of falling behind of a drum. In that case it is unfavorable to have the block connected to a spring-damper system, because this system will then be constantly interacting with the drums.

In case of wire failure the free motion of the block will, eventually, result in a free fall motion of the load. From the case of main hoist failure it is already known that a free fall of the load introduces high tension in the wires, and should therefore be prevented as much as possible. The best way to do this is to directly connect the block to the spring-damper, which is exactly opposite to the desired normal operating case.

The goal of this chapter is to optimize the four following variables in such a way that it able to allow motions for catching up and to have a positive result in case of wire failure, see Figure (9.2) for reference:

- $\Delta Free$  – the free motion of the block before the damper acts on it;
- $M_{equalizer}$  – the mass of the equalizer;
- $c_{damper}$  – the damping constant of the damper;
- $k_{damper}$  – the spring constant of the damper.

There is a chance that a variable set-up delivers the best results, this is not necessarily a problem because when preparing for a heavy lift the reeving configurations often have to be changed. If it is simple to change the set-up for the boom hoist equalizer during the preparation time, no valuable time is lost.

## 9.3 Assumptions

It is not possible to entirely model the reeving system of the boom hoist wires at this stage. Therefore some assumptions are required in order to model the mechanism of the equalizer. These assumptions are listed below:

- The movement of the equalizer will result in an evenly distribution over the reeved boom hoist wire system;

Appendix B, Figure (B.5) shows where the equalizer is attached to the boom hoist reeving system. A movement of the equalizer would result in additional wire entering the reeving system. In reality, it would take some time for the system to reach equilibrium, because the wire would need to 'travel' through the system. All sheaves would then rotate a little bit, the effect of this would be that the wires furthest from the equalizer would 'feel' the elongation of the wire much later than the wires close to the equalizer. This effect however, is very hard to implement in a dynamic model. Normally the system is 'closed', but the addition of wire would make the system very complicated, therefore the assumption is made that the movement of the equalizer results in an evenly distribution over the boom hoist wire system.

- For the free path of the equalizer the  $k_{damper}$ ,  $c_{damper}$  and  $k_{buffer}$  are set to 0 in Matlab

When the block moves along its axis over the free path, it will feel no resistance force of the damper and spring. Still, the forces exerted by the damper and spring are dependent on the speed and position of the block, so in the equations of motions it appears that the force is also working in the

free movement area of the block. This is corrected in Matlab by setting the values of the damper and springs to zero for a given path.

### 9.4 Equations of Motion for equalizer

Making use of the graphical representation of the equalizer in Figure (9.2) it is possible to find the equations of motion for the equalizer block.  $x_E$  is the global coordinate chosen in the direction of movement of the equalizer block. Figure (9.2) shows the equalizer block after wire failure of the bottom wire. This is also the way how the equalizer is implemented in the system, therefore the bottom spring, damper and wire can be neglected. Up to the moment where the wire fails, a contra-force is applied on the equalizer to simulate the other boom hoist wire.

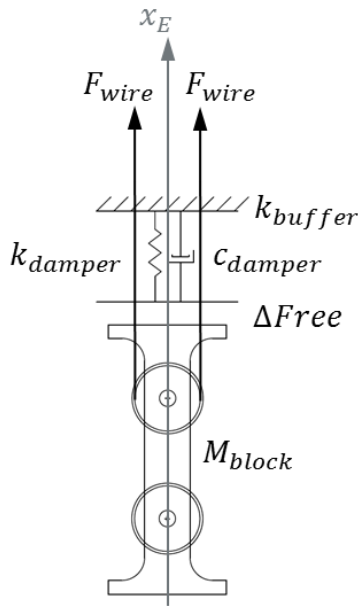


Figure 9.2: Equalizer coordinate system and forces

The equations of motion for the equalizer block can be found in Equation (9.1):

$$\ddot{x}_E = \frac{k_{damper} \cdot (x_E - \Delta Free) + c_{damper} \cdot \dot{x}_E |\dot{x}_E| - 2 \cdot F_{wire}}{-M_{block}} \tag{9.1}$$

Where the force of the buffer is left out of the equation, because it is unsure if the damper will hit the end buffer.

The force in the boom hoist wire has to be corrected for the extra wire. Two partitions of the wire will gain  $\Delta Free$ , which then is spread equally over 40 partitions:

$$\Delta L_{BH} = \left( L_{BH}(\theta(t)) - L_0 - \frac{x_E}{20} \right) \tag{9.2}$$

## 9.5 Results without end buffer

At first the end buffer was left out of the equations. Hitting the buffer would lead to high peak loads, which makes it impossible to determine the effects of the equalizer. The damping factor and stiffness are taken as constant in the calculations. This is not exactly complying with reality, as the stiffness of a damper cylinder changes over the pressure in the cylinder. The load case used in these analyses is the load case with maximum outreach with a 10 000 *mt* load. Each parameter is varied whilst all other parameters are kept constant; the results are shown in Figure (9.3) and (9.4).

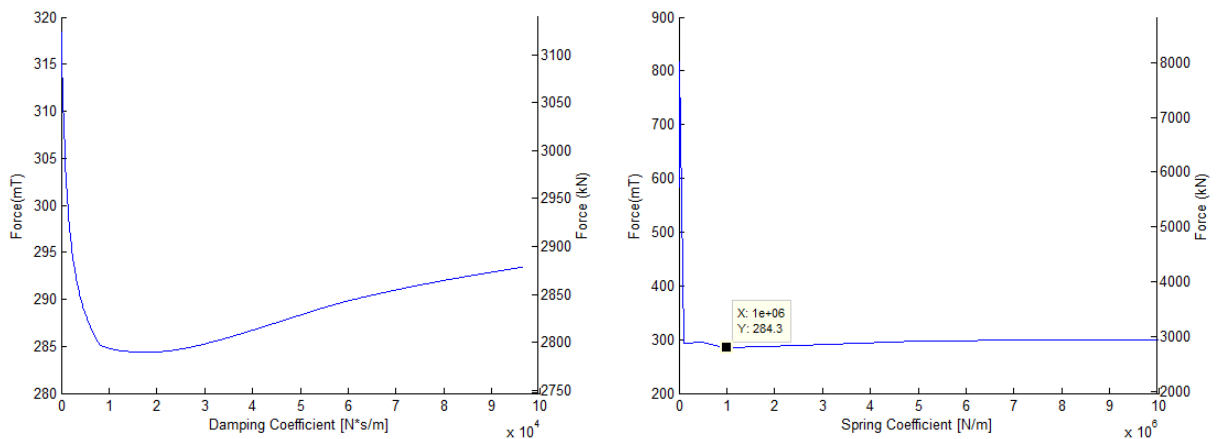


Figure 9.3: Varying damping coefficient and stiffness

From Figure (9.3) it can be obtained that the equalizer does have an influence, however it is not significant. The minimum force that can be obtained with the equalizer is 284.3 *mt*. From Figure (9.4) the conclusion can be drawn that the free path of the block has a negative effect on the maximum force in the wire.

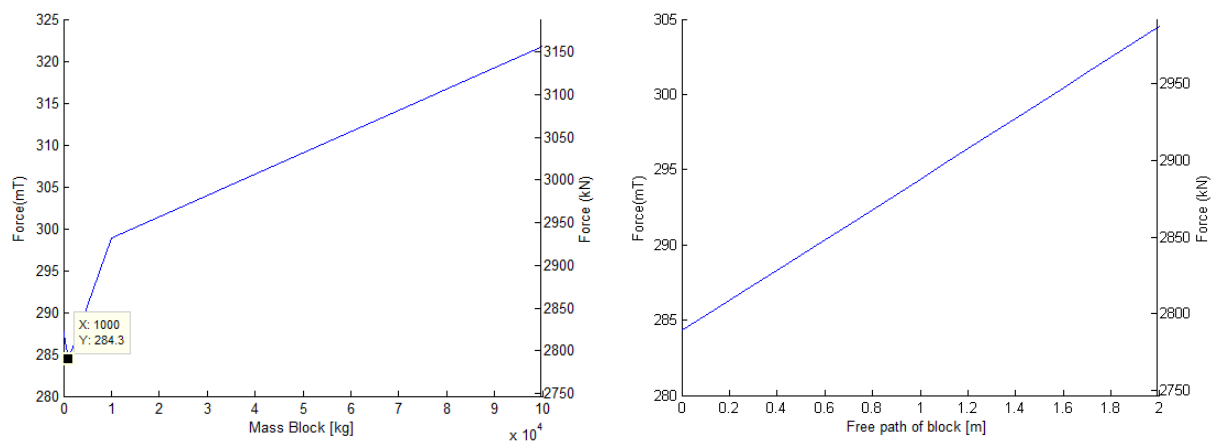


Figure 9.4: Varying mass and free path of the block

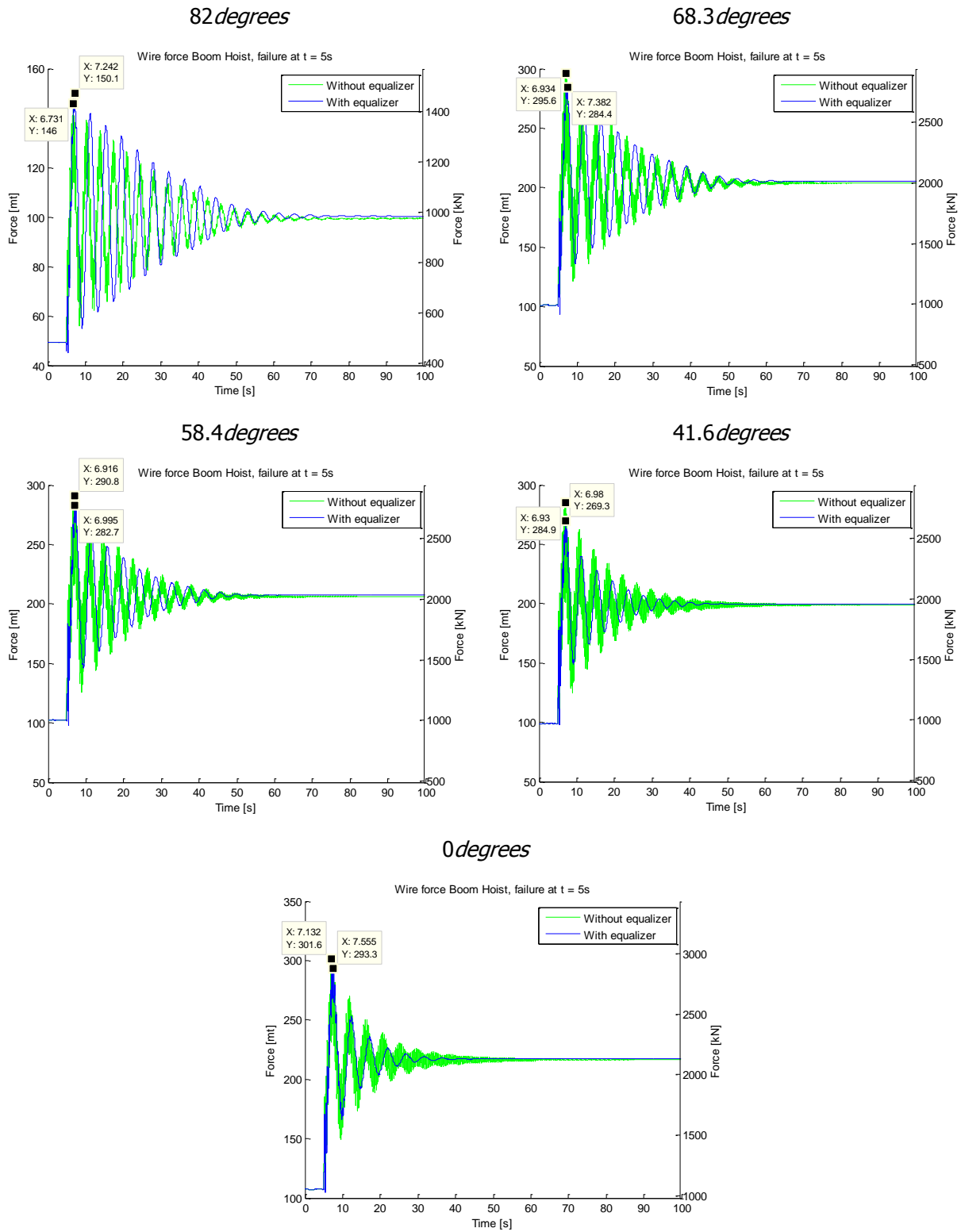


Figure 9.5: Wire force for all load cases

Figure (9.5) shows the wire force for all load cases. With these results it is possible to explain why the equalizer has only limited influence, and why the design is very restricted which does not lead to improvements. The *82degrees* load case shows a negative effect when the equalizer is added to the system. This is due to the rotation of the boom due to the extra wire that comes into the system. This has a more significant effect on the *82degrees* load case because there it leads to more displacement in  $x$  – direction of the load, which increases the overturning moment. It must be stated that the *82degrees* load case is the case with the lowest force in the boom hoist wires, so an increase for this case is not problematic.

For all other cases slight improvement can be witnessed when the equalizer is implemented. Still, these improvements remain small. Due to the fact that a movement of the equalizer yields a rotation of the boom, and consequently a lowering of the load, it is hard to improve the current design with only changing the parameters. A lower damping and/or spring constant of the damper would theoretically reduce the force in the wire; the only compromise would be that the cylinders should become very long in order to allow for movement of the piston. In this case, lowering the damping and/or spring constant results in a larger movement of the equalizer block, which then results in a rotation of the boom and lowering of the load. This makes the overturning moment of the crane worse, and this results in a higher wire force where one would expect a lower wire force. Subsequently, adding more equalizers to more wire partitions would lead to the same issues, and therefore is not regarded as a design improvement.

## 9.6 Main hoist shock absorber

Instead of applying the equalizer concept to the boom hoist wires, the concept could also be applied to the main hoist wires. This excludes the disadvantageous effects of the rotation of the boom, and theoretically it should be able to decay the speed of the dropping load gradually, and thus reducing the maximum tension in the boom hoist wires. This is the same principle as used by Krukowski [10].

Figure (9.6) shows the shock absorber principle of the main hoist system.

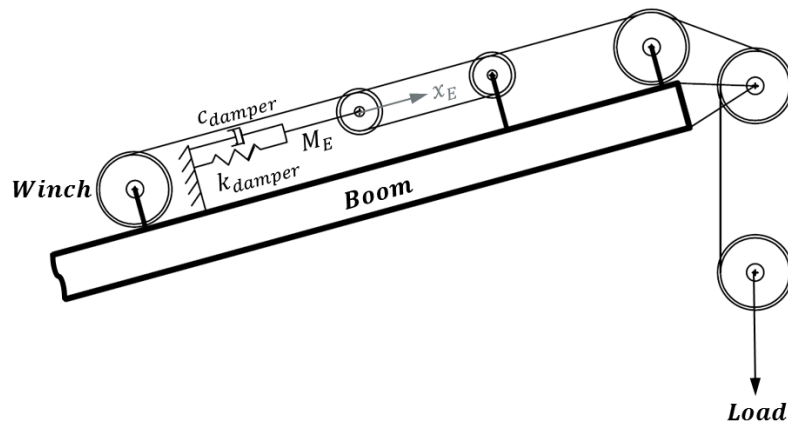


Figure 9.6: Main hoist shock absorber system

This shock absorber should be applied to all four independent main hoist wires, for reference see Figure (3.2) where the reeving configuration of the main hoist system is shown. The translation of the equalizer will result in an increase of length of the main hoist system. The assumptions that were given for the boom hoist system also hold for this system. Where for the boom hoist system a translation resulted in an elongation of twice  $x_E$ , here a translation of the shock absorber will result in an elongation of one time  $x_E$ . However, Equation (9.2) still holds for this system, as the translation here is spread over 20 wire partitions, where in the boom hoist system it was spread over 40.

There is still a difference to be distinguished from the other case, where in that case the equalizer was balanced by the force in the wires; here it is balanced by the force in the equalizer itself. For the figures shown below the luffing frame stiffness has been neglected, this is done because the luffing frame has a high frequency, which makes the figure harder to read. Figure (9.7) shows a case that theoretically could be achieved with an equalizer. However, it must be noted that the stiffness of the equalizer has been set low, which leads to a large required cylinder stroke to balance the initial force. The purpose of Figure (9.7) is to show that larger reductions are possible when applying the equalizer to the main hoist system, the restrictions for this lay in the space that is available for an equalizer system. Also this system could act as a heave compensation system when operating in normal conditions, which could improve the workability of the crane.

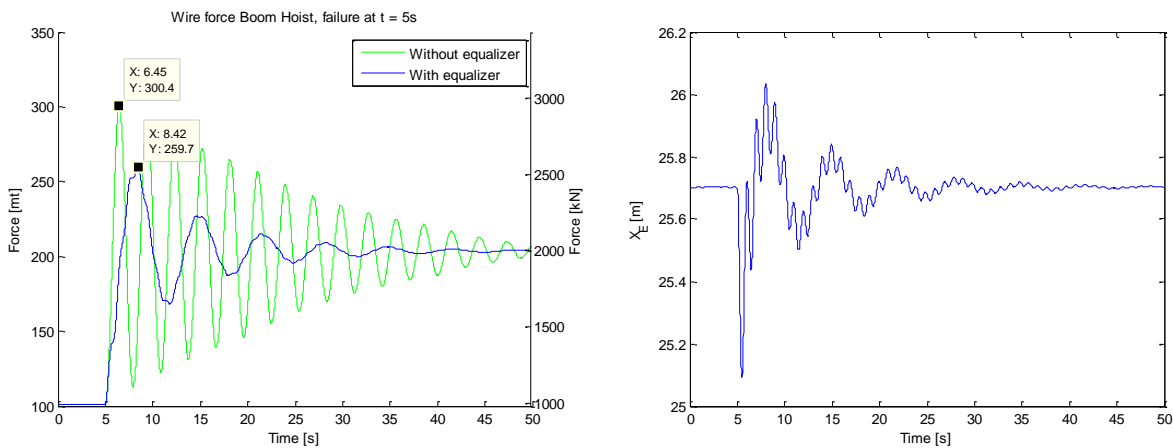


Figure 9.7: Boom hoist force and equalizer position  $X_E$

As can be seen in Figure (9.7), the influence of the shock absorbers depends on its parameters. A low stiffness will be more favorable in terms of gradually slowing the load, but it also requires a long cylinder stroke. Furthermore the speed will also increase of the piston, and this could lead to damage of the shock absorber. Appendix F elaborates on the passive heave compensator which has already been applied by Huisman in Subsea 7's Seven Waves. From these data, a realistic model is implemented with the properties of the Passive Heave Compensator (PHC), these can be found in Table (9.1).

**Table 9.1: PHC parameters**

Property	Value	Unit
Damper stiffness	3e6	N/m
Damping coefficient	251.2	kNs <sup>2</sup> /m <sup>2</sup>

Again, the stiffness is taken as constant value, where in reality it varies with the position of the piston in the cylinder. The value shown in Table (9.1) is approximately the stiffness when the PHC is in equilibrium with the load. The results of the analysis are shown in Figure (9.8).

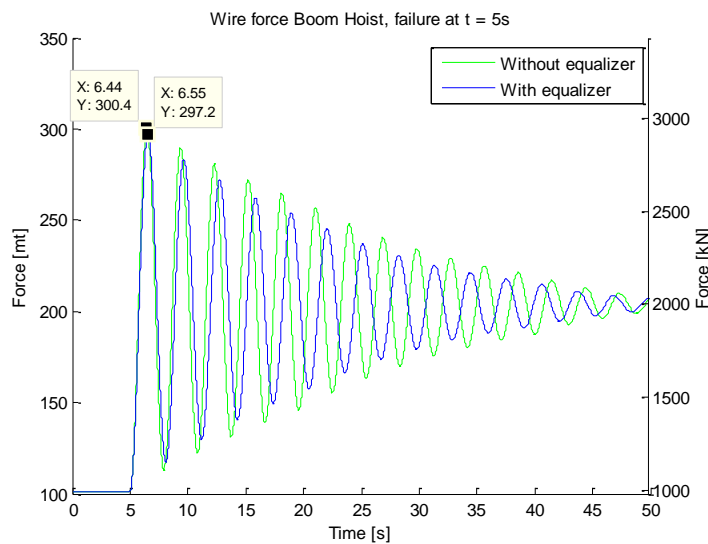


**Figure 9.8: Implementation of existing PHC**

The differences obtained with or without equalizer are small. For the first peak the difference is only in the order of 1%. This is due to the high stiffness of the heave compensator, which allows for little movement of the load. This way the deceleration of the load is still high, resulting in a high peak force. One way to reduce the deceleration is to extend the path over which the load decelerates; this can be achieved by reducing the stiffness of the PHC system.

Figure (9.9) shows the maximum wire force against the stiffness, which ranges from 1e5N/m to 3e6N/m. The damping coefficient has remained constant at the value presented in Table (9.1). From Figure (9.9) the conclusion is drawn that it is possible to significantly reduce the force in the wire, however a low stiffness of the damper is required to achieve this. This could lead to large cylinder lengths, which are undesired. Comparing these results with the boom hoist equalizer results, the conclusion is drawn that the main hoist equalizer can be more effective if the right parameters can be achieved within the restrictions of the cylinders.

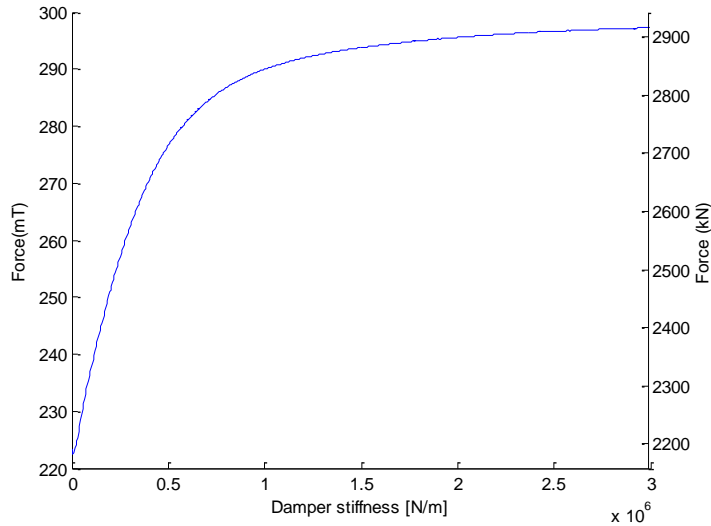


Figure 9.9: Maximum wire force against damper stiffness

### 9.7 Effect of shock absorber on main hoist failure

With a shock absorber attached to the main hoist wires there could be a possibility that there is a positive effect on main hoist failure as well. In order to determine this effect the shock absorber was implemented in the system with the parameters shown in Table (9.1). The results are shown in Figure (9.10)

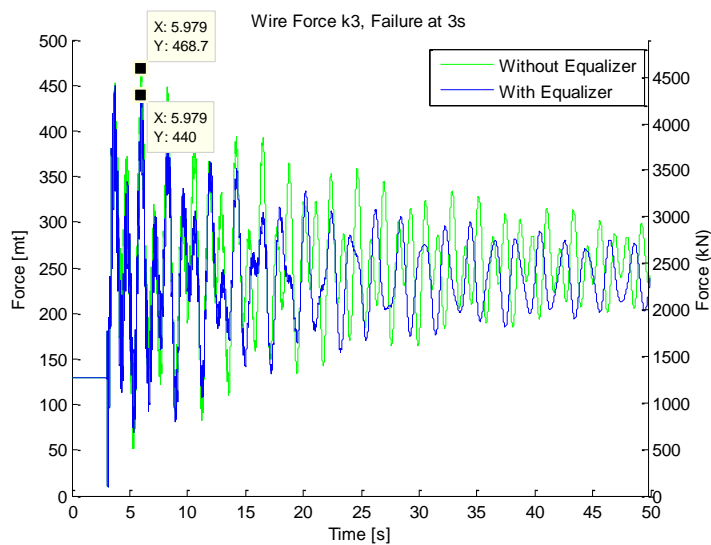


Figure 9.10: Main hoist wire force, outer wire failure

The effects of the shock absorber are visible in Figure (9.10), the system is damped more which leads to less fluctuation in the force. However, the peak forces are only reduced minimally; the highest peak is reduced by 6% when the equalizer is active.

Varying the stiffness in the range which was presented in Figure (9.9) didn't significantly improve the shock absorber, which is contradictory to the results obtained in Figure (9.9). Due to the much higher force that occurs in this case, it is possible that the speed of the piston increases, which will result in larger forces due to the damping. In order to get more insight, the same analysis has been done but now with keeping the stiffness constant and changing the damping. The results of this are shown in Figure (9.11). The maximum force that occurs in the wires decreases with a lower damping coefficient. However, the changes are small, which leads to the conclusion that the influence of the parameters of the shock absorber are low and that it isn't a good mechanism to reduce the maximum wire force in case of main hoist failure. The forces remain around the MBL of the wire, thus the possibility still exists that the wire will fail, especially when one takes wave actions into account which could increase the acceleration of the load.

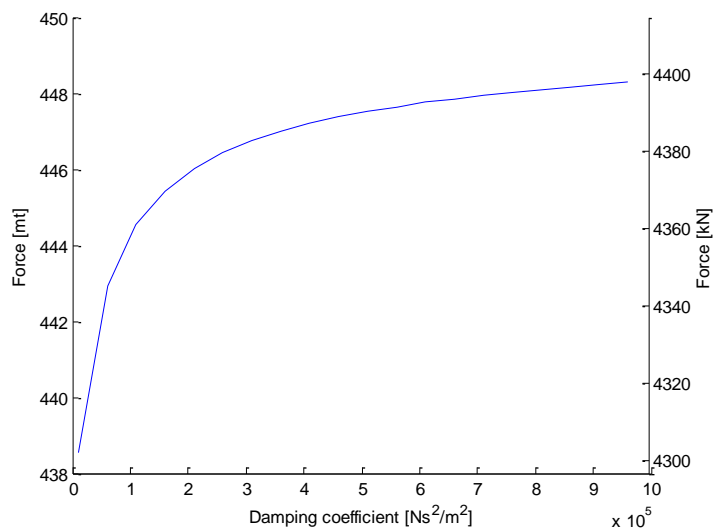


Figure 9.11: Maximum force against damping coefficient

## 9.8 Conclusions

Instead of using control systems to control the winches in the boom hoist system, one might prefer a mechanical equalizer to equalize the forces. This offers the possibility to include a shock absorber in the system, which could reduce the dynamic overloads that exist when wire failure occurs. The implementation of such systems was investigated in this section.

Two types of equalizer were investigated:

- Boom hoist equalizer
- Main hoist equalizer

Their influences on both the boom hoist failure case and the main hoist failure case were investigated and the following results were found:

### Boom hoist equalizer

A parameter study was performed to see what the best combination of parameters was for the boom hoist equalizer. From this study the conclusion was drawn that the improvements that can be achieved are very limited. The movement of the load is connected to the equalizer, so changing the parameters of the equalizer has an effect on boom rotation and vertical velocity of the load. Table (9.2) shows the theoretical best dynamic factors that could be obtained this way.

In terms of practical implementation, it was found that implementing this system would lead to undesirable damping during normal operation. This leads to the conclusion that implementing such a system is a compromise; it reduces the wire force, but is constantly acting when the boom is lifted/lowered.

**Table 9.2: Dynamic factor boom hoist wire**

<b>Boom angle [°]</b>	<b>Load [mt]</b>	<b>Dynamic Factor No Eq.</b>	<b>Dynamic Factor With Eq.</b>	<b>Reduction [%]</b>
82.0	10 000	1.47	1.51	+2.8
68.3	10 000	1.46	1.40	-3.8
58.4	7000	1.41	1.37	-2.8
41.6	4000	1.43	1.35	-5.6
0	1588	1.39	1.35	-2.8

### Main hoist equalizer

An advantage of the main hoist equalizer compared to the boom hoist equalizer is that the boom angle isn't affected by the equalizer position. This way the overturning moment remains equal, and the damping in the main hoist wires slows the load gradually, which reduces the force for boom hoist failure. With the right parameters it is possible to reduce the maximum force significantly, however the design will be limited by the space that can be used for the equalizer(s).

The biggest drawback of this system is that there is need for four independently operating equalizers, which will take a lot of space, power and are very costly.

In case of main hoist failure the influence of an equalizer remains small, the forces occurring in main hoist failure are three times higher, which makes the effect of the equalizer smaller. Therefore if one requires reducing the maximum force in case of main hoist failure, it is recommended to change the lowerblock design instead of implementing an equalizer. Appendix H elaborates on the current main hoist design of other large offshore cranes, and what their (dis)advantages are.

In general, there is sign of improvement possibilities when using equalizers/shock absorbers to reduce the dynamic effects. However, these improvements remain small and the fact that there is little known about how the force translates through the reeving. Therefore it can be concluded that a lot of further analysis is required before such a system can be implemented.

---

# 10 Conclusions and recommendations

---

This study was set out to investigate three possible failure cases on the new 10 000mt Tub Mounted Cranes for Heerema's NSCV. These will be the largest offshore cranes in the world. Such large and complex designs often impose a new critical look at certain subsystems, especially within the offshore industry where the focus lays more and more on safety. It became clear that there was insufficient knowledge about the following three failure cases:

- single boom hoist cable failure;
- single main hoist cable failure;
- drop of the load (due to other reasons than cable failure; rigging failure, hook failure etc.).

This research investigated all three cases, in order to determine what the dynamic effects are of these failure cases and what the most important parameters are. Additionally the possibilities to reduce the dynamic effects were investigated.

## 10.1 Conclusions

### Modeling

For each failure case two models have been created; one simplified model with only one or two degrees of freedom and a detailed model with multiple degrees of freedom. For the derivation of the equations of motions the Lagrange's equations were used. These proved to be very straightforward to use, especially for the main hoist model, which was a multi-body system. The simplified analyses proved to be a good validation for the complex models. The main hoist failure case and the drop of the load failure case have also been validated with the use of animations created from the data obtained in Matlab.

### Boom hoist failure

From an impulse/energy balance the dynamic factor for the boom hoist failure case had already been determined by Huisman. The main goal of the analysis in this thesis was to determine if there are parameters that are not in the energy-balance that do have an influence on the dynamic factor. The influence of several parameters was investigated, but none of them has a significant influence on the dynamic factor.

Therefore the following is concluded:

- The dynamic factor for the boom hoist failure case is 1.5 with respect to the nominal wire force after failure, independent of any variables.
- The wire force never exceeds the MBL of the wire; therefore the crane will not fail to carry the load in case of a single boom hoist failure.
- A shock absorber in combination with an equalizer attached to the boom hoist wires will only have minor influences (max 5.6% reduction), and the constant interaction of the shock absorber and the wires is undesirable. Therefore it is recommended to not further investigate the implementation of a shock absorber attached to the boom hoist wires.
- A main hoist shock absorber can have a reducing effect on the dynamic factor of boom hoist failure. However, no existing shock absorber/heave compensator has the right parameters in order to have a significant influence.
- No stress wave effects are found, although the model is able to 'show' them if they are present. So it can be concluded that stress waves are not present in this case.

### **Main hoist failure**

The main hoist failure case proved to be much more sensitive to various parameters than the other cases. The conclusions that are drawn are:

- Outer wire failure is the most severe case for the system.
- The luffing frame and boom hoist stiffness have a significant influence on the main hoist failure case. It reduces the maximum force by 12%.
- The main hoist length has a large influence on the maximum force; a longer length reduces the maximum force.
- The rigging has a large influence on the maximum force in the main hoist wires, reductions have been found in the order of 15-25%. However, the influence of the rigging is dependent on the eigen-frequencies of the system.
- The influence of a stress wave is low; a calculation proved that the influence is maximum 5% compared to the static weight of the load. A simple analysis with a discretized wire showed no stress wave effects.
- The force in the wire reaches values that are close to the MBL of the wire, based on these analyses no guarantee can be given on the fact if the wire will hold or not.
- A shock absorber has little influence on the maximum force in the wires in case of failure.

There are more conclusions that have been drawn from investigating this case. First the term 'dynamic factor' as used by Huisman cannot provide enough insight for this case. The dynamic factor is based on the force in the wire after failure, which is different for the inner and outer wire failure

case. Therefore the dynamic factor presented in this thesis is based on the wire force before wire failure.

Secondly the conclusion can be drawn that using advanced multibody software still can lead to wrong results. This has been the case during the writing of this thesis, where another company executed a similar analysis with wrong assumptions and then declared the design safe.

Another conclusion that can be drawn is that with the current design no guarantee can be given that the main hoist will hold in case of a wire failure. However, it is questionable if it should be designed for such a case. For example, there are cranes with a 400 *mt* single fall hook. If the wire fails in that case, the load drops as a consequence, but is the crane therefore unsafe to use?

It may be argued that in this case the load is 10 000 *mt*, which is significantly heavier and much more costly. However, the safety-factor in normal operating case is three, so a failure due to overload is very unlikely. Other parameters such as wear and corrosion of the wire are good to monitor, this way the risks of wire failure can be mitigated. An extensive FMECA is advised in order to determine if there is ground to change the design, or to declare the current design safe to use.

### Drop of load

- This is the least severe loadcase for the crane.
- Stress wave effects have an influence; still the force hardly exceeds the initial load before dropping the load.
- The boom stop will fail under the compression load of the boom in case of a drop of the load in the 82 *degrees* loadcase. This done by design to prevent damage to other parts.

## 10.2 Recommendations

The largest shortcoming of the model is the lack of knowledge about the behavior of the sheaves. The wires are reeved many times over many sheaves. For this thesis these sheaves have been left out of the analysis completely. If there is a way to add these to the model, it would improve the insight a lot. The problem with adding the sheaves is that there is wire added to the system or wire running over the sheaves in case of failure. The slip over the sheaves has to be modeled correctly, which is very complicated to do with numerical analysis.

Another possibility is to do scale model tests, however it would be complicated to find materials with the right properties to resemble the crane. Still, creating such a model and perform tests could provide more insight about the time it takes for the wires to un-reeve, and for the system to lose its carrying capacity.

Further recommendations are:

- Include vessel motions; the ship motions could have influences on the maximum forces that are present in the wires at the time of failure. This would also make other analyses possible; for example analyses on swinging or slewing motions. The principle of the Lagrange's equations provides a solid base for this. The model can be attached to a base which is excited with the vessel accelerations, as is done in previous theses by Dix [2] and Demmer [3].
- Add compression of the boom and the interaction with the luffing frame pivot. The boom is in compression when subjected to the load, this has not been taken into account in this model. The effect is expected to be low because the axial stiffness of the boom is high.
- Add bending of the boom. As there is little bending in the cases presented in this report, the bending of the boom has been left out of the equations. However, in the drop of the load – case bending could become important. A vibration analysis could be conducted in ANSYS to determine if damage to the boom could occur in this case.
- Optimize main hoist design. The main hoist has been designed in order to equalize the force between the four tackles, and to cope with sidelead. With the knowledge from this thesis the design could be changed in order to reduce the dynamic factor in case of failure.
- The damping in the main hoist blocks is an important parameter, if this is set to a low value this leads to numeric instability. It could be improved by calculating the normal force on the block and multiply this by friction factor. This has been investigated, but it is hard to exactly extract the normal force on the block and as far as this research went, it didn't have any influence. For further research it could be worthy to further investigate this.
- Further investigate main hoist shock absorber. This is closely related to the behavior of the sheaves. The shock absorber is attached to one partition of wire only, how does it behave through the whole system?
- Investigate the influence on the brakes and winches. The brakes and winches also have to be able to cope with the high peak loads that occur when wire failure occurs, this has not been a part of this investigation but could become of interest.
- Investigate hoisting/lowering operations. When the model is expanded with the winches and brakes, it becomes also interesting to model entire lifting operations with hoisting and lowering.

---

# Bibliography

---

- [1] T. Brzobohaty, *Analysis of a Crane Losing a Load*  
Thesis [in Czech], Huisman CZ, 2006
- [2] Z. Dix, *Reducing the swing motion of a hook load of an offshore crane*  
Master Thesis, Huisman Twente, March 2012
- [3] F. Demmer, *Reducing the swing motion of a hook load of an offshore crane using active tuggers*, Master Thesis, Huisman Twente, December 2013
- [4] D.J. Nugteren, *Investigation in the swing motion of a load in an offshore crane*  
Master Thesis, Huisman Equipment B.V., February 2010
- [5] Lloyd's Register, *Code for Lifting Appliances in a Marine Environment 2013*  
August 2013
- [6] DNV, *Rules for Lifting Appliances*  
June 2013
- [7] Pieter van Oers, *Boom Hoist Tackle Failure Analysis Design Report*  
Huisman Equipment B.V., November 2014
- [8] Singiresu S. Rao, *Mechanical Vibrations, Fifth Edition in SI Units*  
Pearson Education South Asia Pte Ltd, 2011
- [9] Maczynski and Szczotka, *Comparison of Models for Dynamic Analysis of a Mobile Telescopic Crane*, Journal of Theoretical and Applied Mechanics, Volume 40 No. 4, 2002
- [10] Krukowski *et al.*, *The Influence of a Shock Absorber on Dynamics of an Offshore Pedestal Crane*, Journal of Theoretical and Applied Mechanics, Volume 50 No. 4, 2012
- [11] R.Q. van der Linde and A. L. Schwab, *Multibody Dynamics B*  
Lecture Notes, Delft University of Technology, 1997
- [12] E. Wittbrodt *et al.*, *Rigid Finite Element Method in Analysis of Dynamics of Offshore Structures*, Ocean Engineering & Oceanography, Springer, 2013
- [13] R. Huston and H. Josephs, *Practical Stress Analysis in Engineering Design*  
CRC Press, December 2008
- [14] B.D. van den Berg, *Optimization of the buffer in a passive heave compensator*,  
Master Thesis, Huisman Equipment B.V., September 2014
- [15] Heerema Marine Contractors, digital image, viewed on 30-5-2015. Retrieved from <http://www.heerema.com/content/video/image-4-a-hfg-home-heerema-thialf-removal.jpg>
- [16] DIY Trade, digital image, viewed on 1-7-2015. Retrieved from [http://www.diytrade.com/china/pd/9096926/Steel\\_wire\\_rope.html](http://www.diytrade.com/china/pd/9096926/Steel_wire_rope.html)

- [17] Siemens, *Siemens successfully installs third HVDC platform in the North Sea for ThenneT*, press release, July 2010, viewed on 25-06-2015. Retrieved from [http://www.siemens.com/press/pool/de/pressebilder/2014/energy/wind-power/soew201403/300dpi/soew201403-16\\_300dpi.jpg](http://www.siemens.com/press/pool/de/pressebilder/2014/energy/wind-power/soew201403/300dpi/soew201403-16_300dpi.jpg)

# Appendix A: Boom Angles

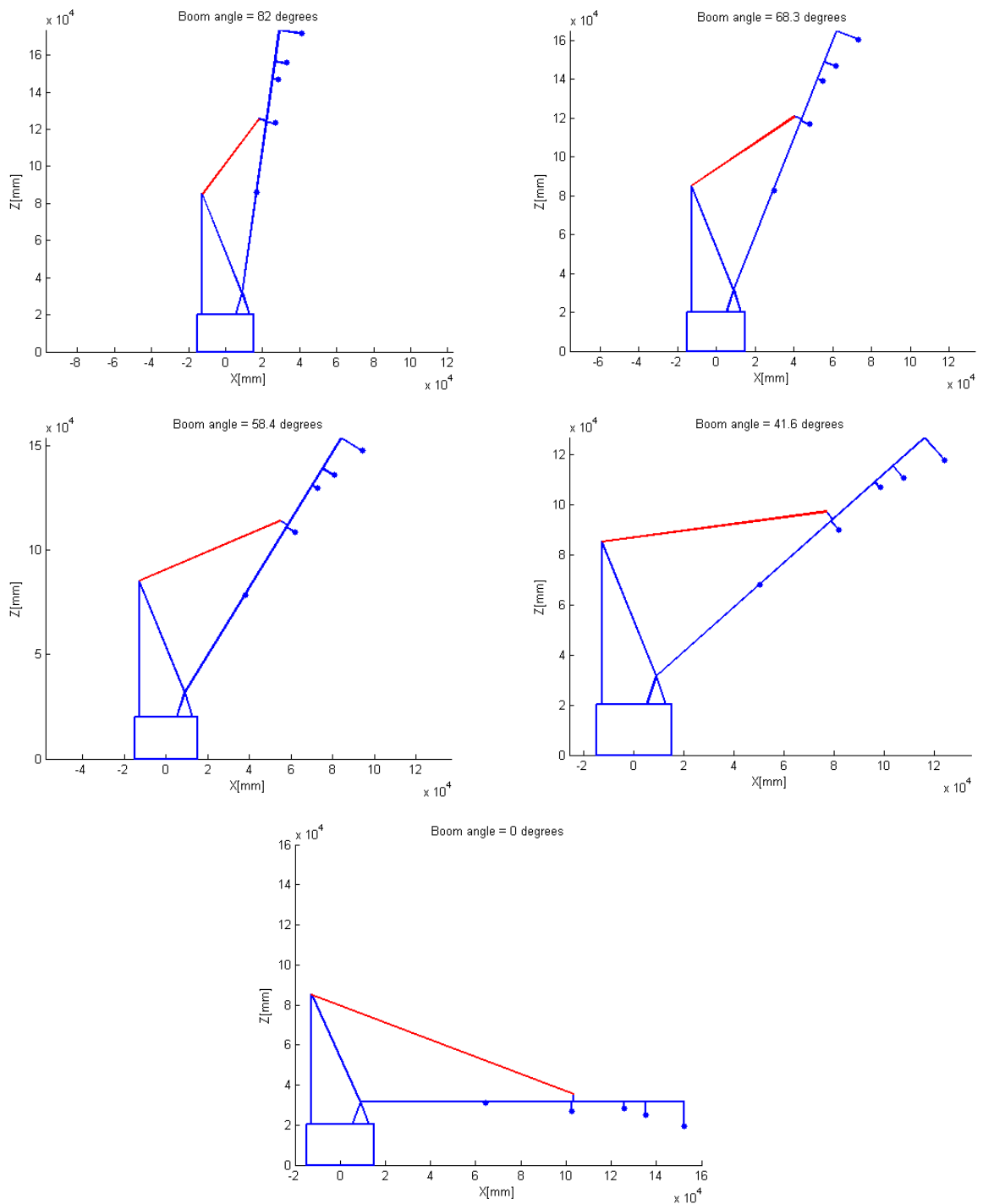


Figure A.1: Boom angles



---

## Appendix B: Crane Details cont'd

---

This Appendix elaborates a bit more on technical crane details. The load curves of the cranes can be found here, and the reeving diagram for the boom hoist. Also the ANSYS plot of the luffing frame stiffness is displayed in this section, and a table from which the bearing friction can be obtained. Other things that can be found here are the main hoist block geometry and the location where the boom hoist equalizer is implemented.

### Load Curves

Different load curves are shown for different reeving configurations. For this thesis, only the maximum load case is examined, which is with an 80 falls main hoist.

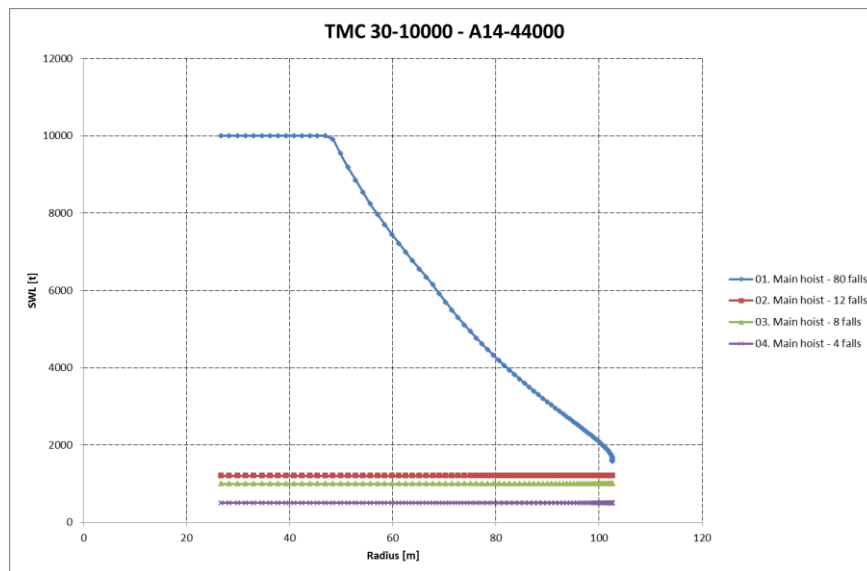
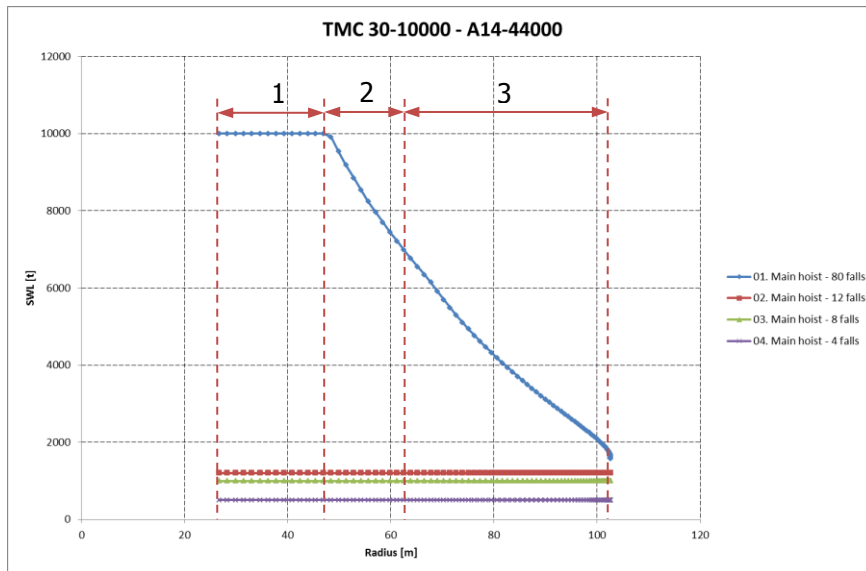


Figure B.1: Load Curves

The blue depicted loadcurve in Figure (B.1) consists of three sections. For more understanding these sections will be explained on the next page.



1. Main hoist governing
2. Boom hoist governing
3. Luffing frame governing

Figure B.2: Governing sections

Figure (B.2) shows the same loadcurve diagram with the three sections. In the first section the main hoist is the limiting parameter for the crane. At the point of maximum outreach with maximum load, which is 10 000mt at 48m, the boom hoist becomes governing. This is due to the fact that the overturning moment is the largest here.

At the transition point from 1 to 2 the bearing of the tub is also governing. At this point the overturning moment is the largest, which also has the most impact on the bearing. The bearing has been designed to be able to cope with this overturning moment, hence it is also governing at this point.

Where point 3 starts an additional criterium has been set. At this stage the force in the luffing frame becomes the governing parameter for the system. The force in the boom hoist stays approximately equal to the force found at 48m outreach. However, the angle at which the force is applied to the luffing frame changes, which increases the compression in the front legs.

### Boom hoist wire reeving configuration

The reeving configuration for the boom hoist wires can be found in Figure (B.2). There are two independent operating boom hoist wires, which are placed symmetric over the boom centerline. This way no unwanted moments are created when there is a difference in load in the two boom hoist wires. Boom hoist wire 1 can be operated by Winch 1 and Winch 4, where Boom hoist wire 2 makes use of Winch 2 and Winch 3.

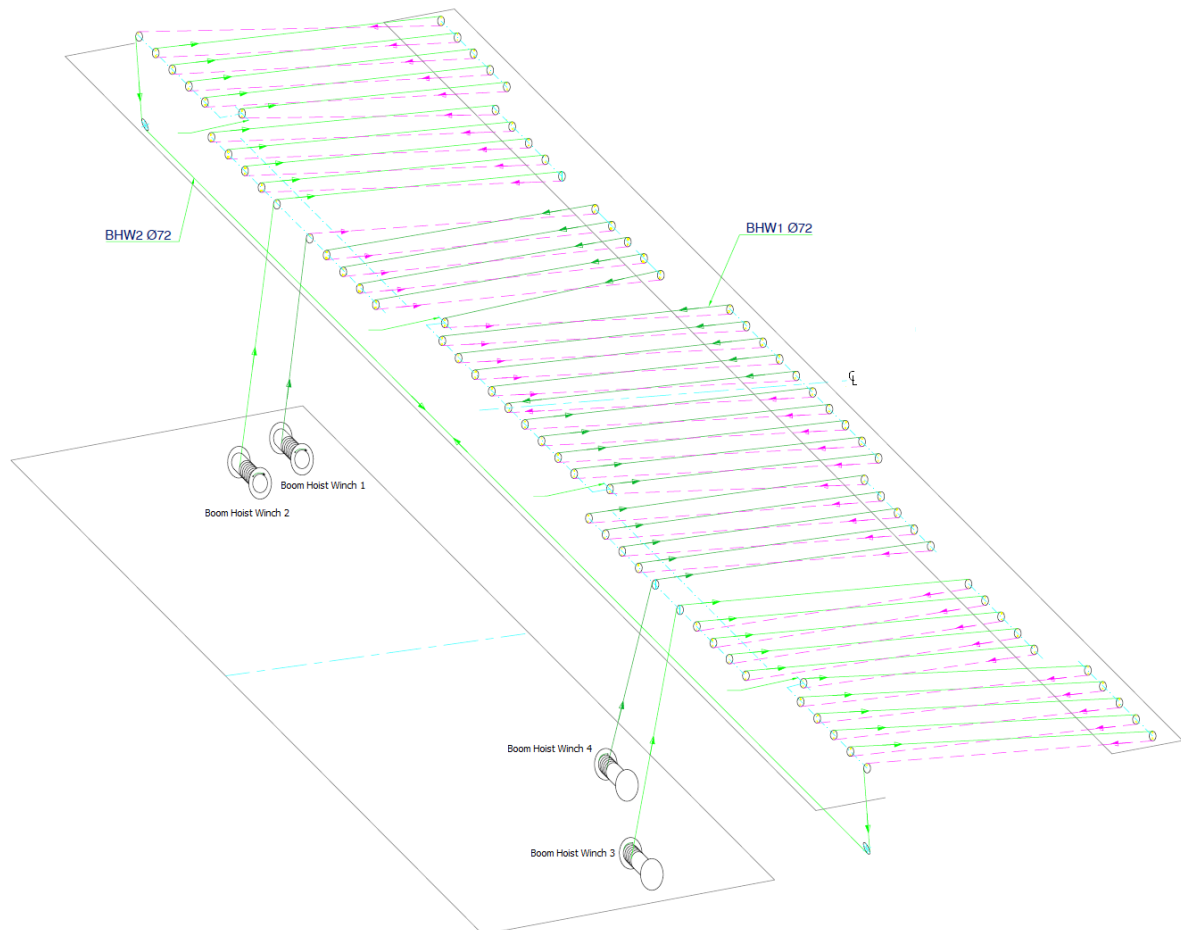


Figure B.2: Boom hoist wire reeving

### Luffing frame stiffness

The luffing frame stiffness is determined in ANSYS by Huisman. The result of the ANSYS plot is shown in Figure (B.3). A force of 1 kN results in a horizontal displacement of 0.007 mm. The corresponding stiffness of the crane house is then determined by:

$$k_{crane} = \frac{1000}{0.007e^{-3}} \approx 1.43e^8 [N/m]$$

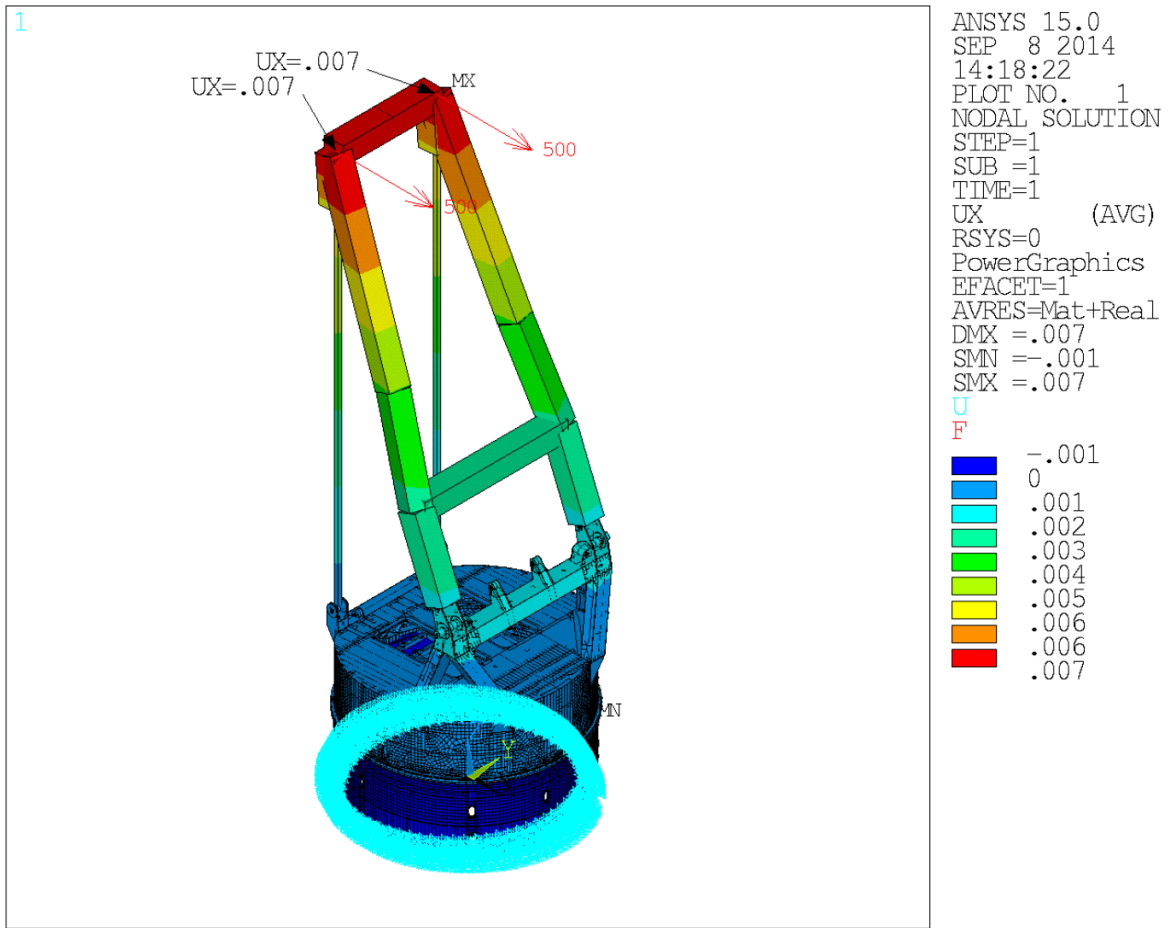


Figure B.3: ANSYS luffing frame stiffness

Main hoist geometry

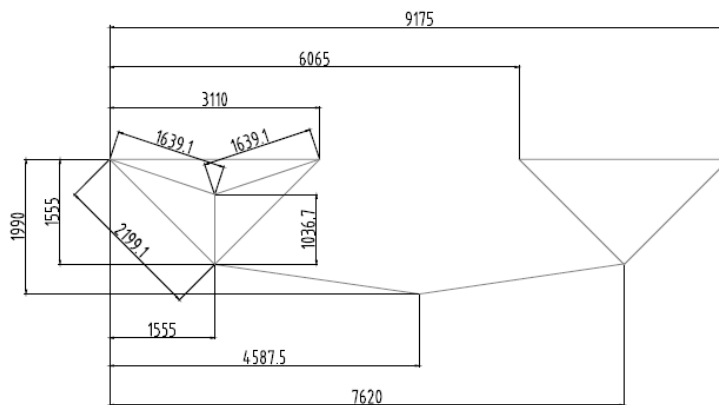


Figure B.4: Main hoist system geometry

### Bearing Material Selection

Bearing type	Subtype	Preference [-]	Translating / rotating [-]	Friction coefficient	Rotation angle [°]	Deflection angle [°]	Continuous running time [min]	Allowable surface pressure [N/mm <sup>2</sup> ]	Allowable environn
Bronze	CuSn12-C	Most preferred	both	15%	360	0.1	10	w.p. 70, wo.p. 90	All
	CuAl10Fe5Ni5-C*				360			w.p. 125, wo.p. 165	All
	CuAl11Fe6Ni6-C				360			w.p. 160, wo.p. 210	Splash zone, (marin
	CuZn25Al5Mn4Fe3-C**				360			w.p. 225, wo.p. 300	Splash zone**, (marin
	Toughmet 3 CX1Q5				360			w.p. 330, wo.p. 460	Splash zone**, (marin
	Wieland B09***				360			N.A.	All
Fibre reinforced plastic	Orkot TLM	Least preferred	both	10%	30	0.5	10	Quasi static 120	(marine) air
	Orkot TXM			5%	360	0.5	30	Dynamic 80	(marine) air
Spherical plain bearing	Bronze		rotating only	15%	360	10	10	Dep. on bronze type	submerged
	Orkot TLM		rotating only	10%	30	10	10	Quasi static 120	Marine air
	Orkot TXM		rotating only	5%	360	10	30	Dynamic 80	Marine air
Roller bearing	Deep groove ball bearing			rotating only	0.15%	360	0.15		Allowable load
	Cylindrical roller bearing			0.20%	360	0.05		depending on Co and Cdyn	zone, (marine) air
	Spherical roller bearing			0.18%	360	1.5 - 2.5	∞		
	Toroidal roller bearing			0.18%	360	1.5 - 2.5			
	Tapered roller bearing			0.18%	360	0.05			

\*: Cannot be used in combination with St.52-3N as sliding counter material

\*\*: Splash zone only if sealed properly

\*\*\*: Only thin-walled bushes without solid lubrication plugs

w.p. = with solid lubrication plugs

wo.p. = without solid lubrication plugs

Figure B.5: Bearing Material

### Boom hoist equalizer

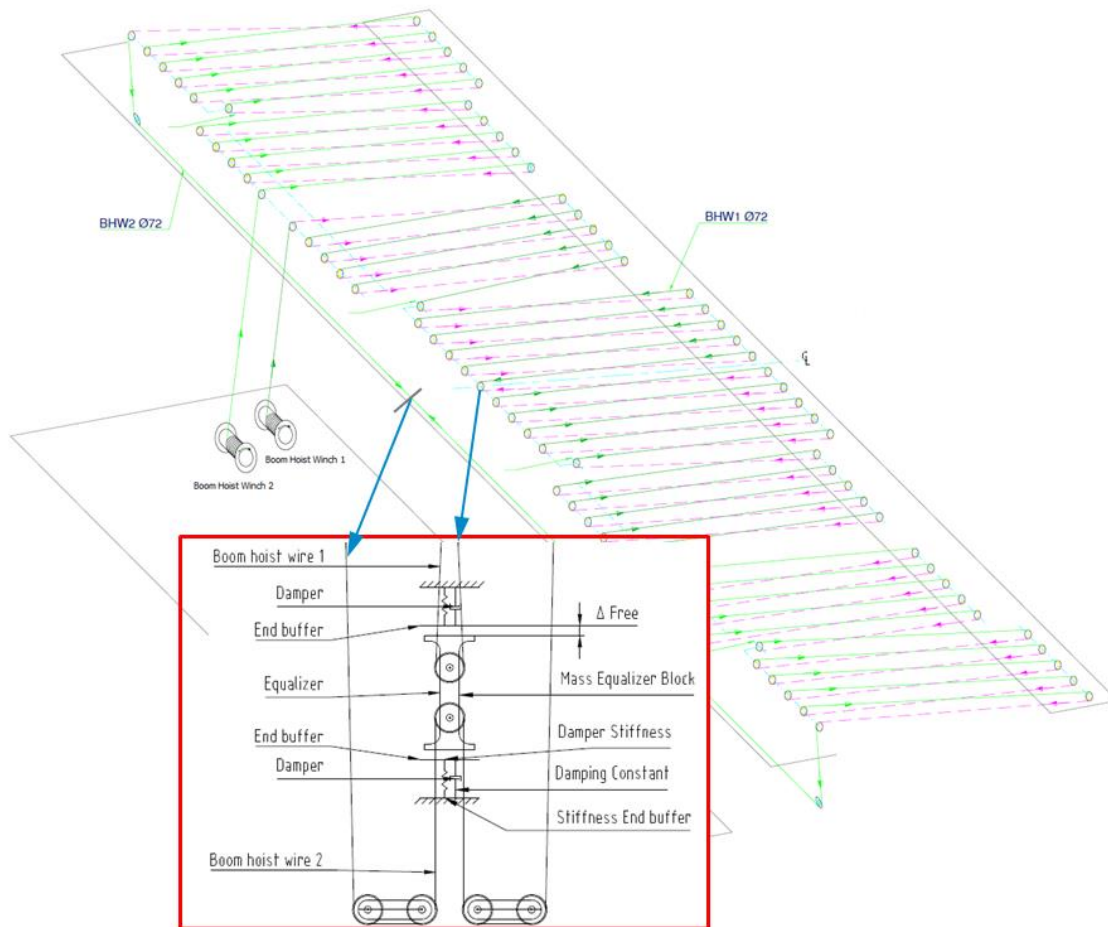


Figure B.6: Location of BH – equalizer

**Boom stop**

In this section the information for the boom stop can be found. First, Figure (B.7) shows the general side view of the Boom with boom stop. As can be obtained from this figure, at  $82\text{ degrees}$  the boom is against the boom stop. Figure (B.8) shows the top view and the main chord dimensions, based on this dimensions an estimation is given on the stiffness of the boom stop.

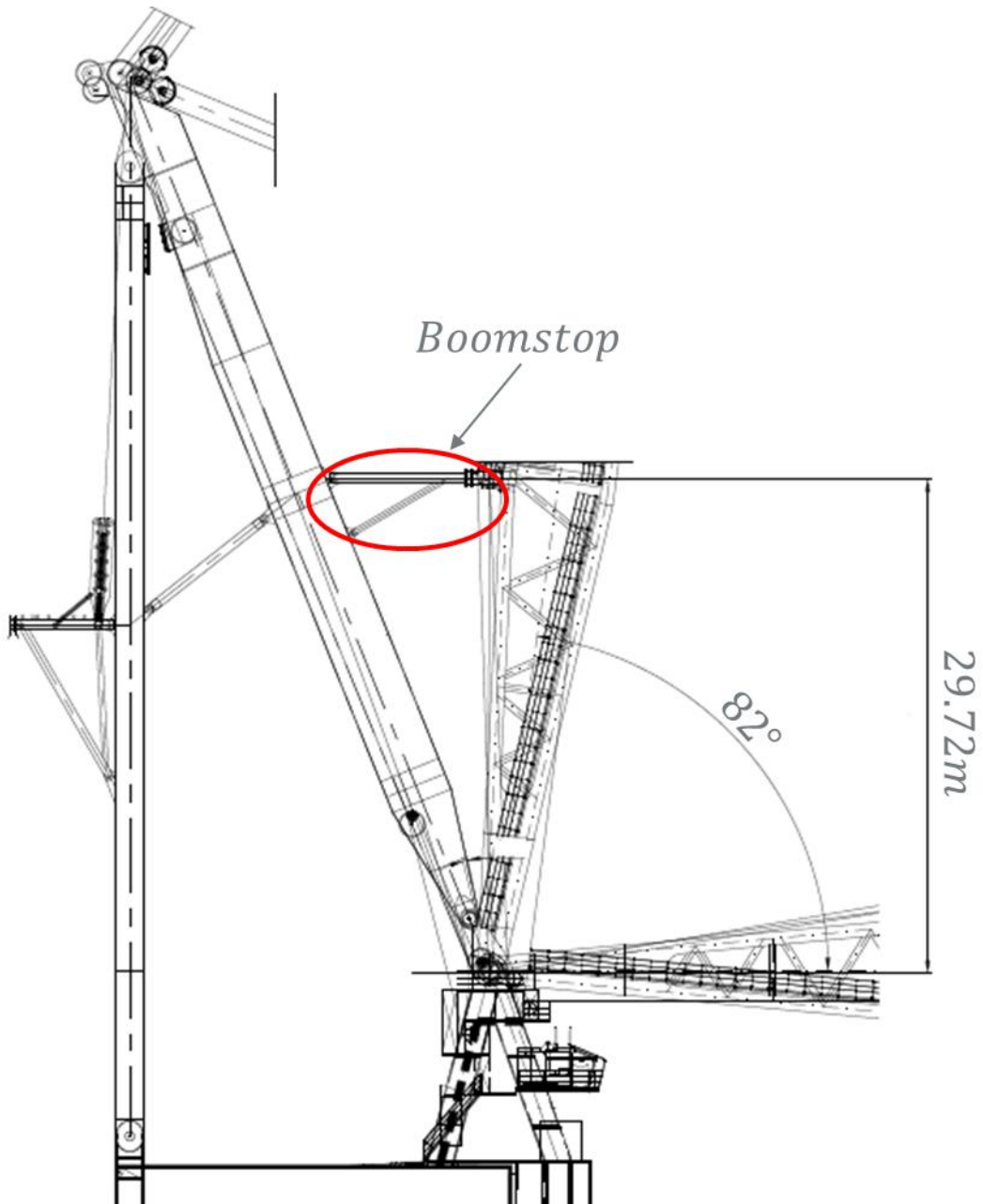


Figure B.7: Boom stop general side view

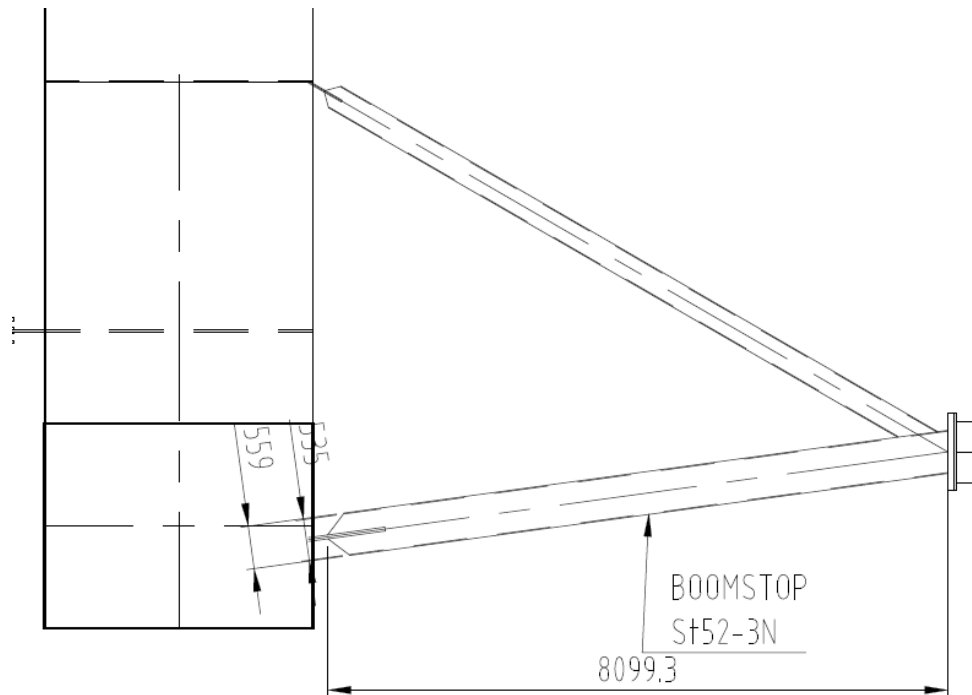


Figure B.8: Boom stop top view & main chord dimensions

The axial stiffness of the boom stop is based on the main chord dimensions. The two 'diagonals' to the side and to the bottom is neglected in order to get a conservative estimation, as a lower stiffness leads to more rotation of the boom.

The stiffness can then be determined by:

$$k = \frac{EA}{L} \quad (\text{B.1})$$

$$k = 2 \cdot \frac{210e9 \cdot (0.559^2 - 0.535^2)\pi}{4 \cdot 8.0993} = 1069e6 \text{ N/m} \quad (\text{B.2})$$

The multiplication by 2 is due to the boom stop being implemented twice; once on each luffing frame.



---

# Appendix C: MATLAB Code

---

## Boom Hoist Model

Only the ODE – function is shown below:

```
function dydt = rhs(t,y)
```

```
global GL
```

### assign variables

```
k=GL.k;
k_MH = GL.k_MH;
L_0=GL.L_0_MH;           % [m]
M_load=10000e3*(1-heaviside(t-5)); % [kg]
M_MH = 480 * 1000; % [kg]
g = 9.81;
r_pivot = 0.5; % [m]
N = GL.N;
d = GL.d;
m_element = GL.mass_element;
k_element = GL.k_element;%*(1-0.5*heaviside(t-5));
L_BHs=GL.L_BHs;
angle_BHs = GL.alpha3_BHs;
M_LF = 0.75*1115e3 ; % [kg]
k_LF = GL.k_LF;

X_LF=-21.700;
Z_LF=53.8;

Lboom = sqrt(GL.X(3)^2+GL.Z(3)^2);
z_tip = Lboom*sin(y(N*4+3) +GL.alpha3(3));
x_tip = Lboom*cos(y(N*4+3) +GL.alpha3(3));

ztiptest= Lboom*sin(GL.init_theta+GL.alpha3(3));
```

### Elongation speed of wire for Damping

```
L1 = sqrt(21.7^2+53.8^2);
L2 = sqrt(96^2+4.2^2);
a = pi - atan(-Z_LF/X_LF)-y(N*4+3)-GL.alpha3_BHs;
b = pi - atan(-Z_LF/X_LF)-GL.init_theta -GL.alpha3_BHs;
Elongation_speed = (2*L1*L2*sin(a)*y(N*4+4)) / (2*sqrt(L1^2+L2^2-2*cos(a)));
```

### Location of Boom hoist sheaves on Boom

```
X_BHs = cos(y(N*4+3)+angle_BHs)*L_BHs;
Z_BHs = sin(y(N*4+3)+angle_BHs)*L_BHs;
```

### Pivot Friction

```
mu_pivot = 0.01; % Friction coefficient pivot

% sign is for direction of rotation
fr_moment_pivot = GL.Normal_force*mu_pivot*sign(y(N*4+4))*r_pivot;
```

### Get CoG locations

```
X = [0;y(3:4:4*N)];
Z = [0;y(5:4:4*N+1)];

X(end+1) = X_BHs;
Z(end+1) = Z_BHs;

X(1) = y(1);
Z(1) = Z_LF;
```

### Get CoG velocities

```
dXdT = [0;y(4:4:4*N)];
dZdT = [0;y(6:4:4*N+2)];

dXdT(1) = y(2);

dXdT(end+1) = -cos(y(N*4+3)) * y(N*4+4) * L_BHs; % X component of velocity of Boom hoist sheaves
dZdT(end+1) = sin(y(N*4+3)) * y(N*4+4) * L_BHs; % Z component of velocity of Boom hoist sheaves
```

### diff X

```
dX = diff(X);
dZ = diff(Z);

% dX(1) = dX(1) - y(1); % y(1) is X - component of luffing frame

ddXdT = diff(dXdT);
ddZdT = diff(dZdT);
```

### Spring forces

```
Lnew = sqrt(dX.*dX + dZ.*dZ);

% X direction
LnewX = dX./Lnew;
LnewZ = dZ./Lnew;

F_spring_element = k_element .* (Lnew - d);
```

### Damping forces

```
fr_wire = 0.01 * 2*sqrt(2*GL.k_element*m_element); % friction coefficient wire * critical damping cor:

% Relative velocity
rV = ddXdT.*LnewX + ddZdT.*LnewZ;
F_damp_element = rV.* fr_wire;
```

### Combine Spring & Damping

```
F_element = F_spring_element+F_damp_element;

if F_element <=0
    disp('0')
    F_element = F_element;
else
    F_element = F_element;
end

Fx_element = F_element.*LnewX;
GL.Fx_element = Fx_element;
Fz_element = F_element.*LnewZ;
```

### Luffing frame

```
dxLFdt = y(2);
d2dxLFdt2 = (- k_LF * (y(1) - X_LF) + Fx_element(1) - y(2)*0.005*2*sqrt(k_LF*M_LF))/M_LF;
```

### E.o.M. Elements

```
%E = zeros(N*4,1);
for i = 1: N
    E(1+(i-1)*4) = y(4+(i-1)*4);
    E(2+(i-1)*4) = (-Fx_element(i)+Fx_element(i+1))/m_element;
    E(3+(i-1)*4) = y(6+(i-1)*4);
    E(4+(i-1)*4) = (-Fz_element(i)+Fz_element(i+1))/m_element;
end

GL.E=E;
```

### Boom

#### Boom stop

```
F_X_BS = (cos(GL.init_theta)-cos(y(N*4+3)))*30.086*GL.k_BS;

M_X_wires = Fx_element(end)*Z_BHs;
M_Z_wires = -Fz_element(end)*X_BHs;
M_stat = (GL.M(1)*cos(y(N*4+3)+GL.alpha3(1))+GL.M(2)*cos(y(N*4+3)+...
    GL.alpha3(2))+GL.M(3)*cos(y(N*4+3)+GL.alpha3(3))+GL.M(4)*cos(y(N*4+3)+...
    GL.alpha3(4))+GL.M(5)*cos(y(N*4+3)+GL.alpha3(5)));

dthetadt = y(N*4+4);
d2thetadt2 = (-1/(sum(GL.I)))*((M_stat)-M_X_wires-M_Z_wires)+...
    k_MH*(Lboom*sin(y(N*4+3)+GL.alpha3(3))-y(N*4+5)-GL.L_0_MH)*x_tip +...
    F_X_BS*29.72+ (0.02+0.02*heaviside(t-20)+0.06*heaviside(t-40))*2*...
    sqrt(sum(GL.I)*k)*Elongation_speed + fr_moment_pivot);
```

### Main Hoist

```
dzMHdt = y(N*4+6);  
d2dzMHdt2 = ((k_MH)/(M_load+M_MH))*(z_tip-y(N*4+5)-L_0) - g -...  
    (0.008*2*sqrt(k_MH*(M_load+M_MH))*(y(N*4+6))/(M_load+M_MH));
```

### ODE input values

```
dydt = [dxLFdt; d2dxLFdt2; E'; dthetadt; d2thetadt2; dzMHdt; d2dzMHdt2];
```

### Main Hoist Model

As the MATLAB code is too lengthy, it is not shown in the report.

### Drop of the load Model

The essence of this model is the same as the Boom hoist model.

---

## Appendix D: End positions MH after failure

---

The easiest way to check whether a model is valid, is to check if the equilibrium position corresponds with the expectations. Therefore the end-of-simulation plots are shown in this section for inner and outer wire failure of the main hoist. For both cases the main hoist length is set at  $30m$ .

### Inner wire failure:

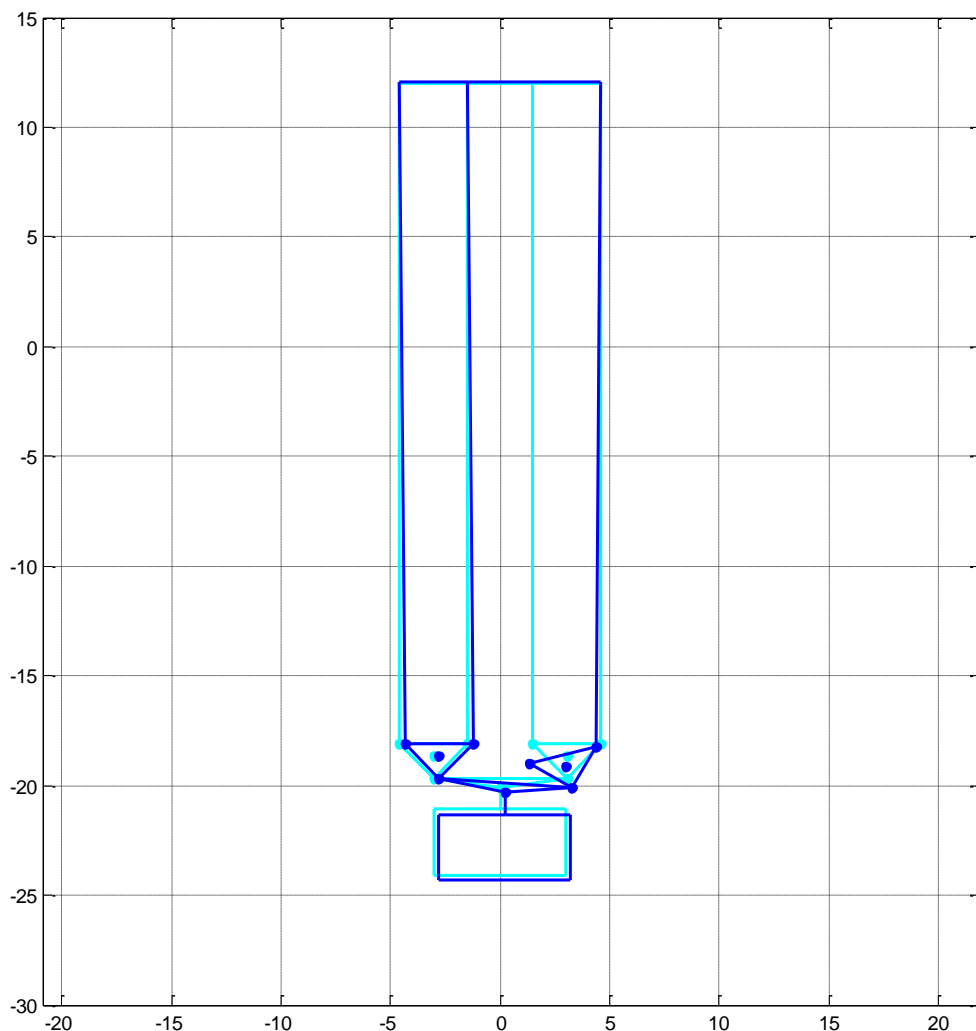
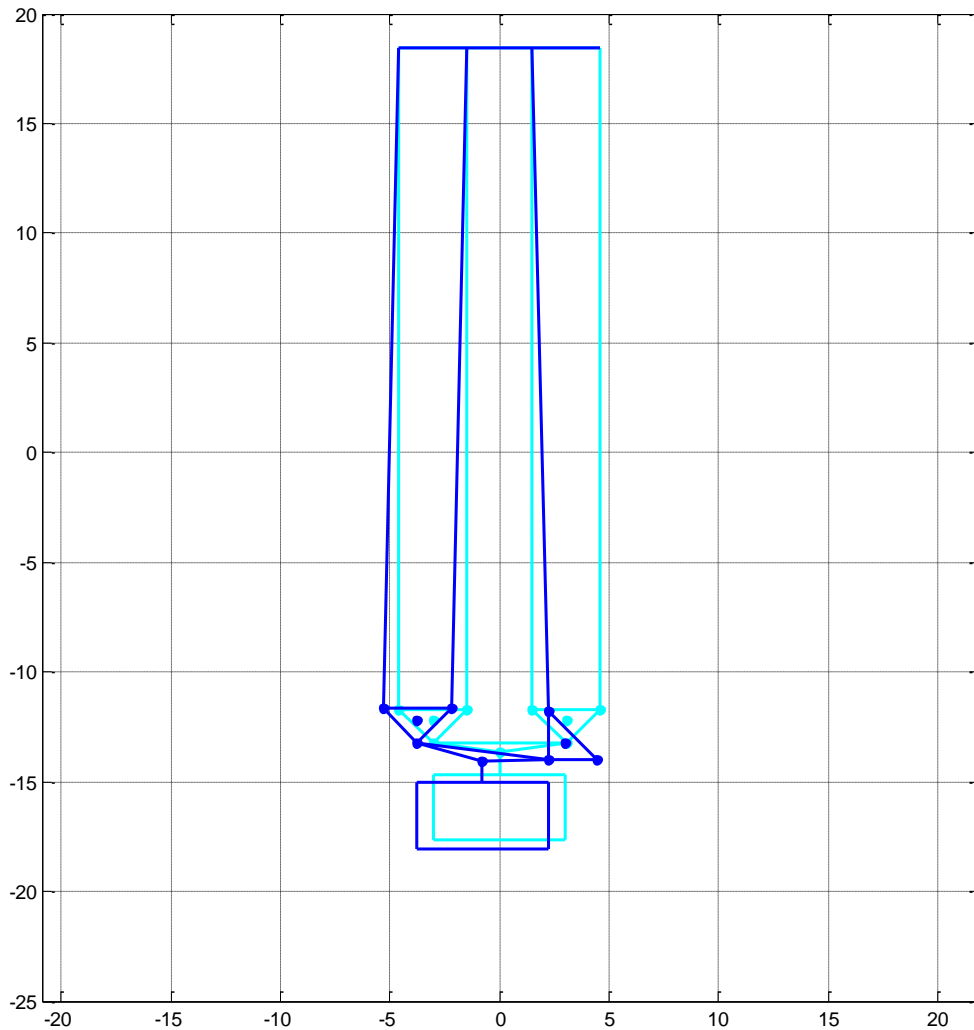


Figure D.1: Inner wire failure

The rotation of the right triangle is blocked by the way the lower block is constructed; therefore the rotation is limited to  $15\text{degrees}$ . Due to this rotation the load is shifted slightly to the right, which can also be witnessed in Figure (D.1).

**Outer wire failure:**

The end-of-simulation plot in case of outer wire failure is shown in Figure (D.2) below:



**Figure D.2: Outer wire failure**

As expected, the load shifts to the left because of the changed moment arm due to the failure of the outer wire. The rotation of the right triangle is not blocked in this case, which causes the rotation of *45 degrees*.

---

## Appendix E: Stress wave effect MH wire

---

This appendix is an addition to Chapter 7.3 about the stress wave effect in the main hoist wire. There are no effects witnessed that indicate the presence of a stress wave in case of wire failure. The lengths which were viewed in these cases are rather restricted; therefore a more elaborate analysis has been carried out in order to determine when the stress wave effect is most present. Figures (E.1)-(E.2) show the results of these analyses.

To see if there is any load-case where the stress wave effect is present, the lower limit load-case has also been examined. This is with a load of  $1588\text{ mt}$ ,  $L_0$  of  $10\text{ m}$ , an initial speed of  $1.74\text{ m/s}$  and 0 initial deflection of the wire.

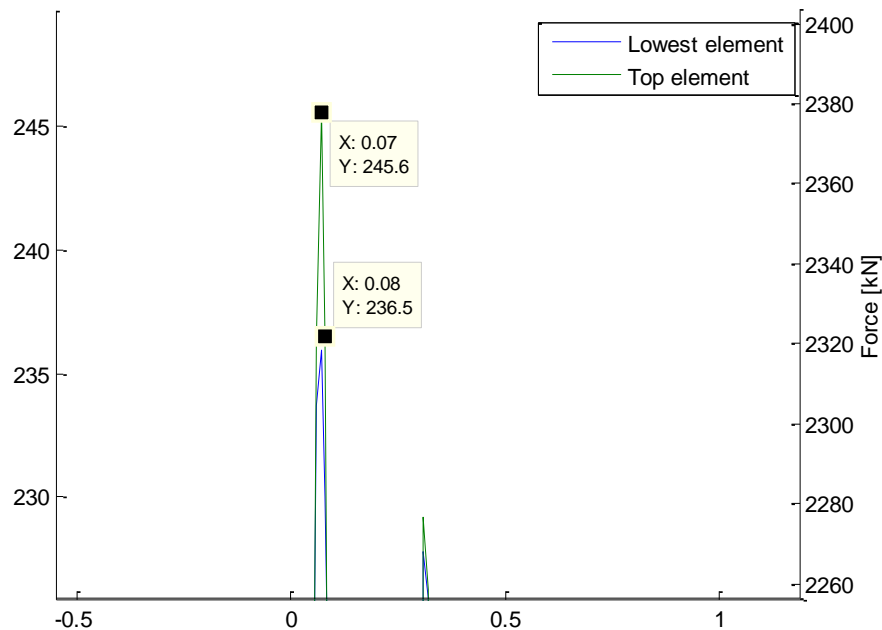
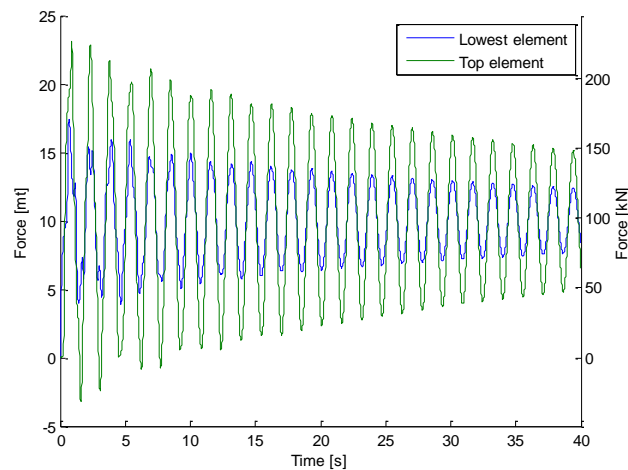


Figure E.1: Lower limit case

To determine whether the model is valid, a case has been used to check if the stress wave effect can be witnessed with this model. A theoretical load-case has been used, with a load of  $1mt$  and a  $L_0$  of  $1000m$ . The results of this can be found in Figure (E2). In this figure clearly the effect of the shockwave is present. The load in the top element is almost 1.5 times higher than the load in the lowest element. So the model is able to show stress wave effects if present. It also proves that in the load-cases shown in this report the stress wave effect is not present, or only in small magnitude compared to the static force. Therefore the assumption to leave the stress wave effect out of the complex main hoist model is valid.



**Figure E.2: Theoretic load-case of  $1mt$  and  $L_0$  of  $1000m$**

---

# Appendix F: Heave Compensation System

---

Working principles:

- Load is balanced by nitrogen pressure
- Stiffness of passive system depends on nitrogen volume
- Movement of load depends on external force (drag, inertia, etc.)
- Load remains stationary after landing

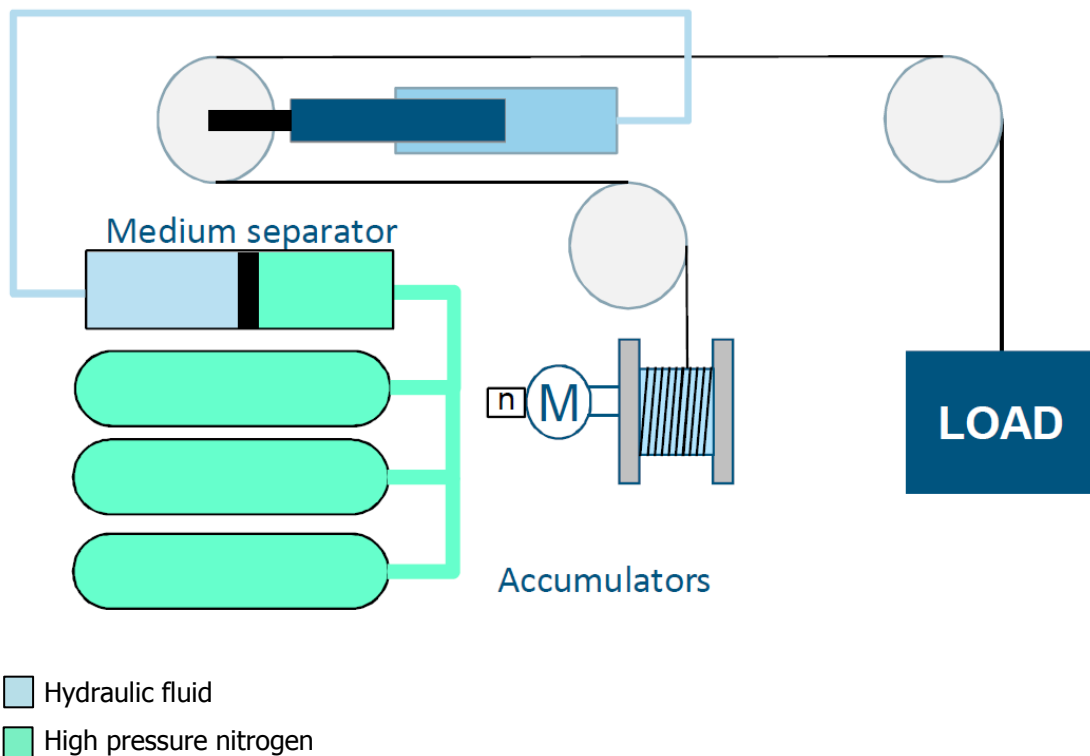


**Figure F.1: Heave compensation system**

Relevant parameters for the heave compensation system can be found in Table (F.1). These parameters are the values from Subsea 7's Seven Waves, on which Huisman installed a 400 mt offshore mast crane with heave compensation, see Figure (F.2). The linepull for a SWL of 1 fall is 200 mt, this is comparable with the linepull of the Main hoist system of the cranes used in this thesis, which is 131 mt. Therefore these parameters provide a solid base for an analysis to find out whether the shock absorber has a positive influence on the maximum Boom hoist force.



Figure F.2: Subsea 7's Seven Waves

Table F.1: Parameters Heave Compensation System

Parameter	Value
SWL 1 fall	200mt
Translating mass	10150kg
Viscous damping	251.2kNs <sup>2</sup> /m <sup>2</sup>
Maximum operating pressure	300bar
Maximum allowable piston speed	0.63m/s
Minimum gas volume at mid position	0.703m <sup>3</sup>

The stiffness of the gas spring in the passive compensator can be calculated using Equation (F.1):

$$k_p = \left( \frac{p_0 V_0^n}{(V_0 - y_p A)^n} - p_0 \right) \cdot \frac{A}{y_p} \quad (F.1)$$

Where:

$n$  = Adiabatic index, determined empirically, for the described case this is 1.7;

$y_p$  = Piston position.

# Appendix G: FMECA

Severity categories						Likelihood of occurrence					
						Probability	Less than once in 20 years	Between once in 20 years and once in 2 years	Between once in 2 years and once in 1 year	Between once in 1 year and once in 3 months	More than once in 3 months
Repair time	Safety	Damage cost	Environmental harm	Description	Description	Very Unlikely	Unlikely	Possible	Likely	Very Likely	
					Grade	1	2	3	5	7	
Severity levels	Less than 1/2 day	No injury / First Aid Case (FAC)	Less than € 1000	Less than 1ltr	Negligible	1	1	2	3	5	7
	1/2 day - 1 day	Medical Treatment Case (MTC)	€ 1000 - 10k €	1ltr - 10ltr	Slight	2	2	4	6	10	14
	1 day - 3 days	Restricted Work Case (RWC)	10k € - 100k €	10ltr - 100ltr	Moderate	3	3	6	9	15	21
	3 days - 7 days	Large Permanent Injury (LPI)	100k € - 1M €	100ltr - 10m <sup>3</sup>	High	5	5	10	15	25	35
	More than 7 days	Multiple LPI / Casualty	More than 1M €	More than 10 m <sup>3</sup>	Very high	7	7	14	21	35	49

The ranking of the Failure Modes is divided into three criticality levels, for which the following holds:

- **Green** (low): criticality acceptable (no action required).
- **Orange** (medium): criticality should be reduced As Low As Reasonably Practicable (ALARP) by appropriate mitigation/control measures, procedures and/or design modifications (cost/effort of the mitigation action should be weighed against its benefit).
- **Red** (high): criticality should be reduced as a priority by design, mitigation/control measures, effective reporting systems, procedures, etc.

Figure G.1: FMECA



---

# Appendix H: Main hoist concepts

---



Figure H.1: Main hoist of Heerema's Hermod

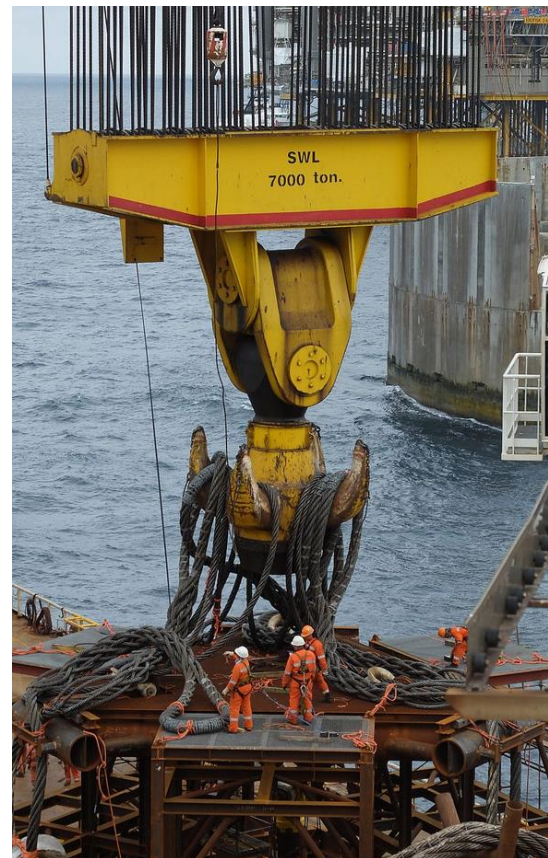
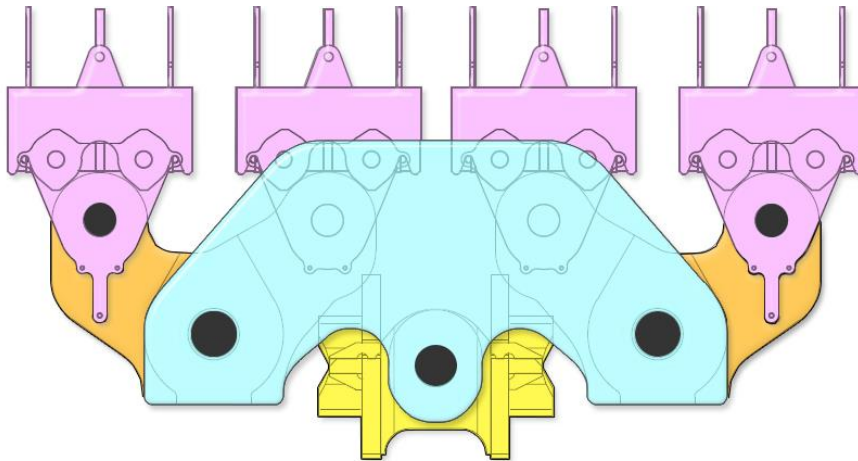


Figure F.2: Main Hoist of Heerema's Thialf (left) and Saipem's 7000 (right)



**Figure H.3: Main hoist of Heerema's NSCV**

The concept of the main hoist block for the NSCV is an innovative concept compared to the existing concepts of today's largest crane vessels. The orange parts displayed in Figure (H.3) are able to rotate, which makes it able to 'equalize' the forces in the wires. This is especially favorable when there is inconsistency in the speed of the winch drums of the wires. Also this way the block can cope with sidelead better.

The major drawback of the system is the increased freefall of the load in case of wire failure. In this case the MH blocks in Figure (H.1) and (H.2) would perform better. At a preliminary stage this concept was also used for the NSCV, which is shown in Figure (H.4). With this concept the dynamic factor in case of wire failure would be significantly reduced.



**Figure H.4: Preliminary concept of MH**



